

**CHROMIUM AND TITANIUM BASED STANNUM
NANOCOMPOSITES MATERIALS AS ELECTRON
ACCEPTORS FOR NEXT GENERATION BULK
HETEROJUNCTION PHOTOVOLTAIC CELLS**



**UNIVERSITY of the
WESTERN CAPE**



NALEDI RALEIE

*BSc Honours Chemistry (North West University),
MSc Nanoscience (University of Johannesburg)*

A thesis submitted in fulfilment of the requirements for the degree of

Philosophiae Doctor

Faculty of Science, Department of Chemistry

University of the Western Cape

Cape Town, South Africa

Supervisor: Prof Emmanuel I. Iwuoha

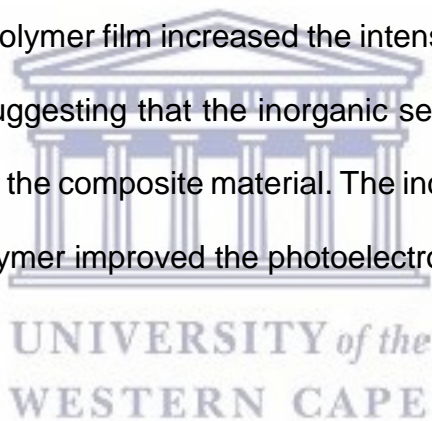
May 2018

ABSTRACT

Renewable energy has become the centrepiece of research in resolving the energy crisis. One of the forms of renewable energy is solar energy. This form of energy is costly to develop. Organic molecules are promising materials for the construction of next generation photovoltaic cells considering their advantage of lower cost compared to crystalline silicon that is currently used in solar cells. This forms the basis of this research, which focused on the synthesis and characterisation of poly(3-hexylthiophene) P3HT, stannum (Sn) nanoparticles and stannum-based bimetallic stannum-titanium (SnTi), stannum-chromium (SnCr) and stannum-vanadium (SnV) nanoparticles for the application in the construction of heterojunction photovoltaic cells (PVCs). The composite materials formed with the stannum-based bimetallic nanoparticles and either P3HT or the commercially available poly[N-9'-heptadecanyl-2,7-carbazole-alt-5,5-(4',7'-di-2-thienyl-2',1',3'-benzothiadiazole)] (PCDTBT) were used as active materials in the photovoltaic cells (PVCs). The optical and electronic properties of the polymers (P3HT and PCDTBT) and the bimetallic nanoparticles were investigated. X-ray diffraction (XRD) analysis indicated that P3HT had a higher level of crystallinity than PCDTBT. The bimetallic materials exhibited well defined sharp bands (due to the increase in crystallinity caused by the combination of two metals) and poly-orientation of the nanoparticles. The photoluminescence (PL) of the pristine polymers, the bimetallic nanoparticles and the nanocomposites were investigated on glass and on indium-tin oxide (ITO)-coated glass substrates. The PL spectral band observed at 422 and 691 nm for PCDTBT and P3HT, respectively, were due to the relaxation of the excitons and the formation of excimers associated with the polymers.

The combination of the bimetallic nanoparticles and the P3HT produced an enhancement in the PL intensity for a thin film. There was a complete quenching of the fluorescence from the acceptor with the donor in both glass and ITO coated substrates. This implied that there was charge dissociation that occurred on the donor in the presence of bimetallic nanoparticles. The electrochemical behaviour of P3HT, PCDTBT and stannum-based bimetallic nanoparticles was investigated using cyclic voltammetry (CV) and electrochemical impedance spectroscopy (EIS). The oxidation and reduction peaks were used to calculate the HOMO, LUMO and bandgap of the polymers and the bimetallic nanoparticles. PCDTBT had lower bandgap values as determined from both CV (0.62 eV) and UV-Vis (1.4 eV) measurements, than P3HT CV (1.68 eV) and UV-Vis (1.60 eV). The maximum phase angle values determined from EIS measurements were 82.1° and 81.4° for P3HT and PCDTBT, respectively. There was relatively fast electron transfer process in P3HT, since the maximum capacitive effect was observed at relatively higher phase angle compared to PCDTBT. Thus, P3HT was chosen as the preferable semiconductor for photovoltaic applications. The vibrational and electronic spectra of the nanoparticles were interrogated. The band gap of the stannum-based bimetallic nanoparticles was extrapolated from the Tauc plot. It was observed that SnTi had the highest bandgap value compared to SnCr and SnV. Small angle X-ray scattering spectroscopy (SAXS) was used to determine the particle size and shape of the nanoparticles. The SAXS measurements indicated particle sizes of 23 nm, 30 nm and 31 nm for SnCr, SnV and SnTi nanomaterials, respectively.

The scattering pattern for all the bimetallic nanoparticles were well-defined broad peaks, which confirmed that the nanoparticles were spherically shaped. P3HT derivatised with the bimetallic nanoparticles was used in the formation of photoelectrochemical cells, in which the bimetallic nanoparticles acted as acceptor materials. The current-voltage (I-V) characterization curves for the photoelectrochemical cells were obtained, and the photovoltaic parameters such as the fill factor (FF), open circuit voltage (V_{oc}), short circuit voltage (I_{sc}) and power conversion efficiency (η) were calculated from these curves. The photoelectrochemical cell used in the measurements (at a potential window of 0.01 to 0.1 V) contained 0.1 M $LiClO_4$ in acetonitrile as electrolyte. The addition of SnCr nanoparticles in the P3HT polymer film increased the intensity of the photocurrent and the incident solar power, suggesting that the inorganic semiconductor increased the number of charge carriers in the composite material. The incorporation of the bimetallic nanoparticles within the polymer improved the photoelectrochemical cell efficiency.



KEYWORDS

Photovoltaic cells

Photoelectrochemical cells

Power conversion efficiency.

Energy

Acceptor

Donor

Nanocomposite

Transition metals

Thin films

Bimetallic nanoparticles

Bandgap



LIST OF ABBREVIATIONS

A - Electrode surface area (cm^{-2})

Ag/AgCl - Silver/silver chloride reference electrode

BHJ – Bulk heterojunction cells

C₆₀ – Fullerene

CB – Chlorobenzene

CT - Charge transfer band

CV - Cyclic voltammetry

E_{oc} - Open Circuit Voltage

E_p - Peak potential

E_{pa} - Anodic peak potential

E_{pc} - Cathodic peak potential

F - Faradays constant

FF – Fill Factor

FeCl₂ - Iron (II) chloride

h - Hours

HOMO - Highest occupied molecular orbital

I_{max} - The current at which there is maximum power output



I_{pa} - Anodic peak current

I_{pc} - Cathodic peak current

I_{sc} - Short Circuit Current

ITO - Indium Tin Oxide

IR – Infrared

I-V – Current voltage

$LiClO_4$ - Lithium perchlorate

LUMO - Lowest unoccupied orbital

MNPs – Metal nanoparticles

n - Number of electrons

N_p – Nanoparticle

OPV – Organic photovoltaic

P3HT - Poly(3-hexylthiophene)

PCBM - [6,6]-phenyl-C61-butylric acid methyl ester

PCDTBT-Poly[N-9'-heptadecanyl-2,7-carbazole-alt-5,5-(4',7'-di-2-thienyl-2',1',3'-benzothiadiazole)]

PV – Photovoltaic

R - Gas constant

R_{ct} - Charge transfer resistance

aSi - Amorphous Silicon



UNIVERSITY of the
WESTERN CAPE

SnCl₂ - Tin (II) chloride

T - Temperature in Kelvin (K)

TGA - Thermal Gravimetric Analysis

TiO₂ - Titanium dioxide

UV-Vis - Ultraviolet-visible

V_{max} - The voltage at which there is maximum power output

XRD - X-ray Diffraction

Z – Impedance



UNIVERSITY *of the*
WESTERN CAPE

DECLARATION

I declare that "***Chromium and Titanium based Stannum Nanocomposites Materials as Electron Acceptors for Next Generation Bulk Heterojunction Photovoltaic Cells***" is my own work and has not been submitted before for any degree or examination in any other university, and that all the sources I have used or quoted have been indicated or acknowledged as complete references.



UNIVERSITY *of the*
WESTERN CAPE

Naledi Raleie

May 2018

Signed: 

DEDICATION

I dedicate this thesis to:

*My loving mother Mrs Magdeline Nkhumisang Raleie; for all the sacrifices,
understanding and encouragement throughout the years.*

*My late Father Mr Trevor Raleie; for always believing me and inspiring me to achieve
my goals.*

My brother Khotso Raleie; for having so much faith in me

My son Reaboka Tswharo Raleie; I love you dearly

&

My aunt Ruth Sebolecwe, for the support, love and valuable prayers

UNIVERSITY of the
WESTERN CAPE

ACKNOWLEDGEMENT

First and foremost, praises and thanks to God, Almighty, for His showers of blessings throughout my research work and strength to complete the research successfully.

To my Supervisor: Prof Emmanuel Iwuoha, thank you for giving me the opportunity to be part of SensorLab, and trusting me enough to carry out this project. For all the words of encouragement, believing in me and support throughout this project.

To my Family: I am truly indebted to my mother Magdeline Nkhumisang Roleie, my brother Khotso Oscar Roleie for considering my dreams as theirs and providing me the strength and enthusiasm to reach my goals. My late father Trevor Roleie, for his unrelenting support and love. Your confidence in my abilities gave me confidence to look beyond the horizon. My son Reaboka Tshwaro Roleie, thank you for understanding all the times I am not with you, your unconditional love was instrumental in helping me stay focused throughout this project.

To Physics Department. My sincere gratitude goes to Prof Adrense for assisting me with my research application. To Sfiso Khanyile and Siphesihle Magubane for the assistance in the lab, *I truly appreciate it.*

To SensorLab Researchers: Dr Natasha Ross, Dr Rachel Fanelwa Ajayi, Dr Chinwe Ikpo, Dr Nomaphelo Ntshongontshi, Dr Mawethu Bilibana, Dr Christopher Sunday, Dr Tesfaye Waryo, Dr Abd Baleg, Dr Milua Masikini, Dr Keagen Pokpas, Dr Francis Ntumba Muya, Dr Vivian John Suru, Dr Usisipho Feleni, Dr Lindsay Wilson, and Dr Unathi Sidwaba, thank you for the advices, assistance and encouragement through these past years.

To Chemistry Department: To Mrs Jackson, thank you so much for your support, kindness and mostly for your assistance in all academic and technical problems. To Prof P. Baker, thank you for the guidance and assistance throughout the years. Also, my appreciation goes to all the technical staff. **May God Bless you.**

To SensorLab Colleagues:, Sinazo Qakala, Candice Franke, Siyabulela Hamca, Siyabonga Mdluli, Emmanuel Ramoroka, Ezo Nxumani, Penelope Mathumba, Miranda Ndipingwi and Anne Lutgarde Djoumessi, thank you for all the advices and suggestions throughout this project. **Thanks for being such good colleagues.**

To Ntuthuko Wonderboy Hlongwa: I truly appreciate everything you have done for me, all the sleepless nights working on this project, motivation and unfailing support.

Special Thanks To: Nozipho Gumbi, Nomxolisi Dywili, Nuria Gonzalez, Samuel Mkhelane, Kim Raleie, Nolukholo Tyombo and Danielle Sass thank you for providing support and friendship that I needed. A good support system is important in surviving and staying sane during post graduate studies. **You guys are the best.**

To my Collaborators (Spain): Prof Alejandro Urena I am extremely grateful for the opportunity. To Prof Silvia Prolongo and Dr Rocio Moriche Tirado for assisting as per abilities and all the support.

To Sponsors: My sincere gratitude and appreciation goes to the National Research Foundation (NRF) for awarding me a Doctoral Scholarship. Also, I wish to gratefully acknowledge the European Union's Erasmus Mundus programme for granting me an AESOP+ (A European and South African Partnership on Heritage and Past Plus) Doctoral Scholarship for a research exchange visit to the Universidad Rey Juan Carlos, Madrid, Spain.

ACADEMIC OUTPUT

Publication

Dywili, N.R., Njomo, N., Ikpo, C.O., Yonkeu, A.L.D., John, S.V., Hlongwa, N.W., **Raleie, N.** and Iwuoha, E.I. Anilino-Functionalized Graphene Oxide with Pt Metal Nanoparticles for Application as Supercapacitor Electrode Material, Journal of Nano Research, 44 (2016) 79-89. (**Published**).

Raleie, N., Mathumba, P and Iwuoha, E.I. Electron flow in S-N doped Graphene/P3HT Schottky Junction solar cells, Journal of Material Chemistry A. (**Submitted**).

Raleie, N., Mthumba, P., Yonkeu, A.L.D., Dywili, N.R., and Iwuoha, E.I. Improving the Power Conversion Efficiency in P3HT/nanoparticles Based in Photoelectrochemical Cells, International Society of Electrochemistry. (**Submitted**).

Raleie, N., Dywili, N.R., Njomo, N., Ikpo, C.O., Yonkeu, A.L.D., John, S.V., Hlongwa, N.W., and Iwuoha, E.I. Effect of Active Layer Thickness on Current and Photon Response of PCDTBT-doped graphene Based Bulk Heterojunction Solar Cells, Journal of Material Chemistry A. (**Submitted**).

Conferences

Title: The effect of surface-functionalized graphene oxide on the morphology, mechanical and thermomechanical properties of PLA. **Poster presentation.** 2014 Postgraduate symposium. University of Johannesburg. 17 October 2014.

Authors: N. Raleie, J. Ramontja, S. Sinha Ray and X.Y. Mbianda.

Title: The effect of surface-functionalized graphene oxide on PLA: Towards orthopaedic applications. **Oral presentation.** 7th international symposium on macro and supramolecular architecture and materials. Johannesburg. 23-27 November 2014.

Authors: N. Raleie, J. Ramontja, S. Sinha Ray and X.Y. Mbianda.

Title: Improving the power conversion efficiency of P3HT/Stannum nanocomposites photoelectrochemical cell. **Poster presentation.** 4th International Symposium on Electrochemistry "Pure and Applied Electrochemistry". University of Johannesburg.

3-5 April 2018. **Authors:** N. Raleie and E.I. Iwuoha.

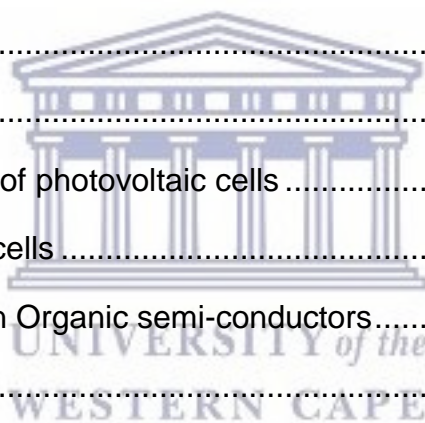
TABLE OF CONTENTS

Contents

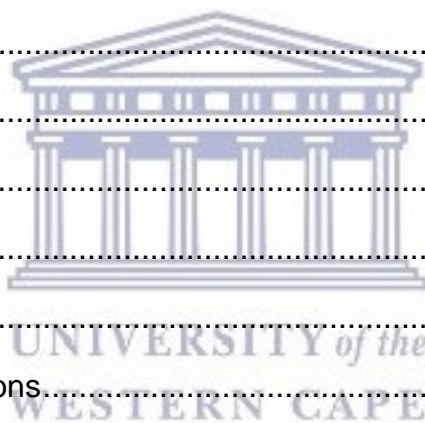
ABSTRACT	i
KEYWORDS	iv
LIST OF ABBREVIATIONS	v
DECLARATION.....	viii
DEDICATION	ix
ACKNOWLEDGEMENT	x
ACADEMIC OUTPUT.....	xii
Publication	xii
Conferences.....	xiii
TABLE OF CONTENTS	xiv
LIST OF FIGURES.....	xix
LIST OF TABLES	xxiii
CHAPTER ONE	1
INTRODUCTION	1
<i>Summary</i>	1
1. Background.....	2
1.1 Problem Statement	4
1.2 Rationale and Motivation.....	5
1.3 The aims and Objectives of the Research	5
1.4 Outline of the Thesis	7
Bibliography	9



CHAPTER TWO.....	11
Literature review	11
Summary	11
Transition Metals and Polymers in Electron acceptors/donors for Photovoltaic Cells	12
Abstract.....	12
2.1. Introduction	13
2.2. Energy.....	14
2.2.1 Challenges regarding energy	14
2.2.2 Clean energy technologies	15
2.2.3. Different types of energy	15
2.3 Photovoltaic cells	17
2.3.1 Introduction	17
2.3.2 Working principle of photovoltaic cells	18
2.4 Organic photovoltaic cells	19
2.4.1 Light absorption in Organic semi-conductors.....	20
2.4.2 Single-layer cells.....	20
2.4.3 Bilayer heterojunction cells	21
2.4.4 Hybrid Heterojunction cells	23
2.4.5 Bulk heterojunction cells	24
2.5 Photoelectrochemical cells.....	25
2.6 Bandgap.....	27
2.6.1 Effect of bandgap modulation in organic photovoltaic cells	27
2.6.2 The target for low band gap materials and design	29
2.6.3 Roles of transition metals in solar cells for low band gap	30
2.7 Properties of nanoparticles and polymers in PV cells	32
2.7.1 Electrical properties	33

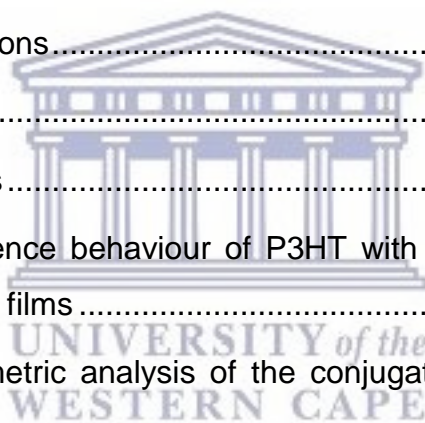


2.7.2 Optical properties.....	34
2.8 Photovoltaics performance parameters.....	35
2.8.1 The upper limit of V_{oc}	36
2.8.2 Short circuit current (I_{sc}).....	37
2.8.3 Fill Factor (FF).....	37
2.8.4 Power Conversion Efficiency (η).....	38
2.9 Conclusion.....	39
Bibliography.....	40
CHAPTER THREE.....	48
Summary.....	48
Analysis of PCDTBT and P3HT Thin Films as Potential Donor Materials for Photovoltaic Applications.....	49
Abstract.....	49
3.1 Introduction.....	50
3.2 Experimental.....	52
3.2.1 <i>Materials</i>	52
3.2.2 Sample preparations.....	52
3.2.3 Instrumentation.....	53
3.3 Results and Discussion.....	53
3.3.1 Chemical structures of the polymers.....	53
3.3.2 Optical analysis.....	54
3.3.3 Electrochemical analysis.....	59
3.4. Conclusion.....	68
Bibliography.....	69
CHAPTER FOUR.....	80
Summary.....	80
Novel Stannum-based Nanoparticles as Acceptor Material for.....	81



Organic Photovoltaic Devices	81
Abstract.....	81
4.1 Introduction	82
4.2 Experimental.....	84
4.2.1 Materials and Synthesis Procedure	84
4.2.2 Instrumentation	85
4.3 Results and Discussion.....	86
4.3.1 Structural properties of nanoparticles	86
4.3.2 Morphological properties of nanoparticles	90
4.3.3 Optical Properties	95
4.3.4 Structural analysis	99
4.3.5 Electrochemistry analysis	101
4.4 Conclusion	108
Bibilography	109
CHAPTER FIVE	112
Summary.....	112
Investigation of Mechanical Properties by Nanoindentation for P3HT Thin Films Prepared by Sol-Gel Process.....	113
Abstract.....	113
5.1 Introduction	114
5.2 Experimental.....	116
5.2.1 Materials and sample preparation	116
5.2.2 Instrumentation	117
5.3 Results and discussion	117
5.3.1 Structural properties	117
5.3.2 Morphological properties	120
5.3.3 Optical Profilometry	122

5.3.4	Mechanical properties.....	123
5.4	Conclusion	128
	Bibliography	128
CHAPTER SIX	130
Summary.....	130
Effect of Bimetallic Nanoparticle Properties on the Performance of Photoelectrochemical Cell.....	131
Abstract.....	131
6.1	Introduction	132
6.1.1	Working principle of photoelectrochemical cell	133
6.2	Experimental	135
6.2.1	Sample preparations.....	135
6.2.2	Instrumentation	135
6.2.3	Characterizations	136
6.2.3.1	Photoluminescence behaviour of P3HT with different concentrations of SnCr nanoparticles thin films	136
6.2.3.2	Thermal gravimetric analysis of the conjugated polymer and bimetallic nanoparticles	138
6.2.3.3	Atomic force microscopic analysis of the conjugated polymer and bimetallic nanoparticles	140
6.2.3.4	Photoelectrochemical measurements for photovoltaic application.....	142
Bibliography	148
CHAPTER SEVEN	152
Conclusive Summary	152



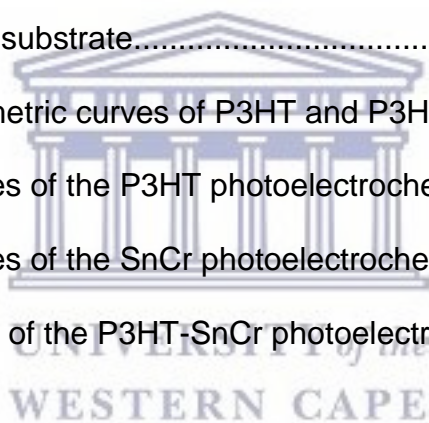
LIST OF FIGURES

Figure 1: Global energy consumption by International Energy Agency 2013	16
Figure 2: The scheme of cross section of a PSC and working principle for a polymer-fullerene BHJ photovoltaic cell	19
Figure 3: Schematic representation of the device architecture in photovoltaic cells	25
Figure 4: Energetics of an n-type semiconductor-electrolyte solution interface before contact and at equilibrium	26
Figure 5: Energetics of a p-type semiconductor-electrolyte solution interface, before contact and at equilibrium	26
Figure 6: Explanation of bandgap	28
Figure 7: Sun irradiance (red) and number of photons (black) as a function of wavelengths	30
Figure 8: Device structure consists of an active layer of P3HT: PCBM: ZnS NP sandwiched between Ca/Al electrode and conducting electrode of PEDOT: PSS on ITO glass substrate	31
Figure 9: Diagram illustrating the evolution of electronic states from an atom to a metal	33
Figure 10: Typical forward bias of I-V characteristic of a PV cell	38
Figure 11: Fourier transform infrared (FTIR) absorption of P3HT and PCDTBT.	54
Figure 12: UV-vis absorption spectra of P3HT thin film.	56
Figure 13: UV-vis absorption spectra of PCDTBT thin film.	57

Figure 14: Tauc plot for P3HT and PCDTBT.	57
Figure 15: Photoluminescence spectra of (a) PCDTBT and (b) P3HT thin films. ...	59
Figure 16: Cyclic voltammogram behaviour of P3HT and bare Pt electrode in 0.1M LiClO ₄ at 100 mV/s.....	61
Figure 17: Cyclic voltammogram of (a) P3HT and (b) PCDTBT.	62
Figure 18: The Bode plots of Bare Pt electrode analysed using 0.1 M LiClO ₄	64
Figure 19: Bode plot that describes impedance behaviour of phase angle for P3HT and PCDTBT analysed using 0.1 M LiClO ₄	65
Figure 20: Bode plot that describes impedance behaviour of absolute value for P3HT and PCDTBT analysed using 0.1 M LiClO ₄	66
Figure 21: Simplified Randles equivalent circuit for P3HT and PCDTBT.....	66
Figure 22: Nquist plot of P3HT and PCDTBT in 0.1 M LiClO ₄ at 80 mV applied potential.....	67
Figure 23: ATR-FTIR interferograms ranging from 500 - 4000 cm ⁻¹ for (a) PVP capped Sn nanoparticles and (b) SnCr, SnV and SnTi.	87
Figure 24: XRD pattern of Sn nanoparticles.	89
Figure 25: XRD pattern of SnCr, SnTi and SnV nanoparticles.	89
Figure 26: HR-TEM images of (a) Sn nanoparticles, (b) SnCr, (c) SnV and (d) SnTi bimetallic nanoparticles.	91
Figure 27: Selected area electron diffraction pattern (SAED) of (a) Sn nanoparticles, (b) SnCr, (c) SnV and (d) SnTi bimetallic nanoparticles.	92
Figure 28: Energy dispersive X-ray spectrum of nanoparticles (a) Sn nanoparticles, (b) SnCr, (c) SnV and (d) SnTi bimetallic nanoparticles.	94
Figure 29: (a) UV-vis spectra and (b) Tauc plots for Sn-based bimetallic nanoparticles.....	96

Figure 30: (a) The excitation and emission spectra of SnCr nanoparticles and (b) Photoluminescence spectra of Sn-based nanoparticles.....	98
Figure 31: SAXS measurements of (a) particle size, (b) volume size and (c) intensity distributions for Sn-based nanoparticles.	101
Figure 32: Cyclic voltammograms for (a) Sn nanoparticles and (b) Pt bare electrode with SnTi nanoparticles in 0.1 M LiClO ₄	103
Figure 33: Cyclic voltammograms for (a) SnCr nanoparticles, (b) SnTi nanoparticles and (c) SnV nanoparticles in 0.1 M LiClO ₄ at different scan rate.....	104
Figure 34: The Bode plot gives direct information on the (a) frequency and (b) phase angle for the bimetallic nanoparticles SnCr, SnV and SnTi.....	106
Figure 35: Simplified Randles equivalent circuit for the bimetallic nanoparticles. ...	107
Figure 36: Nyquist plot the bimetallic nanoparticles SnCr, SnV and SnTi.	107
Figure 37: XRD patterns of (a) P3HT thin film and (b) TiO ₂ nanoparticles.....	119
Figure 38: XRD patterns for P3HT thin films with 1 wt%, 5 wt% and 10 wt% TiO ₂ nanoparticles content.	119
Figure 39: (a) TEM image of P3HT thin film with 10 wt% content of the TiO ₂ nanoparticles and (b) SAED image of P3HT thin film with 10 wt% content of TiO ₂ nanoparticles.....	120
Figure 40: AFM topography of (a) TiO ₂ and (b) P3HT:TiO ₂ (10 wt%) of films spin-coated from toluene solvent.	121
Figure 41: Thickness image of the 10 wt% content P3HT film obtained from the optical profilometry.	123
Figure 42: A load-displacement curve for the P3HT thin films at (a) 1 wt%, (b) 5 wt% and (c) 10 wt% content of TiO ₂ nanoparticles.	126

Figure 43: The Hardness-Young's modulus curves for the P3HT thin films at 1, 5 and 10 wt% content of the TiO ₂ nanoparticle.....	127
Figure 44: Plot of experimental data of hardness versus the particle size. The dashed line is a fit to the data obtained from the Hall-Petch equation.....	127
Figure 45: Different types of photoelectrochemical cells with the working electrode (WE) made of semiconductor (n- or p-type) and the counter electrode (CE)	134
Figure 46: Working principle of photoelectrochemical cells	134
Figure 47: PL spectra of P3HT: SnCr for different concentrations at room temperature on glass substrate.....	137
Figure 48: PL spectra of P3HT: SnCr for different concentrations at room temperature on ITO coated substrate.....	138
Figure 49: Thermal gravimetric curves of P3HT and P3HT-SnCr.....	139
Figure 50: The I-V curves of the P3HT photoelectrochemical cell.....	143
Figure 51: The I-V curves of the SnCr photoelectrochemical cell.....	144
Figure 52: The I-V Curves of the P3HT-SnCr photoelectrochemical cell.....	146



LIST OF TABLES

Table 1: Calculated electrochemical and optical bandgaps of the polymers.....	63
Table 2: Calculated electrochemical impedance parameters from the Nquist plot. .	67
Table 3: Ultraviolet and Visible light regions for nanomaterials. Ultraviolet and Visible light regions for nanomaterials.	97
Table 4: Calculated electrochemical and absorption band gaps for bimetallic nanoparticles.....	105
Table 5: Summary of the impedance spectroscopy data analysis for Bimetallic nanoparticles.....	108
Table 6: Root mean square roughness values for the compounds.....	122
Table 7: Hardness, Young's modulus and particle size of the P3HT thin films.	126
Table 8: AFM topographical images of (50 x 50 μm^2) of P3HT, SnCr and P3HT-SnCr spin coated from chlorobenzene	141
Table 9: Comparison of HOMO and LUMO between P3HT and SnCr nanoparticles.	143
Table 10: The photovoltaic response of the conjugated polymer (P3HT) in different scan rates for photoelectrochemical cell.	144
Table 11: The photovoltaic response of the acceptor (SnCr) in different scan rates for photoelectrochemical cell.....	145
Table 12: The photovoltaic response of the active layer (P3HT-SnCr) in different concentrations for photoelectrochemical cell.....	147



UNIVERSITY *of the*
WESTERN CAPE

CHAPTER ONE

INTRODUCTION

Summary

As both population and energy use per capital increase, modern society is approaching physical limits to its continued fossil fuel consumption. The immediate limits are set by the planet's ability to adapt to a changing atmospheric chemical composition, not the availability of resources. In order for a future society to be sustainable while operating at or above our current standard of living, a shift away from carbon based energy sources must occur. An overview of the current state of active solar (photovoltaic) energy technology is provided here to outline a partial solution for the environmental problems caused by accelerating global energy expenditure. The technical, social, and economic benefits as well as limitations of photovoltaic technologies to provide electricity in both off-grid and on-grid applications is critically analysed in the context of this shift in energy sources. It is shown that photovoltaic electrical production is a technologically feasible, economically viable, environmentally benign, sustainable, and socially equitable solution to society's future energy requirements. This chapter will exhibit a concise background to the study in which will emphasize, amongst other items the significance evolution from non-renewable to renewable energy source (photovoltaic cells). The prominence is more proclaimed on the application of transition metals (bimetallic nanoparticles) as electron acceptors to improve the efficiency in the bulk heterojunction photovoltaic cells. The problem and its significance, scope, the research's aim, objectives and the thesis outline are further discussed.

1. Background

Energy is an essential commodity and is closely entwined with climate change and development. Energy is required for primary human needs such as: cooking, heating, lighting and other household based activities. It is also needed to support and amplify economic processes: agriculture, electricity production, industries, services and transport. It has been commonly suggested that alleviating energy poverty will be essential to fulfil the Millennium Development Goals (Vatansever *et al*.; 2012). Advances in science and technology have provided us with several alternative means of producing energy on a sustainable level, such as wind, geothermal, biomass, and solar. Solar energy constitutes a class of promising candidates also known as photovoltaic (PV). It is clean and infinitely obtainable and this technology utilizes the sun to produce heat, light and electricity. The phrase “photo” means light and “voltaic” electricity. Fossil energy resources are restricted and their use is linked to a number of pessimistic environmental effects, thus energy has grown to be a prime geo-political and socio-economic issue (Yu, *et al*; 2014). It has become a crucial necessity to invest in renewable energy resources, which would dominate the future abundantly without degrading the environment through greenhouse gas discharge (Timmons *et al*.; 2009). The energy potential of the sun is huge, but regardless of the unlimited solar energy resources, harvesting is a challenge predominately because of the restricted efficiency of the array cells. PV effect was first discovered by a French Scientist Edmond Becquerel in 1839 but wasn't all-inclusive until the development of quantum theory of light and solid state physics in the 1900s by Albert Einstein, who gave a detailed interpretation of the PV effect in 1905 (Jardas, 2012).

When sunlight strikes PV cells, the photons of the absorbed sunlight remove the electrons from the atoms of the cell, these free electrons then move through the cell, creating and filling in holes in the cell. The predominant component of a photovoltaic device is a semi-conductor material, since it is basically the one that regulate how much energy is taken up by the photovoltaic device. This limitation can be overcome using a system that has an acceptor and a donor. Hence in this work we investigate stannum-based bimetallic nanoparticles as an acceptor and a polymer as a donor (Jeon *et al.*, 2010). Large-scale application of PV solar energy will also contribute to the diversification of energy sources resulting in more equal distribution of energy sources in the world (Timmons *et al.*, 2009). It has been reported that PV solar energy contribution is only a tiny part of the total energy production. At present, the total energy production is estimated to be 1.6×10^{10} kW compared to 1.0×10^6 kWp that can be delivered by all solar cells installed worldwide. By Wp (Watt peak) we understand a unit of power that is delivered by a solar cell under a standard illumination kWp in 2030. This demonstrates that there must be a steady growth in solar cells production so that PV solar energy becomes a significant energy source (Heremans *et al.*, 2009). When PV starts to make a substantial contribution to the energy production and consequently to the decrease in the gas emissions depends on the growth rate of the PV solar energy production.

1.1 Problem Statement

There is a growing need for energy in the world and since the traditional energy sources based on the fossil fuels are limited and will be exhausted in future, PV solar energy is considered a promising energy source candidate. The most extensively used semi-conductor is the crystalline silicon. This is due to the reported high efficiency (24%) in converting the light energy into electrical energy; they are also known to be very stable. Amorphous silicon (a-Si) has also been considered for photovoltaic devices and it has been reported to have efficiency of 13% but with time, that went down to 5% (Brongersma *et al.*, 2006). This has been ascribed to the low stability of the a-Si caused by the breaking down of the hydride bonds. There has also been a development of the latter that challenged the low efficiencies which is known as cadmium and gallium selenide, though cadmium is known to be a very toxic element. The development of the solar energy is hindered by the cost of the materials since the most commercially used materials like crystalline silicon (c-Si) tend to be very expensive (Zhong *et al.*, 2016). Thus organic materials have been very attractive in photovoltaic device research because they are known for being low in costs (Ahmed *et al.*, 2011). Inherently conducting polymers such as polyaniline; polythiophene, etc. (Woo *et al.*, 2010) have been potentially studied as good conducting materials for photovoltaic devices. A problem encountered with organic materials based photovoltaic devices is the recombination of the excited molecules upon absorption which limits the amount of energy that can be generated.

1.2 Rationale and Motivation

Organic Photovoltaics (OPVs) are emerging as promising development of low cost solar energy conversion technologies. Among all the OPV device architectures explored to date, going from single layer to bilayer solar cells and including the Schotcky barrier solar cells, the bulk heterojunction (BHJ) cell, with an active layer consisting of a blend of electron donor (polymer) and an acceptor material provides the most efficient excitonic solar cells. Once the photons contained in the solar light are absorbed in the BHJ active layer, the strongly bound excitons, instead of free electron-hole pairs as produced in organic materials, are generated; an efficient electron donor-acceptor interface with suitable HOMO/LUMO energy level offsets is therefore of first importance for efficient charge photogeneration (Alsalme *et al.*, 2014). Among all the classes of acceptor materials which have been studied, fullerene-based acceptor materials have demonstrated excellent electron-accepting and electron-transporting properties and still dominate in OPV technologies. In this work, new acceptor material will be fabricated from nanoparticles, as nanoparticles are known for their small dimension structures to enhance properties of polymers (Shafiee *et al.*, 2011 and Yang *et al.*, 2015).

1.3 The aims and Objectives of the Research

This work included using different stannum-based bimetallic nanoparticles, titanium dioxide (TiO₂) nanoparticles (acceptors) and two types of polymers (donors) namely P3HT and PCDTBT. These will be compared in electrical, mechanical and optical properties for better efficiency donor in photoelectrochemical cell.

Fabrication of an organic bulk heterojunction photovoltaic cells will be based on a blend of a highly semiconducting material P3HT or PCDTBT with stannum-based bimetallic nanoparticles as the acceptor material and the photovoltaic properties of fabricated cells will be studied. This study will focus mainly on preparing and characterising the electron acceptor materials based on different stannum-based nanoparticles namely chromium, titanium and vanadium. The bimetallic nanoparticles will be blended onto the electron donating materials P3HT and PCDTBT fabricating nanocomposites. Also, the study of applicability of these nanocomposites towards the conversion of solar energy into electrical current will be studied. To achieve this, the following objectives must be met:

1.3.1 *Synthesis of poly(3-hexylthiophene) as a potential donor in photovoltaic application*

- Determination of optical and structural properties of the polymeric material using Ultraviolet-visible (UV-Vis) spectroscopy, photoluminescence (PL) spectroscopy and Fourier transformed infra-red spectroscopy (ATR-FTIR).
- Determination of electrochemical properties of the polymeric material using cyclic voltammetry (CV) and electrochemical impedance spectroscopy (EIS)

1.3.2 *Synthesis of Sn, SnCr, SnTi and SnV nanoparticles in the presence of PVP as a capping agent*

- Determination of optical and structural properties of the polymeric material using UV-Vis, PL, X-ray diffraction (XRD), Raman spectroscopy and ATR-FTIR.
- Determination of electrochemical properties of the polymeric material using CV and EIS.

1.3.3 Fabrication of the bulk heterojunction photovoltaic device

- Synthesis of the composites in different concentrations of the nanoparticles
- Determination of thermal, structural and morphological properties using thermal gravimetric analysis (TGA), atomic force microscopic (AFM) and PL.
- Development and testing of the bulk heterojunction photovoltaic cell.
- Determination of the fill factor, power conversion efficiency, short open circuit and voltage open circuit using BioLogic VMP300.

1.4 Outline of the Thesis

Outline of the chapters follows:

Chapter 1; presents a brief background information of the main aspects of the study, that is: photovoltaic cells with more emphasis on the use of bimetallic nanoparticles as electron acceptor materials. In addition the problem and its significance, the research's aim and objectives are also discussed.

Chapter 2; entails an extensive literature review of the concepts of the study which were briefly introduced in the previous chapter. The concepts, discussed amongst others, include: the working principles and classification of different types of photovoltaics. This is followed by the advantages of the organic materials in the photovoltaic devices. Nanotechnology and applications of nanomaterials are further described with the background of characterisation techniques applied in this study finalising the scope of discussion for this chapter.

Chapter 3; describes the synthesis, characterisation and application of P3HT and PCDTBT covering mostly the electrochemical behaviour and optical properties. Several analytical techniques such as FTIR, CV, UV-Vis and PL were used to characterize these polymers. The characterization results were sufficiently analysed and discussed.

Chapter 4; specifies the synthesis and characterizations of Stannum-based bimetallic nanoparticles. The developed electrochemical, optical, and its chemical composition were characterized using CV, UV-VIS, PL, FTIR and HR-TEM. The optical and electronic properties of these nanoparticles are important in obtaining the HOMO, LUMO and bandgap.

Chapter 5; outlines the synthesis of TiO₂ and the blend between the nanoparticles and poly(3-hexylthiophene) with different content concentrations of the nanoparticles. This chapter focuses mainly in the mechanical properties nanocomposites towards photovoltaic cells application. These properties of the nanoparticles and nanocomposites are revealed by XRD, HR-TEM, AFM, and nanoindentater.

Chapter 6; illustrates the fabrication of the photovoltaic device by photoelectrochemical route for P3HT-SnCr. The important properties in photovoltaics such as thermal and optical were characterized by TGA and PL. The important parameters in photovoltaics application are obtained from the I-V curves obtained from photoelectrochemical characterization.

Chapter 7; Gives a summary of the work done as well as recommendations for future work.

Bibliography

Ahmed, E., Ren, G., Kim, F. S., Hollenbeck, E. C. and Jenekhe, S. A. (2011) 'Design of new electron acceptor materials for organic photovoltaics: Synthesis, electron transport, photophysics, and photovoltaic properties of oligothiophene-functionalized naphthalene diimides', *Chemistry of Materials*, 23, pp. 4563–4577.

Alsalmeh, A. M., Alghamdi, A. A. B., Alhamdani, A. A. G. Q. and Iraqi, A. (2014) 'Synthesis and properties of alternating vinylene-benzothiadiazole-based copolymers with carbazole and fluorene derivatives for photovoltaic applications', *International Journal of Electrochemical Science*, 9, pp. 1920–1941.

Brongersma, M. L., Peumans, P., Catrysse, P. and Bernard, E. (2006) 'Nanostructured Metal-Organic Composite Solar Cells', *Scanning Electron Microscopy*, 1, pp. 1–7.

Heremans, P., Cheyns, D. and Rand, B. P. (2009) 'Strategies for increasing the efficiency of heterojunction organic solar cells: Material selection and device architecture', *Accounts of chemical research*, 42, pp. 1740–1747.

Jardas, D. (2012) 'Photovoltaic systems'.

Jeon, I. and Baek, J. (2010) 'Nanocomposites Derived from Polymers and Inorganic Nanoparticles', pp. 3654–3674.

Shafiee, A., Salleh, M. M. and Yahaya, M. (2011) 'Determination of HOMO and LUMO of [6,6]-phenyl C61-butyric acid 3-ethylthiophene ester and poly (3-octyl-thiophene-2, 5-diyl) through voltametry characterization', *Sains Malaysiana*, 40, pp. 173–176.

Timmons, D., Harris, J. M. and Roach, B. (2009) 'The Economics of Renewable Energy', *Renewable Energy*, 6, pp. 1341–1356.

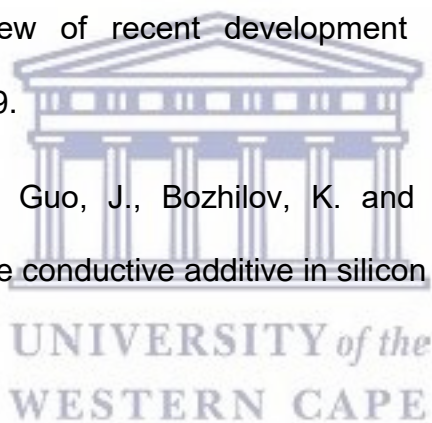
Vatansever, D., Siores, E. and Shah, T. (2012) 'Alternative Resources for Renewable Energy : Piezoelectric and Photovoltaic Smart Structures', 14, pp. 3.

Woo, C. H., Beaujuge, P. M., Holcombe, T. W., Lee, O. P., and Fréchet, J. M. J. (2010) 'Incorporation of Furan in Low Band Gap Polymers for Efficient Solar Cells', *Journal of the American Chemical Society*, 132, pp. 15547–15549.

Yang, J., Clark, N., Long, M., Xiong, J., Jones, D. J., Yang, B. and Zhou, C. (2015) 'Solution stability of active materials for organic photovoltaics', *Solar Energy*. Elsevier Ltd, 113, pp. 181–188.

Yu, J., Zheng, Y. and Huang, J. (2014) 'Towards high performance organic photovoltaic cells: A review of recent development in organic photovoltaics', *Polymers*, 6, pp. 2473–2509.

Zhong, L., Beaudette, C., Guo, J., Bozhilov, K. and Mangolini, L. (2016) 'Tin nanoparticles as an effective conductive additive in silicon anodes', *Nature*. pp. 1–8.



CHAPTER TWO

Literature review

Summary

New power generation and storage equipment, ranging from batteries to power plants, must be continually developed and manufactured to meet the ever-increasing demand for electrical power around the globe for a wide variety of applications. Photovoltaic cells have the ability to meet some of these power demands by directly converting sunlight into electricity and can potentially generate power anywhere there is light. Alexandre-Edmond Becquerel first observed the photovoltaic effect in an electrolyte solution in 1839, and the modern era of solid-state photovoltaic cells was ushered in with developments at Bell Labs in 1954. Even with over 50 years of research, photovoltaic cells accounted for only about 1,636 GWh of the 18,307 TWh of electricity produced globally in 2005 according to the International Energy Agency. Solar energy has great potential because the surface of the earth receives, on average, about 1.2×10^{17} W of solar power. Polymer photovoltaic cells have attracted considerable attention in the past few years owing to their potential of providing environmentally safe, flexible, lightweight, inexpensive, efficient photovoltaic cells. This chapter presents an immense overview of concepts which were briefly introduced in the previous chapter. Amongst others these concepts include: the working principles and classification of different types of photovoltaic cells. This is followed by the important properties and parameters involved in photovoltaic cells. Nanotechnology and applications of nanomaterials are further described with the background of challenges regarding energy are discussed in this chapter.

Transition Metals and Polymers in Electron acceptors/donors for Photovoltaic Cells

Abstract

At present, most of the energy the population of the world consumes originates from fossil resources. Communities are aware of the major impact of the uses of fossil fuel on the environment as an energy source, and the failing support. As such, there is an urgent need for societies around the globe to convert from using brown energy to green energy in order to sustain the resources and enhance the quality of life. Unlike traditional and alternative energies sources such as wind, hydropower and biomass, solar energy is the most abundant energy which is less costly to harvest. The power of the sunlight that reaches the earth's surface amounts to 120,000 TW and vastly exceeds the world's energy demand (~15 TW). The AM1.5 spectrum of the energy flux of the sunlight recorded on the ground passed through a mass of air that is 1.5 times as large as under normal incidence. This spectrum is referred to as the solar spectrum and it contains light with photon energies varying roughly from 4 down to 0.5 eV, with a broad peak around 2 eV. The total power of the AM1.5 spectrum is 1000 Wm⁻². The organic photovoltaic cell (OPVC) is very promising owing to their potential of, providing environmentally safe, flexible, lightweight and inexpensive photovoltaic cell. There are however, main unsolved problems of low power conversion efficiency. Up to now about 6% power conversion efficiencies on the device level have been realized. The efficiency of the OPVC is limited by several factors.

2.1. Introduction

Harvesting energy directly from sunlight using photovoltaic technology is regarded as being one of the key roles in addressing the growth of global energy needs using renewable sources. Tang *et al.* (2012) implemented a bilayer heterojunction configuration containing of a p-type layer for hole transport and an n-type layer for electron transport to improve the photocurrent of the solar cell device (Ye *et al.*, 2012). The general working principle in these types of solar cells involves firstly the photoexcitation of the donor material by the absorption of light energy to generate excitons. The Coulomb-correlated exciton and electron hole pair diffuses to the donor-acceptor (D-A) interface where exciton dissociation occurs via an electron-transfer process (Karzazi *et al.*, 2014). Their fully separated free charge carrier transport to the respective electrodes in the opposite direction with the aid of the internal electric field, which then generates the photocurrent and photovoltage. Since their limited lifetimes only allow excitons to diffuse a short distance, usually between 15 and 14 nm; donor excitons that are created far away from the heterojunction interface decay to the ground state without any chance to reach the acceptor (Yin *et al.*, 2017). Leading to the loss of absorbed photons and quantum efficiency (Rodríguez-Martínez *et al.*, 2017). Consequently, the performance of bilayer heterojunction devices is greatly limited by the small area of charge-generating interface between the donor and acceptor (Ye *et al.*, 2012). Overcoming this difficulty, the concept of a bulk heterojunction (BHJ) was then introduced by the pioneering work of Yu *et al.* (2014) where it was explained that by blending the donor and acceptor materials together a large interfacial area can be achieved through controlling the phase separation between the two components in bulk (Guo *et al.*, 2012).

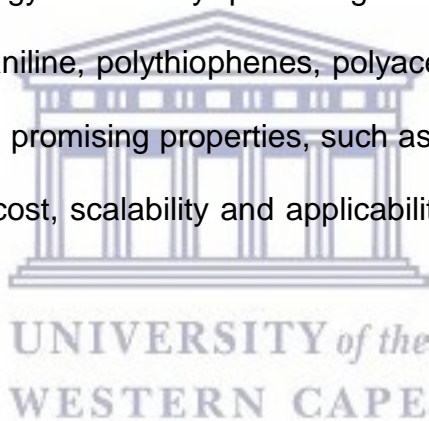
2.2. Energy

2.2.1 Challenges regarding energy

The necessitate for energy has tended to exceed the supply and dreadfully, it is expected to further increase by as much as an order of magnitude by 2050, at the same time primary-energy demands are expected to escalate by 1.5 to 3 times (Vatansever *et al.*, 2012). This increasingly demand for developing countries such as South Africa is met through incinerating fossil fuels emanating greenhouse gases and pollutants. Coincidentally, this development will eventually lead to energy-related environmental problems such as acid precipitation and global climate change amongst others in future (Joffe, 2012). Transformation from non-renewable energy to renewable energy is inevitable to prevent CO₂ emission which could increase and reach more than 50% of the world's CO₂ emission. South Africa is presently struggling to deal with an energy crisis which was monitored by Eskom, resulting in cutting the power supplies to the estimation of 90 days in 2016 as a strategy to ease the strained grid. The South African energy department has taken into consideration the evaluation of power-generation mixes after the 2016 crisis, incorporating renewable resources to restrain the energy shortages. Furthermore, the energy department not only is coming up with power plans, scientists too are finding means to innovate organic materials and photovoltaic cells technologies to achieve succeeding sustainable energy systems. Not only will these technologies improve energy supply security but also reduce air pollutants whilst alleviating climate change (Vatansever *et al.*, 2012).

2.2.2 Clean energy technologies

Energy is crucial to all countries because it is a predominant human's need. The world at large needs energy for various daily operations such as cooking, transportation, warming buildings, etc. In recent years, the department of energy has collaborated with the Department of Science and Technology (DST) expending in clean energy technologies by encouraging, supporting research and developing clean and sustainable energy technologies to improve the economy and to minimize the dependence in foreign oil and combustion of coal. This serves as an approach to solve the energy challenges facing the country. Currently, organic materials towards photovoltaic cells technology is a very promising clean energy plan. Organic conducting polymers (polyaniline, polythiophenes, polyacetylene, etc.) with a variety of chemical structures have promising properties, such as easy processing, possible recyclability, relatively low cost, scalability and applicability as sustainable materials (Alsalmé *et al.*, 2014).



2.2.3. Different types of energy

Recently our daily lifestyle depends utterly on electrical energy this is evident from the effect that a 24 – 48 h load shedding has on our essential daily activities, and without energy life becomes exceedingly challenging. Power-cuts tend to make daily activities very difficult and sometimes impossible. In 2012, Joffe reported that keeping the lights on is tenably the most rapid and pressing challenge for South Africa's electricity supply industry since 2008 and will be for the next few years unless the new power stations can deliver the capacity needed to relieve the shortage of the supply (Joffe, 2012).

To date there has been a need to make a transition to a more diverse source of supply. There are different types of power plants which are currently utilized around the world for supplying energy. These power plants include solar, thermal, nuclear, hydroelectric, wind, and geo-thermal (**Figure 1**). Hydroelectric, thermal and nuclear power plants attain energy from non-renewable fuels, whereas wind, solar and geo-thermal power plants are derived from renewable sources such as the wind, the sun and hot geysers, respectively. This makes renewable energy sources and fuels like solar, wind, biofuels and biomass to be in high demand. These renewable energies originate from natural resources and are naturally replenished (Timmons *et al.*, 2009 and Celik Bedeloglu *et al.*, 2010).

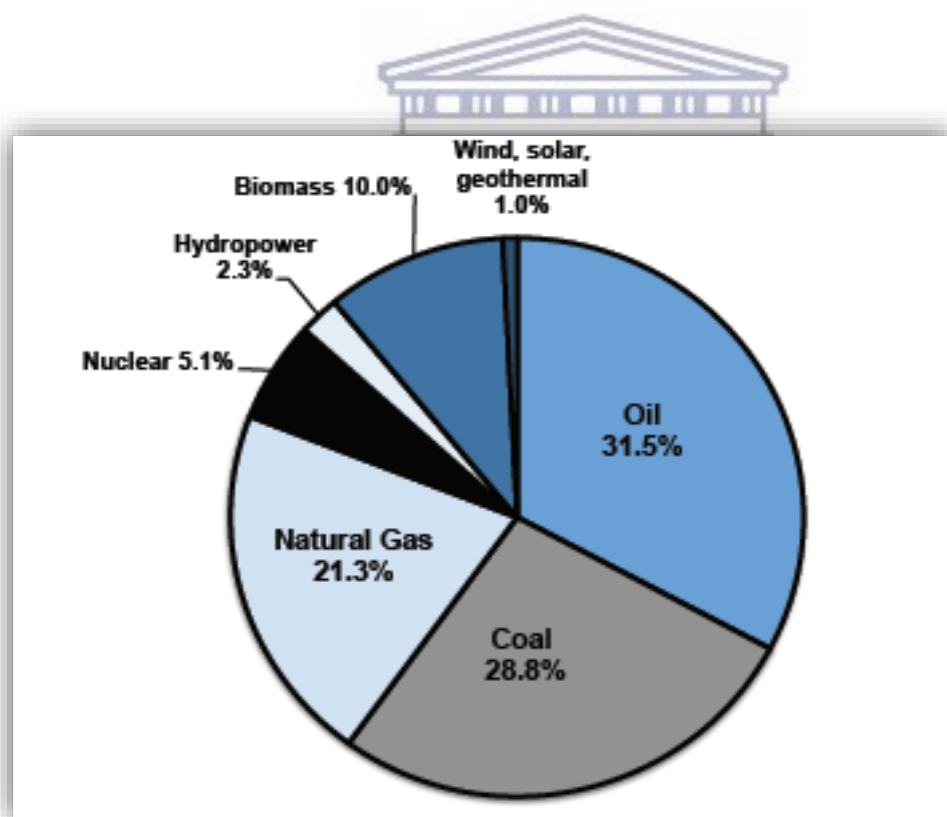


Figure 1: Global energy consumption by International Energy Agency 2013 (Luber *et al.*, 2013).

2.3 Photovoltaic cells

2.3.1 Introduction

Solar energy is radiant light and heat from the sun that utilizes a range of ever-evolving technologies such as: solar heating, photovoltaics and solar thermal energy. Solar powered electrical generation depends strongly on photovoltaics and heat engines. Solar photovoltaic transforms light into electricity utilizing semi-conducting materials. Photovoltaic cells known as solar cells, are solid state electrical devices that converts the energy of light directly into electricity. The cell's assemblies are often referred to as solar modules or panels. These solar modules are normally deployed as an array of single modules on rooftop, building facades or in large-scaled ground-based arrays (Mora *et al.*, 2017). A module is embodied by many jointly connected solar cells. In the past it was reported that crystalline silicon modules consisted of 60 - 72 cells. Photovoltaic system supplies direct current which must be converted to alternating current through an inverter for the output from the system to be used in the grid (Li, 2011). Conventionally, a photovoltaic cell efficiency is about 15%, meaning that it can convert about 1/6 of solar energy into electricity. Photovoltaic cell has been reported to have a lifetime of more than thirty years and is one of the most reliable semiconductor product. Photovoltaic systems do not require substantial maintenance and at the end of its life cycle, photovoltaic modules can almost be completely recycled (Doeleman, 2012 and Scharber *et al.*, 2013).

These modules bring electricity to rural areas where there is no electric power grid, and thus increase the life value of these areas. To date, the industry of photovoltaic modules and related renewable energies are growing at a rate of 40% per year, therefore, it has been one of the fastest growing industry in the last decade. In the year 2010, the capacity of installed power has reached an enormous number of 17.5 GW.

2.3.2 Working principle of photovoltaic cells

Conversion of light energy in electrical energy is based on a phenomenon called photovoltaic effect. When semiconductor materials are exposed to light, some of the photons of light ray are absorbed by the semiconductor crystal which causes a significant number of free electrons in the crystal. This is the basic reason for producing electricity due to photovoltaic effect. Photovoltaic cell is the basic unit of the system where the photovoltaic effect is utilised to produce electricity from light energy. The basic working principle of a BHJ photovoltaic cell is often described in five steps

(Figure 2):

- Light absorption and exciton generation in the active layer **(step 1)**
- Diffusion of the photogenerated excitons to the donor/acceptor interfaces **(step 2)**
- Charge transfer to form an excited charge transfer complex at the donor/acceptor interfaces **(step 3)**
- Separation of charge transfer complex, and generation of free charge carriers **(step 4)**
- Charge carrier transport to electrodes and collection **(step 5)**

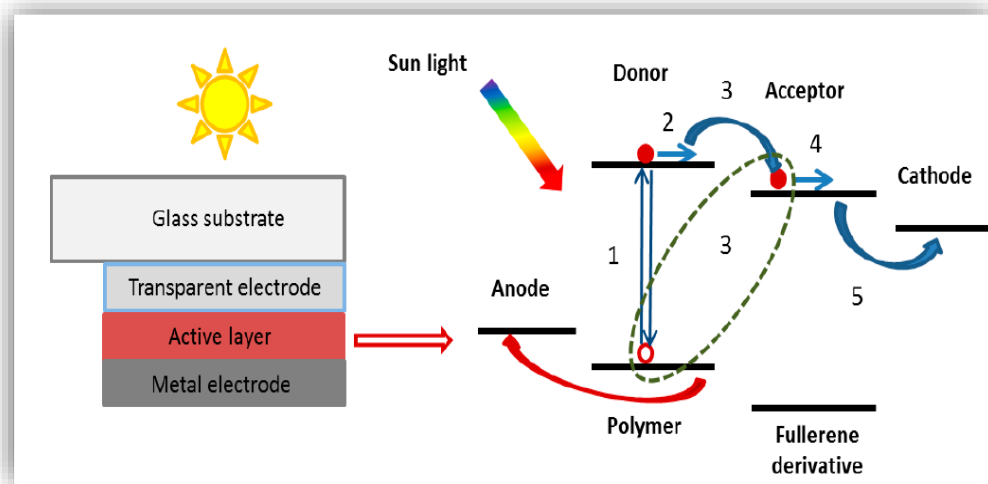


Figure 2: The scheme of cross section of a PSC and working principle for a polymer-fullerene BHJ photovoltaic cell (Nelson, 2011).

2.4 Organic photovoltaic cells

The field of OPVs has progressed quite significantly in the last decade, not only for their academic interest but also their potential as an affordable energy technology with high throughput roll-to-roll solution processing driving down costs to the point of competitiveness with current technologies. OPVs generally consist of a donor and acceptor, which are similar in concept to the two types of doped silicon (Mohammad *et al.*, 2014). Unlike silicon solar cells, the donor and acceptor in an OPV are completely different materials. Each material has a characteristic HOMO (highest occupied molecular orbital) and LUMO (lowest unoccupied molecular orbital) energy. Usually, the HOMO and LUMO of the donor (anode) is known to be higher in energy than their respective counterparts in the acceptor (cathode).

The operation of an organic photovoltaic device involves three consecutive fundamental steps: (1) absorption of light, (2) creation of separate charges at the donor-acceptor interfaces, and (3) selective transport of the charges through the bulk of the device to the appropriate collecting electrodes (Kopidakis *et al.*, 2005).

2.4.1 Light absorption in Organic semi-conductors

The band gap for an organic molecule originates from the molecular orbitals that make up a conjugated π -bonding system. For an organic molecule or polymer to be a candidate for use in an OPV device, it must have a conjugated π electron system. The existence of a band gap in a one-dimensional system of conjugated chains was predicted in the 1950s by Rudolf Peierls. The phenomenon of Peierls instability splits the originally half-filled pz-molecular orbital into two: the π - and π^* - bands. In the lower energy ground state, the valence electrons need to occupy the π -orbital (bonding orbital), the valence electrons occupying this energy level is known as the (HOMO) (Shafiee *et al.*, 2011). Absorption of a photon of sufficient energy, electrons will be excited from the bonding π into the anti-bonding π^* - band, corresponding to the first optical excitation from the HOMO to the LUMO. The common band gap value of these HOMO - LUMO molecules should be in the range of 1.5 – 3 eV (Shafiee *et al.*, 2011).

2.4.2 Single-layer cells

The first organic solar cells were situated on a single thermally evaporated molecular organic layer sandwiched between two metal electrodes (**Figure 3**), usually a layer of indium tin oxide (ITO) with high work function also a layer of low work function metal such as aluminium, magnesium or calcium.

The structure using 50 - 320 nm thickness of poly (pphenylenevinylene) (PPV) sandwiched between an ITO and a low work function cathode was created by Marks *et al.*, 1994. The reported quantum efficiencies for this device were 0.1% under 0.1 mW/cm² intensity (Marks *et al.*; 1994 and Shastry *et al.*, 2016). The low quantum efficiency resulted from intrinsically low mobility of charges through semiconducting organics. The carrier mobility of semiconducting organics remained around 10⁻³ cm²/Vs, while the mobility of single crystalline silicon was about 10³ cm²/Vs orders. This indicated that the photogenerated charges in semiconducting organics required more time to be collected from electrodes (Heremans *et al.*, 2009). In single-layer cells, the built-in potential is derived from the difference in work function of the electrodes or a Schottky-type potential barrier at the metal/organic interfaces. The difference of work function between the two conductors sets up an electric field in the organic layer, when the organic layer absorbs light, then the electrons will be excited to the LUMO and leave holes in the HOMO, thereby forming excitons (Shafiee *et al.*, 2011). In both cases, the photovoltaic properties are strongly dependent on the nature of the electrodes. An additional characteristic of such single-layer cells is their poor fill factor, in which can be usually attributed either to a large series resistance associated with the insulating nature in organic photoconductors. The major losses in single-layer structures are due to short exciton diffusion lengths and recombination of the excited charge carriers.

2.4.3 Bilayer heterojunction cells

Overcoming the limitations mentioned in the single-layer cell, the bilayer introduces an electron acceptor layer between the active material and the negative metal electrode as seen in **Figure 3**. Thus both the exciton diffusion range and the poor shunt resistor can be improved.

The acceptor and donor materials must be in close proximity at the heterojunction for efficient exciton dissociation. The optimum length scale is in the range of the exciton diffusion length, normally a few tens of nanometres. However, the thickness of the active layer should be comparable to the penetration length of the incident light, which for organic semi-conductors is typically 80 - 200 nm (Lu *et al.*, 2012). Addition of a second semi-conducting material doesn't only improve exciton separation but has two significant advantages over single-layer devices; the fact that electrons and holes are localized in different materials after the exciton is separated implies that each material needs to transport only one type of charge, therefore reducing design constraint on the materials. Secondly, since the electrons and holes are already partially separated upon photogeneration, there is therefore many holes in the donor and electrons in the acceptor, giving rise to a chemical potential that promotes that photovoltaic effect. A major problem in bilayer polymer solar cells is the short diffusion length of excitons in organic semiconductors (5 - 20 nm) (Ohshimizu *et al.*, 2011). To absorb enough light, the polymer donor layer must be sufficiently thick (~100 - 200 nm). The first relatively successful OPV was reported by Tang *et al.* (1986), which was based on a double-layer structure of p-type copper phthalocyanine and n-type perylene diimide derivative (Ye *et al.*, 2012). In 1986 Tang *et al.* reported that copper phthalocyanine and a perylene tetracarboxylic derivatives were used as active materials and ~ 1% PCE was delivered (Tang; 1986). The first bilayer polymer solar cell fabricated using MEH-PPV and C₆₀ was reported by Sariciftci *et al.* in 1993 (Bao *et al.*, 1993).

The bilayer solar cell was fabricated by sandwiching two organic layers, one being an electron donor layer and the other being an electron acceptor, in between two metallic electrodes. The energy offset between the LUMO levels of the two organic materials facilitated exciton dissociation at the interface between the two organic layers, thus improving the performance of organic solar cells. The energy levels of the donor and the acceptor in the bilayer solar cell need to be well designed for efficient exciton dissociation. The LUMO offset needs to be large enough to provide sufficient energetic driving force for electrons transferring from the donor to the acceptor (Yang *et al.*, 2015).

2.4.4 Hybrid Heterojunction cells

A very different kind of heterojunction has emerged because of trying to improve the efficiencies of organic solar cells; this is the hybrid heterojunction (Gutmann, 2010). The hybrid heterojunction utilises the two concepts practised in bilayer heterojunction and bulk heterojunction, with the only difference being that there is use of an organic and inorganic compound in the active layer of the cell (Liu, 2014). Consequently, they merge the exclusive properties of inorganic semiconductor nanoparticles with those of organic/polymeric material. Also, their low cost synthesis, processability and versatile manufacturing of thin film devices make them attractive (Hou *et al.*, 2013). Inorganic semiconductor nanoparticles may have high absorption coefficients and particle size induced tunability of the optical band-gap. Hybrid solar cells are manufactured using different concepts such as solid state dye-sensitized solar cells and hybrid solar cells using the bulk heterojunction concept with different nanoparticles such as TiO₂, ZnO, CdSe etc.

2.4.5 Bulk heterojunction cells

A bulk heterojunction (BHJ) solar cell has provided considerable attention over the last years attributed to their potential as a low cost photovoltaic technology. Presently, the understanding of BHJ solar cells suggests that the maximum efficiency is in the range of 10 - 12%. Higher interfacial areas and enhanced exciton dissociation efficiencies can be achieved, if both the electron donor (usually a polymer) and acceptor (usually a fullerene derivative) layers are prepared in a mixture (**Figure 3**) (Seyler *et al.*, 2013 and Yin *et al.*, 2017). The main benefit of the BHJ is being able to dissociate excitons very efficiently over the whole extent of the solar cell, thus promoting polaron pairs anywhere in the film (Heremans *et al.*, 2009). In concept, the donor/acceptor interface area is maximized in the BHJ active layer, then all photogenerated excitons diffuse to a donor/acceptor interface within their lifetime. The efficient exciton dissociation occurs when the energy offset between the LUMO levels of the two organic materials is sufficient. In 1995, Yu *et al.* was the first to investigate the BHJ polymer solar cell (PSC) with a power conversion efficiency (PCE) of 2.9% under monochromatic light illumination by mixing poly[2-methoxy-5-(2'-ethyl-hexyloxy)-1,4-phenylene vinylene] (MEH-PPV) as a donor and cyano-PPV (CN-PPV) as an acceptor in the active layer (Hou *et al.*, 2008). Currently, BHJ is the dominant active layer geometry in PSCs and the PCEs (Yang *et al.*, 2015).

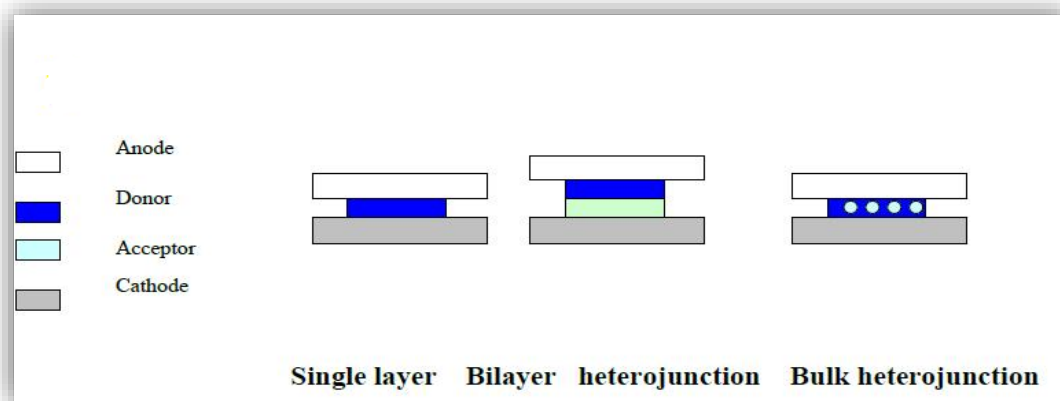


Figure 3: Schematic representation of the device architecture in photovoltaic cells (Ahmed *et al.*, 2011).

2.5 Photoelectrochemical cells

Photoelectrochemical cells (PECs) are solar cells based on a semiconductor–electrolyte interface. Photoelectrochemical cells allow the conversion of light to electricity. Their main characteristic is a semiconductor-electrolyte solution interface, which was intensely studied by *Gerischer et al.* (2001). For an n-type semiconductor, a scheme of the energetics of the interface before and after contact is shown in **Figure 4**. After contact, the former different redox potential E_{redox} of the electrolyte solution and the Fermi level (E_F) of the semiconductor equilibrate. As a result, the interface gets charged, which leads to a bending of the valence band (VB) and the conduction band (CB) of the semiconductor (*Ge et al.*, 2017). Due to illumination of the semiconductor electrons may be excited, jumping from the valence band to the conduction band. In the space charge layer the generated charges are now separated, because the holes are attracted towards the interface and the electrons to the opposite direction. As a result, a current is observed in an outer circuit (*Habelhames et al.*, 2014).

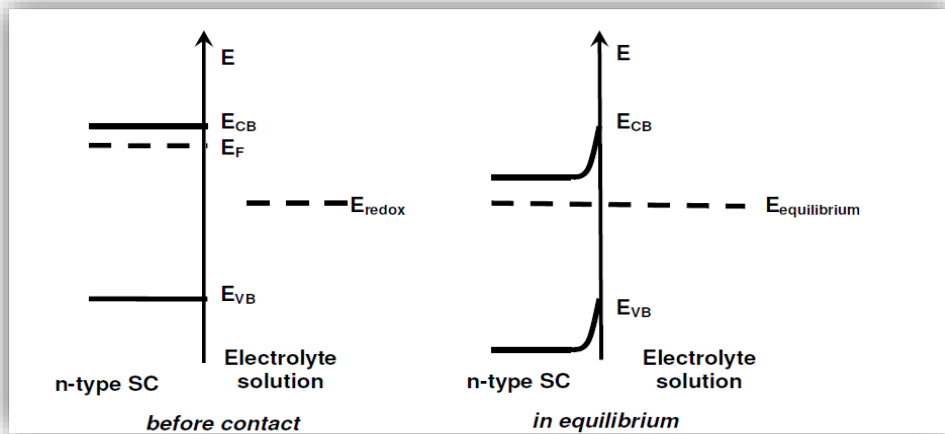


Figure 4: Energetics of an n-type semiconductor-electrolyte solution interface before contact and at equilibrium (Wei *et al.*, 2007).

For a p-type semiconductor the situation is reversed. Valence and conduction bands are now bent downwards, and consequently the electrons excited by illumination are attracted by the interface, pushing the holes away. The current flowing through an outer circuit has now opposite sign. A scheme of the situation in a p-type semiconductor is shown in **Figure 5**.

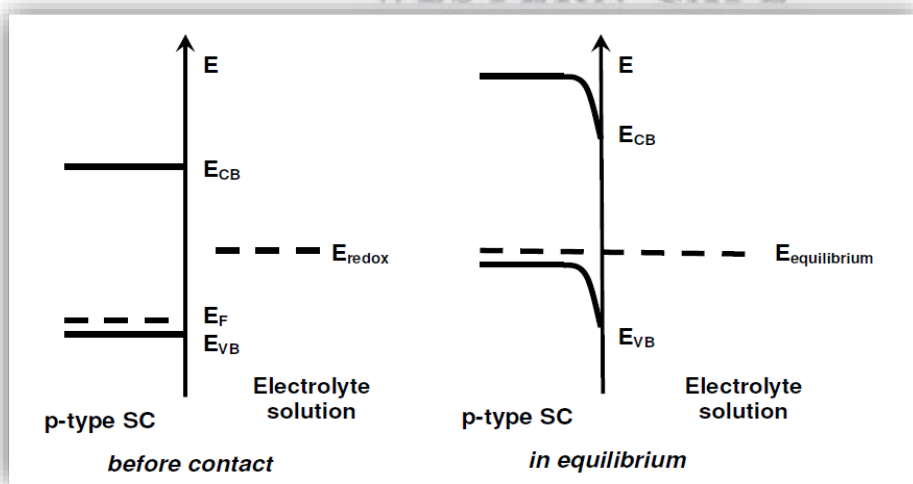


Figure 5: Energetics of a p-type semiconductor-electrolyte solution interface, before contact and at equilibrium (Wei *et al.*, 2007).

2.6 Bandgap

2.6.1 Effect of bandgap modulation in organic photovoltaic cells

In practice, low bandgap (E_g) solar cells suffer from a great loss of power output when their operating temperature becomes $\gg 25^\circ\text{C}$. This is referred to as the thermal coefficient of efficiency (or power) loss and sometimes is quoted as a percentage loss of power (or voltage) in commercial modules. A characteristic of organic solar cells is their narrow absorption window, compared to the absorption band of inorganic semiconductors (Choi *et al.*, 2012). A possible way to capture a wider band of the solar spectrum and thus increasing the power conversion efficiency is using more solar cells with different bandgaps. The optimum of the bandgap E_{g2} of the second subcell is always such that the absorption window of the second subcell borders (or overlaps) the cut-off wavelength of the first subcell, and analogous for E_g . Hence, in all optimal bandgap configurations, (nearly) the entire solar spectrum between the outside borders of the absorption windows is absorbed. The term “band gap” refers to the energy difference between the top of the valence band to the bottom of the conduction band (**Figure 6**); electrons can jump from one band to another. For an electron to jump from a valence band to a conduction band, it requires a specific minimum amount of energy for the transition, the band gap energy. A diagram illustrating the bandgap is shown in **Figure 6**. Measuring the band gap is important in the semiconductor and nanomaterial industries.

The band gap energy of insulators is large (> 4 eV), but materials with a small band gap (< 3 eV), which behave as insulators at absolute zero and allow excitation of electrons into their conduction bands (at temperatures below their melting point) are known as semiconductors (Minnaert *et al.*, 2012 and Tumuluri *et al.*, 2014). An alternative strategy is to use layers of varied materials coated onto the silicon base material. This is employed in the solar industry in the construction of photovoltaic (PV) solar cells. The bandgap is important as it determines the portion of the solar spectrum a photovoltaic cell absorbs. Much of the solar radiation reaching the Earth is comprised of wavelengths with energies greater than the band gap of silicon. These higher energies will be absorbed by the solar cell, but the difference in energy is converted into heat rather than into usable electrical energy. Consequently, unless the band gap is controlled, the efficiency of the solar cell will be poor. Using layers of varied materials with different band gap properties is a proven way to maximize the efficiency of solar cells (Doeleman, 2012).

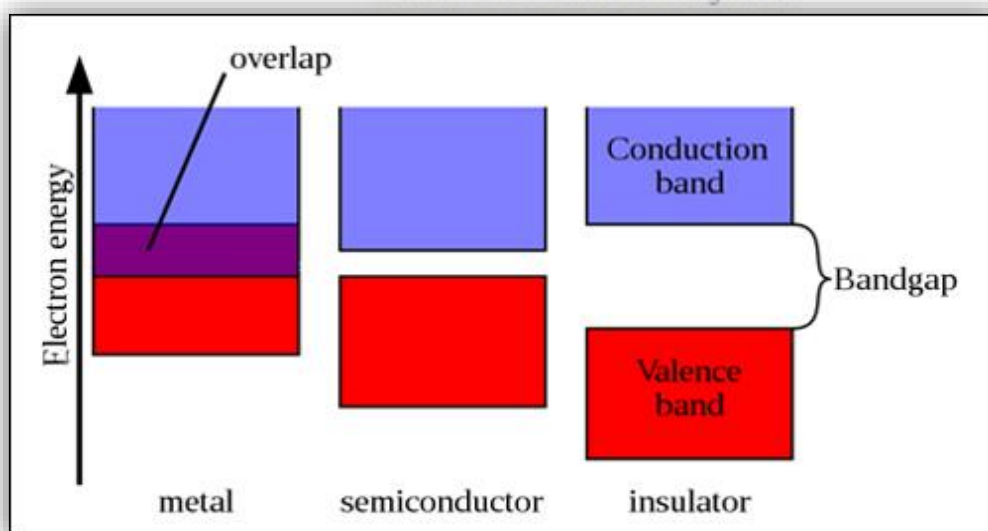
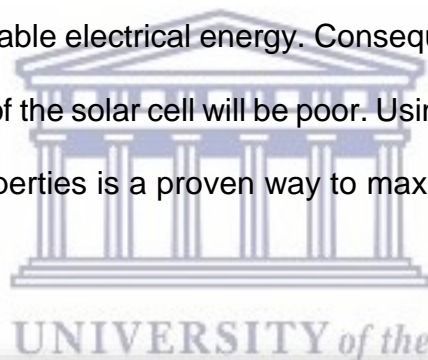


Figure 6: Explanation of bandgap (Doeleman, 2012).

2.6.2 The target for low band gap materials and design

The sun is a stable source of renewable energy and it is estimated to last for another five billion years. At the core of the sun five million tons of energy is released every second in the form of γ -rays, which is equivalent to 3.8×10^{26} J. The γ -rays make their way to the surface of the sun by absorption and re-emission at lower temperature until it reaches the surface mainly as the visible light observed on earth. The air mass (AM1) spectrum corresponds to the solar irradiance with the sun 45° above the horizon (Faculty *et al.*, 2015). It is, however relevant to consider the number of photons available since PVs essentially convert one photon into one electron. According to the National renewable energy laboratory (NREL), the representation of the solar spectrum in photon flux as a function of wavelength give a better picture of how many photons are available for conversion into electrons under ideal condition. **Figure 7** shows a maximum displacement towards the infrared wavelengths when considering the number of photons rather than the energy, thus it is of great interest to the harvest photons at the longer wavelengths. It should be taken into consideration that the energy of the charge carriers at longer wavelengths is lower and this will limit the voltage difference that the device can produce, thus there is an optimum band gap which is currently a subject matter for excitonic devices. This view describes efficiencies that can be obtained for low band gap materials that may not coincide with predicted value for the optimum band gap. According to past literature low band gap polymers have the possibility to improve the efficiency of OPVs due to a better overlap with the spectrum, thus for maximum photon harvesting in the OPV devices low band gap materials are needed (Doeleman, 2012). Most PVs cannot efficiently utilize the light energy below 350 - 400 nm due to the absorption in the ITO/glass substrate through this part of the spectrum contains very little intensity.

It becomes more evident that one gain considerably in current when increasing the λ_{max} from 650 – 1000 nm, therefore decreasing the band gap, considering that wavelengths ranging from 250 - 400 nm amounts to ~1.4% of possible or ~1 mAcm⁻² of current density.

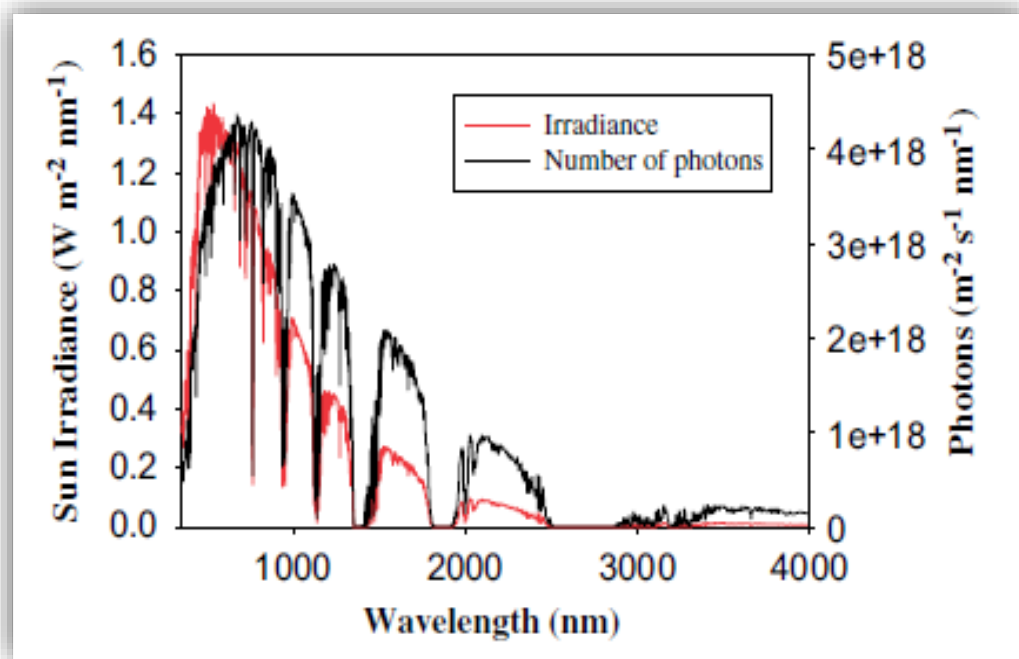


Figure 7: Sun irradiance (red) and number of photons (black) as a function of wavelengths (NREL) (Moujoud *et al.*, 2011).

2.6.3 Roles of transition metals in solar cells for low band gap

Combining the ease of processability of an organic polymer with the improved mechanical and optical properties of an inorganic nanoparticle is of practical use for the fabrication of many new devices. A common structure of organic solar cells is composed of five different layers which is been a result of intense research in the last decade. Arango *et al.*; (1999) developed the first polymer/nanoparticle (MEH-PPV/TiO₂) bulk heterojunction PV cell which was made by sintering together titania nanoparticles then spin casted the polymer on top.

The study showed that the nanoporous titania device indicated an incomplete pore filling by spin coating; which resulted in exciton present in the pore filling and not split to geminate recombination or charge carriers not able to escape the region of interpenetrating titania and MEH-PPV prior to back electron transfer and external quantum efficiency (EQE) attained was 6% (Kwong *et al.*, 2004 and Kawakami *et al.*, 2011). In 2015 Kin-Tak *et al.*; fabricated a hybrid solar cell (**Figure 8**) containing polymer-fullerene with nanoparticle (P3HT: PCBM/ZnS) to enhance the exciton generation and electron carrier transport, also to improve the open circuit voltage (V_{oc}).

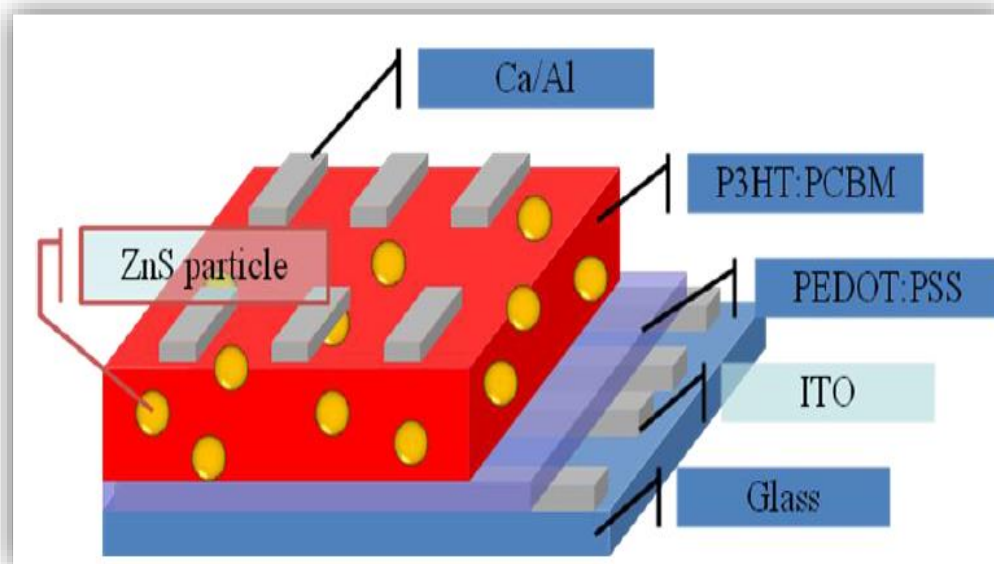


Figure 8: Device structure consists of an active layer of P3HT: PCBM: ZnS NP sandwiched between Ca/Al electrode and conducting electrode of PEDOT: PSS on ITO glass substrate (Yang *et al.*, 2015).

2.7 Properties of nanoparticles and polymers in PV cells

The term metallic nanoparticles are used to describe the nanosized metals with dimensions (length, width or thickness) within the size range 1 - 100 nm. The intrinsic surface defects of metallic nanoparticles make the final power conversion efficiency of hybrid solar cells lower than their fullerene-based counterparts. These defects would trap photo-excited electrons, which not only enlarges series resistance (RS) for electron transport and weaken electronic coupling with polymer donor in hybrid solar cells, but also results in severe back charge recombination due to the lower energy offset between the trap state and highest occupied electron orbit (HOMO) of polymer donor (Agarwal, 2010). Currently, much attention has been paid to investigate the effects of surface modified ZnO as electron transport layer on polymer solar cells containing fullerene derivatives as electron acceptors. Hau *et al.* (2001) used a carboxylic acid functionalized fullerene to modify the surface of ZnO electron transport layer, which reduced the surface defects, improved electronic coupling of ZnO/organic layer and consequently improved the short circuit current density (I_{sc}) and fill factor (FF) of the device. Hsieh *et al.* (2008) inserted a cross-linked fullerene between ZnO electron transport layer and active layer, which can also effectively passivate the shunts in ZnO film, restrain the back-charge recombination and improve the device performance (Habelhames *et al.*, 2014 and Malashchonak *et al.*, 2015). However, little efforts were paid to investigate the effects of surface modification of ZnO nanoparticles on bulk heterojunction hybrid solar cells based on polymers (as electron donor) and ZnO (as electron acceptor).

2.7.1 Electrical properties

The electronic structure of MNPs has considerable implications for their photochemical performance and therefore should to be studied with high accuracy. The electronic properties of MNPs are probed mainly by two methods: photoelectron spectroscopy as a nonlocal technique and scanning tunneling spectroscopy as a local technique. The electronic structure changes related to the transition from a single atom to an extended metal crystal are schematically illustrated in **Figure 9**. X-ray photoelectron spectroscopy (XPS) and ultraviolet photoelectron spectroscopy (UPS) are generally used to probe the electronic structure of MNPs. On one hand, gradual development of metallic bands from single atomic orbitals is observed in the valence band region with increasing cluster size. Additionally, a well-defined Fermi edge develops in clusters containing several thousands of atoms, which separates occupied and unoccupied electronic states. The metallic properties appear at about 1 nm, and a bulk-like band structure is formed at about 3 nm in diameter.

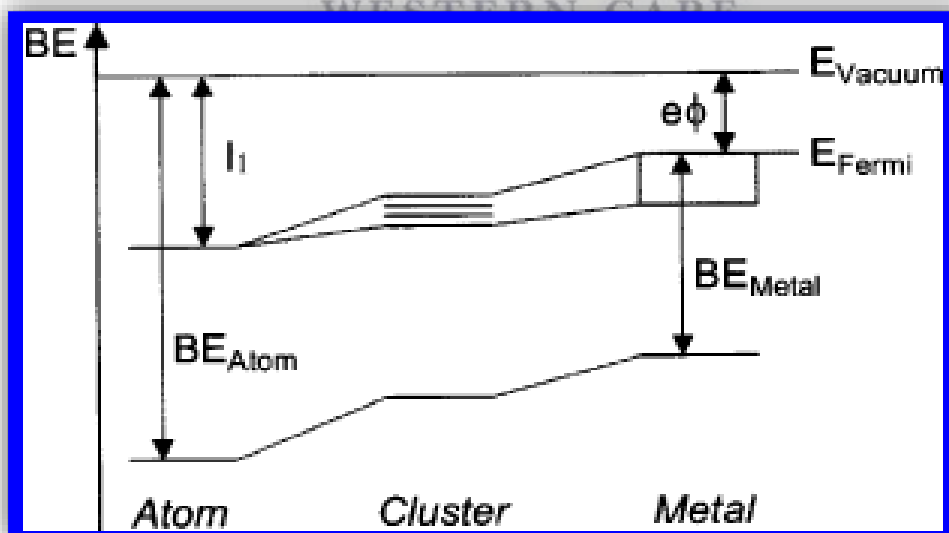


Figure 9: Diagram illustrating the evolution of electronic states from an atom to a metal (Copyright 1999 Elsevier).

2.7.2 Optical properties

Optical properties of thin films towards photovoltaic cell are important for the conversion efficiency and very significant as far as applications in any optoelectronic devices are concerned. Optical band gap and absorption coefficient are the two important parameters of a solar cell material (Agarwal, 2010 and Anefnaf *et al.*, 2016). There are several important features in the structure of the nanomaterials that influence the optical properties such as the short-range order, long-range order, and the coordination defects. The coordination defects feature is the most important because it determines the trapping and the recombination of the electronic properties (Pv *et al.*, 2017). In recent studies, optical characterization was done for the determination of the nature of absorption spectrum and the energy bandgap of CuSe thin films. The optical transmission spectrum of CuSe films was recorded in the wavelength region 400 - 1400 nm. It is of great importance to note that CuSe films were very much transparent in the visible region, the dependence of optical absorption coefficient on photon energy helps to analyse the band structure and the type of transition of electrons (Anefnaf *et al.*, 2016). In earlier research, Kreibig and Vollmer studied the optical characteristics of metal nanoparticles (MNPs) as a consequence of their distinct electronic and geometric properties and of relevance for surface photochemistry. The main concerns here are the dependences of absorption spectra of MNPs on their sizes and shapes, particle-particle interactions, and their environments (Xu, 2007 and Saini *et al.*, 2009).

2.7.2.2 The effect of photoluminescence (PL)

Photo-excitation causes electrons within a material to move into permissible excited states. When these electrons return to their equilibrium states, the excess energy is released and may include the emission of light (radiative process) or may not (non-radiative process). The energy of the emitted light (photoluminescence) relates to the difference in energy level between the two electrons states involved in the transition between the excited state and the equilibrium state. The quantity of the emitted light is related to the relative contribution of the radiative process. There is some detection that can be made from the emitted light patterns for solar cells (Shastry *et al.*, 2016). Generally, it is agreed upon that when a semi-conductor material is exposed to a photon of light, there is excitation of the electron from the valence band to the conduction band thereby leaving a hole in the valence band. An electron hole pair is formed because of the existence of coulombic forces between the particles. The electron hole pair is referred to as an exciton. The effect of the presence of the nanoparticles in the photoluminescence spectra of the polymers is a very important parameter that needs to be explored to determine the applicability of a compound as an acceptor in the photovoltaic system. The study of the fluorescence behaviour of the polymers with the nanoparticles was done to verify whether there is quenching of the emission of the polymer which will be used as a donor in the photovoltaic cell by the nanoparticle which is a potential acceptor (Bakar *et al.*, 2014 and John *et al.*, 2016).

2.8 Photovoltaics performance parameters

When light shines on a solar cell, the current that is measured is called the photocurrent. The value of the photocurrent is dependent on many factors in addition to just the quality of the device.

The quality of the device, the incident wavelength, intensity of the incident light and the area of the device being illuminated are some of factors that affect the photocurrent. Several parameters are used to characterize the efficiency of the solar cell, including the maximum power point (P_{\max}), the energy conversion efficiency (η) and the fill factor (FF). These points are illustrated in **Figure 10**, which shows a typical forward bias current-voltage (I-V) curve of an illuminated photovoltaic cell (Hoppe *et al.*, 2004 and Huong Nguyen *et al.*, 2006).

2.8.1 The upper limit of V_{oc}

Open circuit voltage (V_{oc}) is the maximum voltage, at zero current. The value of V_{oc} increases logarithmically with increased sunlight. This characteristic makes solar cells ideally suited to battery charging. The open-circuit voltage V_{oc} is the voltage across the solar cell when $J = 0$, which is the same as the device being open-circuited. Since, $J = 0$ and power is the product of current and voltage, no power is produced at this voltage. However, the V_{oc} marks the boundary for voltages where power can be produced. The open-circuit voltage can also be thought of as the point at which the photocurrent generation and dark current processes compensate one another. The longest wavelength for which this is finite is limited by its bandgap. Maximum use can only be made of incoming sunlight if the bandgap is in the range 1.0 – 1.6 eV (Heremans *et al.*, 2009). This effect alone acts to limit the maximum achievable efficiency of solar cells to 44% (Shockley *et al.*, 1961).

2.8.2 Short circuit current (I_{sc})

The short circuit current gives the maximum current density that can be obtained when the two leads are connected to each other. When analysing an I-V curve, the short circuit current is the value where the voltage is ~ zero, due to the generation and collection of light-generated carriers. For an ideal solar cell at most moderate resistive loss mechanisms, the short-circuit current and the light-generated are identical, therefore the short circuit current is the largest current which may be drawn from the solar cell (Byun *et al.*, 2011).

2.8.3 Fill Factor (FF)

The fill factor is defined as the ratio of the curve under the maximum power point of the cell ($P_{max} = I_{max} \times V_{max}$) to the area associated with open and closed circuit ($P = I_{sc} \times V_{oc}$). The fill factor is referred to as a quantifying unit for the squareness of the I-V curve. This is also influenced by the materials morphology. In addition to this it is also influenced by the stability of the materials. The fill factor can be calculated using the following equation:

$$FF = \frac{V_{max} \times I_{max}}{V_{oc} \times I_{sc}}$$

Where V_{max} and I_{max} are the current and voltage at the point of maximum power output of the solar cell. I_{max} and V_{max} can be determined by calculating the power output P of the solar cell ($P = I \times V$) at each point between I_{sc} and V_{oc} and finding the maximum of P_{max} . The theoretical limit of a fill Factor (FF) is between 0.25 and 1 (Wanninayake *et al.*, 2015).

2.8.4 Power Conversion Efficiency (η)

Power Conversion efficiency can be defined as the ratio between the maximum power output (P_{\max}) and the power that is from the incident light (P_{in}). As already stated the power conversion efficiency is greatly influenced by the V_{oc} and I_{sc} . The latter is displayed in the following equation used to calculate the efficiency (Scharber *et al.*, 2013).

$$\eta = \frac{FF \times V_{\text{oc}} \times I_{\text{sc}}}{P_{\text{m}}}$$

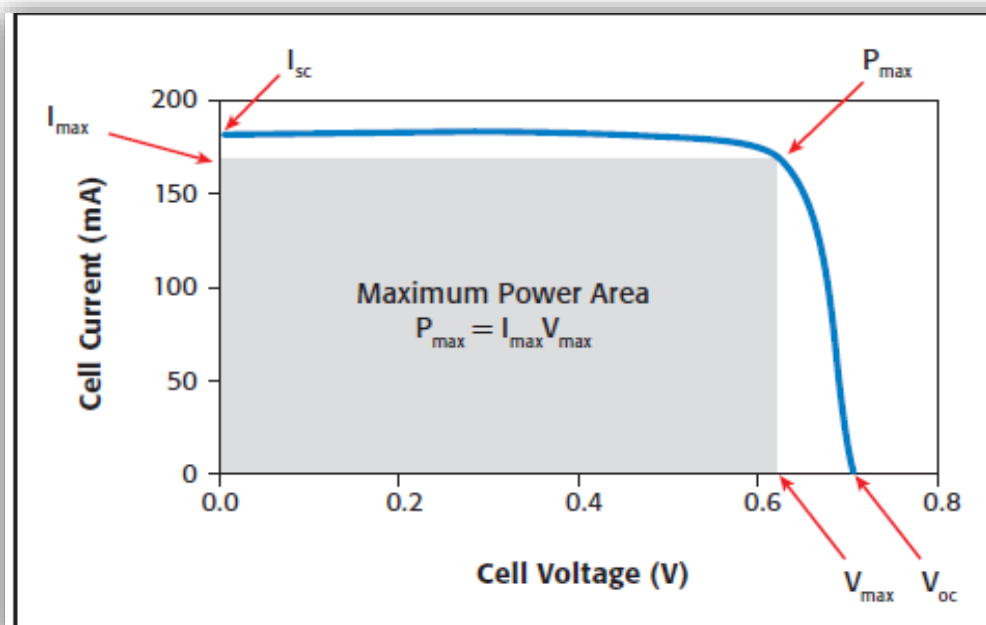


Figure 10: Typical forward bias of I-V characteristic of a PV cell (Minnaert *et al.*, 2012).

2.9 Conclusion

One simple requirement for an efficient polymer-based photovoltaic cell is effective utilization of the solar spectrum. Absorption of light is dependent on the conjugated polymer's band gap energy; however conventional conjugated polymers usually have wide band gaps. For instance, the most widely studied polymer for photovoltaic cells is P3HT, which has a band gap energy around 1.9 eV. Unfortunately, more than 52% of the total solar irradiance is at energies below 1.77 eV and there has been much interest in reducing the polymer band gap to absorb more of the solar spectrum. Increasing the strength of a donor (raising its HOMO) or acceptor (lowering its LUMO) will result in a reduced band gap for photovoltaic application. Morphology control and optimization in polymer photovoltaic cells is a critical factor in determining the power conversion efficiency (PCE). In this study, stannum-based bimetallic nanoparticles will be incorporated as acceptor materials to fabricate new photovoltaic cells. These bimetallic nanoparticles will be blended with the well-known and studied polymer P3HT to improve the absorption by red-shifting the band gap energy. This will result in improving exciton and charge transport by further delocalizing electrons and excited states while reducing the population of carrier trapping sites (Gliboff, 2013). Efficient PSCs should produce a large voltage in addition to a large current density. When characterizing the photovoltaic device, a potential is swept across it from the point of maximum current (I_{sc}) to the point of no current flow (V_{oc}). While losses in I_{sc} are primarily the result of poor transport which can be reduced by improving polymer planarity, both V_{oc} and I_{sc} are influenced by intermolecular energy transfer (Clarke *et al.*, 2012 and Bkakri *et al.*, 2015).

Bibliography

Agarwal, A. (2010) 'Optical Properties and Application of Metallic Nanoparticles and their Assembled'.

Ahmed, E., Ren, G., Kim, F. S., Hollenbeck, E. C. and Jenekhe, S. A. (2011) 'Design of new electron acceptor materials for organic photovoltaics: Synthesis, electron transport, photophysics, and photovoltaic properties of oligothiophene-functionalized naphthalene diimides', *Chemistry of Materials*, 23, pp. 4563–4577.

Alsalmeh, A. M., Alghamdi, A. A. B., Alhamdani, A. A. G. Q. and Iraqi, A. (2014) 'Synthesis and properties of alternating vinylene-benzothiadiazole-based copolymers with carbazole and fluorene derivatives for photovoltaic applications', *International Journal of Electrochemical Science*, 9, pp. 1920–1941.

Anefnaf, I., Benhaddou, N. and Aazou, S. (2016) 'Optical , Structural and Photoconductivity Properties of Organic Photovoltaic Thin Films Based on Polymer / Fullerene', pp. 3.

Bakar, N. A., Supangat, A. and Sulaiman, K. (2014) 'Controlling the morphological, structural, and optical properties of one-dimensional PCDTBT nanotubes by template wetting', *Nanoscale Research Letters*, 9, pp. 1–6.

Bao, Z., Chan, W. and Yu, L. (1993) 'Synthesis of Conjugated Polymer by the Stille Coupling Reaction', *Chemistry of Materials*, 5, pp. 2–3.

Bkakri, R., Chehata, N., Kusmartseva, O. E., Kusmartsev, F. and Song, M. (2015) 'Charge Transfer and Transport Properties in P3HT and P3HT : Graphene Based Organic Solar Cells', 3, pp. 1–5.

Byun, W. B., Lee, S. K., Lee, J. C., Moon, S. J. and Shin, W. S. (2011) 'Bladed organic photovoltaic cells', *Current Applied Physics*. 11, pp. 179–184.

Celik Bedeloglu, A., Demir, A., Bozkurt, Y. and Sariciftci, N. S. (2010) 'Photovoltaic properties of polymer based organic solar cells adapted for non-transparent substrates', *Renewable Energy*. 35, pp. 2301–2306.

Choi, W. S., Chisholm, M. F., Singh, D. J., Choi, T., Jellison, G. E. and Lee, H. N. (2012) 'Wide bandgap tunability in complex transition metal oxides by site-specific substitution', *Nature Communications*, 3.

Clarke, T. M., Eng, M. P., Barlow, S. and McCulloch, I. (2012) 'Charge photogeneration in donor / acceptor organic solar cells Charge photogeneration in donor / acceptor organic solar cells Safa Shoaee Chun Huang Martin Heeney Dirk Vanderzande'.

Doeleman, H. (2012) 'Limiting and realistic efficiencies of multi-junction solar cells', p. 33.

Faculty, T. A., Jung, J. and Fulfillment, I. P. (2015) 'Organic-inorganic nanocomposites for renewable energy conversion devices'.

Ge, J. and Yan, Y. (2017) 'Synthesis and characterization of photoelectrochemical and photovoltaic $\text{Cu}_2\text{BaSnS}_4$ thin films and solar cells', *Journal of Material Chemistry C*, 5, pp. 6406–6419.

Gliboff, M. (2013) 'Molecular Level Understanding of Interfaces and Excited State Electronic Structure in Organic Solar Cells Using Soft X-ray Techniques'.

Guo, X., Kim, F. S., Seger, M. J., Jenekhe, S. A. and Watson, M. D. (2012) 'Naphthalene diimide-based polymer semiconductors: Synthesis, structure-property correlations, and n-channel and ambipolar field-effect transistors', *Chemistry of Materials*, 24, pp. 1434–1442.

Gutmann, J. S. (2010) 'Comparison of Hybrid Blends for Solar Cell Application', pp. 301–312.

Habelhames, F., Zerguine, W. and Nessark, B. (2014) 'Improvement of optical and photoelectrochemical properties of conducting polymer by incorporation of ZnO nanoparticles', *Journal of Materials and Environmental Science*, 5, pp. 2139–2144.

Heremans, P., Cheyns, D. and Rand, B. P. (2009) 'Strategies for increasing the efficiency of heterojunction organic solar cells: Material selection and device architecture', *Accounts of chemical research*, 42, pp. 1740–1747.

Hoppe, H. and Sariciftci, N. S. (2004) 'Organic solar cells: An overview', *Journal of Materials Research*, 19, pp. 1924–1945.

Hou, J., Chen, H. Y., Zhang, S., Li, G. and Yang, Y. (2008) 'Synthesis, Characterization, and Photovoltaic Properties of a Low Band Gap Polymer Based on Silole-Containing Polythiophenes and 2,1,3-Benzothiadiazole', *Journal of the American Chemical Society*, 130, pp. 16144–16145.

Hou, J. and Guo, X. (2013) 'Organic Solar Cells', *Journal of Materials Research*, 46, pp. 968–1485.

Huong Nguyen, L., Günes, S., Neugebauer, H., Serdar Sariciftci, N., Banishoeib, F., Henckens, A., Cleij, T., Lutsen, L. and Vanderzande, D. (2006) 'Precursor route poly(thienylene vinylene) for organic solar cells: Photophysics and photovoltaic performance', *Solar Energy Materials and Solar Cells*, 90, pp. 2815–2828.

Joffe, H. (2012) 'Challenges for South Africa ' s Electricity Supply Industry', *Helen Suzman Foundation Focus*, 64, pp. 32–37.

John, S. V., Mayedwa, N., Ikpo, C., Molefe, L. Y., Ndipingwi, M. M., Dywili, N. R., Van Wyk, J., Mapolie, S. F., Baker, P. and Iwuoha, E. (2016) 'Photoluminescence quenching of poly(octylfluorenylbenzothiadiazole) luminophore by n-type cobalt(II) salicylaldimine metallodendrimer', *Synthetic Metals*. pp. 114–122.

Karzazi, Y. and Arbouch, I. (2014) 'Inorganic photovoltaic cells : Operating principles, technologies and efficiencies - Review', 5, pp. 1505–1515.

Kawakami, R., Ito, K., Sato, Y., Mori, Y., Adachi, M. and Yoshikado, S. (2011) 'Preparation and Evaluation of TiO₂ Nanoparticle Thin Films using Electrophoresis Deposition Method', *IOP Conference Series: Materials Science and Engineering*, 18, pp. 06.

Kopidakis, N., Mitchell, W. and Bozell, J. (2005) 'Bulk heterojunction organic photovoltaic devices using dendrimers', *Solar Energy*.

Kwong, C. Y., Choy, W. C. H., Djurišić, A. B., Chui, P. C., Cheng, K. W. and Chan, W. K. (2004) 'Poly(3-hexylthiophene): TiO₂ nanocomposites for solar cell applications', *Nanotechnology*, 15, pp. 1156–1161.

- Li, Y. (2011) 'Photovoltaic Systems for Solar Electricity Production', pp. 1–4.
- Liu, R. (2014) 'Hybrid Organic/Inorganic Nanocomposites for Photovoltaic Cells', *Materials*, 7, pp. 2747–2771.
- Lu, X., Hlaing, H., Germack, D. S., Peet, J., Jo, W. H., Andrienko, D., Kremer, K. and Ocko, B. M. (2012) 'Bilayer order in a polycarbazole-conjugated polymer', *Nature Communications*. Nature Publishing Group, 3, pp. 795–797.
- Luber, E. J. and Buriak, J. M. (2013) 'Reporting Performance in Organic Photovoltaic Devices BT'. *American Chemical Society Nanotechnology*, 7, pp. 4708–4714.
- Malashchonak, M. V., Streltsov, E. A., Mazanik, A. V., Kulak, A. I., Poznyak, S. K., Stroyuk, O. L., Kuchmiy, S. Y. and Gaiduk, P. I. (2015) 'Band-gap and sub-band-gap photoelectrochemical processes at nanocrystalline CdS grown on ZnO by successive ionic layer adsorption and reaction method', *Thin Solid Films*, 19, pp. 145–152.
- Minnaert, B. and Veelaert, P. (2012) 'Guidelines for the Bandgap Combinations and Absorption Windows for Organic Tandem and Triple-Junction Solar Cells', pp. 1933–1953.
- Mohammad Bagher, A. (2014) 'Comparison of Organic Solar Cells and Inorganic Solar Cells', *International Journal of Renewable and Sustainable Energy*, 3, pp. 53.
- Mora, M. B. De, Monroy, B. M. and Lugo, J. E. (2017) 'Solar Energy Materials & Solar Cells Materials for downconversion in solar cells : Perspectives and challenges', *Solar Energy Materials and Solar Cells*, 165, pp. 59–71.

Moujoud, A., Oh, S. H., Hye, J. J. and Kim, H. J. (2011) 'Improvement in stability of poly(3-hexylthiophene-2,5-diyl)/[6,6]-phenyl-C₆₁-butyric acid methyl ester bulk heterojunction solar cell by using UV light irradiation', *Solar Energy Materials and Solar Cells*, pp. 1037–1041.

Nelson, J. (2011) 'Polymer: Fullerene bulk heterojunction solar cells', *Materials Today*, 14, pp. 462–470.

Ohshimizu, K., Takahashi, A., Rho, Y., Higashihara, T., Ree, M. and Ueda, M. (2011) 'Synthesis and characterization of polythiophenes bearing aromatic groups at the 3-position', *Macromolecules*, 44, pp. 719–727.

Pv, T., Alliance, M. and Asso, E. P. I. (2017) 'Opto-Electronics Review Top PV market solar cells 2016', *Opto-Electronics Review*. Association of Polish Electrical Engineers, 25, pp. 55–64.

Rodríguez-Martínez, X., Vezie, M. S., Shi, X., McCulloch, I., Nelson, J., Goñi, A. R. and Campoy-Quiles, M. (2017) 'Quantifying local thickness and composition in thin films of organic photovoltaic blends by Raman scattering', *Journal of Material Chemistry C*, 5, pp. 7270–7282.

Saini, V., Li, Z., Bourdo, S., Dervishi, E., Xu, Y., Ma, X., Kunets, V. P., Salamo, G. J., Viswanathan, T., Biris, A. R., Saini, D., Biris, A. S., V, D. U. and Carolina, N. (2009) 'Electrical , Optical , and Morphological Properties of P3HT-MWNT Nanocomposites Prepared by in Situ Polymerization', pp. 8023–8029.

Scharber, M. C. and Sariciftci, N. S. (2013) 'Efficiency of bulk-heterojunction organic solar cells', *Progress in Polymer Science* , 38, pp. 1929–1940.

Seyler, H., Subbiah, J., Jones, D. J., Holmes, A. B. and Wong, W. W. H. (2013) 'Controlled synthesis of poly(3-hexylthiophene) in continuous flow', *Beilstein Journal of Organic Chemistry*, 9, pp. 1492–1500.

Shafiee, A., Salleh, M. M. and Yahaya, M. (2011) 'Determination of HOMO and LUMO of [6,6]-phenyl C61-butyric acid 3-ethylthiophene ester and poly (3-octyl-thiophene-2, 5-diyl) through voltametry characterization', *Sains Malaysiana*, 40, pp. 173–176.

Shastry, T. A., Balla, I., Bergeron, H., Amsterdam, S. H., Marks, T. J. and Hersam, M. C. (2016) 'Mutual Photoluminescence Quenching and Photovoltaic Effect in Large-Area Single-Layer MoS₂-Polymer Heterojunctions', *American Chemical Society Nanotechnology*, 10, pp. 10573–10579.

Timmons, D., Harris, J. M. and Roach, B. (2009) 'The Economics of Renewable Energy', *Renewable Energy*, pp. 1341–1356.

Tumuluri, A., Naidu, K. L. and Raju, K. C. J. (2014) 'Band gap determination using Tauc 's plot for LiNbO₃ thin films', *International Journal of ChemTech Research*, 6, pp. 3353–3356.

Vatansever, D., Siores, E. and Shah, T. (2012) 'Alternative Resources for Renewable Energy : Piezoelectric and Photovoltaic Smart Structures'.

Wanninayake, A. P., Gunashekar, S., Li, S., Church, B. C. and Abu-Zahra, N. (2015) 'Performance enhancement of polymer solar cells using copper oxide nanoparticles', *Semiconductor Science and Technology*. Institute of Physics Publishing, 30, pp. 06

Wei, D. and Amaratunga, G. (2007) 'Photoelectrochemical Cell and Its Applications in Optoelectronics', 2, pp. 897–912.

Xu, Q. (2007) 'Optical Properties of Poly (3-hexylthiophene)/ ZnS', pp. 48–63.

Yang, J., Clark, N., Long, M., Xiong, J., Jones, D. J., Yang, B. and Zhou, C. (2015) 'Solution stability of active materials for organic photovoltaics', *Solar Energy*. Elsevier Limited, 113, pp. 181–188.

Ye, C., Li, M., Luo, J., Chen, L., Tang, Z., Pei, J., Jiang, L., Song, Y. and Zhu, D. (2012) 'Photo-induced amplification of readout contrast in nanoscale data storage', *Journal of Materials Chemistry*, 22, pp. 4299.

Yin, H., Lok, K., Hoi, C., Ho, Y., Ka, H., Lee, H., Wa, H., Cheng, Y., Wing, S. and Kong, S. (2017) 'Bulk-heterojunction solar cells with enriched polymer contents', 40, pp. 1–7.



CHAPTER THREE

Summary

The search for renewable and environmentally friendly energy sources has made organic electronics an interesting field of research. Semiconducting polymers stand out because they are cheap and easily processable at a largescale from solution, combined with impressive optoelectronic properties. Polythiophenes, in particular poly(3-hexylthiophene) (P3HT), are the most prominent and investigated representatives of semiconducting polymers and have been applied in various devices such as solar cells and field-effect transistors. For this class of polymers, it has been well established that the morphology of the functional layer has a significant impact on the device performance. However, transport bottlenecks are hard to determine due to the complex semi crystalline microstructure, which is composed of a mixture of crystalline and amorphous domains. Understanding of the correlation between microstructure and functional properties, precise control of nucleation and growth of semi crystalline polymers such as P3HT is crucial. This chapter gives an overview of recent work addressing the morphology and crystallization of regio-regular P3HT, both in solution and thin film, and attempts to correlate these structural features to the functional (i.e. optical and electrical) properties of the polymer.

Analysis of PCDTBT and P3HT Thin Films as Potential Donor Materials for Photovoltaic Applications

Abstract

The search for renewable and environmentally friendly energy sources has made organic electronics an interesting field of research. Semiconducting polymers stand out because they offer cheap and easy processability at a largescale from solution, combined with impressive optoelectronic properties. Polythiophenes, in particular; poly(3-hexylthiophene) (P3HT), are the most prominent and investigated representatives of semiconducting polymers and have been applied in various devices such as solar cells and field-effect transistors. For this class of polymers, it has been well established that the morphology of the functional layer has a significant impact on the device performance. Poly(3-hexylthiophene) (P3HT) and Poly[N-9'-heptadecanyl-2,7-carbazole-alt-5,5-(4',7'-di-2-thienyl-2',1',3'-benzothiadiazole)] PCDTBT thin film were synthesized from chlorobenzene (CB) solvent by spin coating method on ITO glass substrates. The optical properties of the films were studied by using Ultraviolet and visible absorbance (UV-vis) spectrophotometer and photoluminescence (PL), the absorbance spectrum have been recorded at wavelength within the range (300 – 850 nm). The optical absorption (A) was analysed to determine the optical constants such as absorption coefficient (α), refractive index (n), and extinction coefficient (k). Analysis of the absorption coefficient was also carried out to determine the energy bandgap and nature of transitions. Electrical properties were characterised from CV and EIS.

3.1 Introduction

When a semiconducting polymer absorbs incident solar radiation, an electron is excited from the highest occupied molecular orbital (HOMO) to the lowest unoccupied molecular orbital (LUMO), forming electron-hole pair, known as an exciton (Shafiee *et al.*, 2011). The optical band gap is defined as the difference between the HOMO and the LUMO energy levels in a polymer, as illustrated in **Figure 7**, in the previous chapter. In a PV device, this process must be followed by exciton dissociation. The electron must then reach one electrode while the hole must reach the other electrode (Hankins, 1999 and Li, 2011). To achieve charge separation, an electrical field is required, which is provided by the asymmetrical ionisation energy/work functions of the electrodes. This asymmetry is the reason why electron-flow is more favoured from the low-work function electrode to the high work function electrode (Nelson, 2011). Conjugated polymers are polymers with π -electron-rich systems. They possess appropriate optical and electronic properties for optoelectronics due to their delocalized π -electrons (Etgar, 2013 and Lube *et al.*, 2013). However, the electrical conductivity of neat conjugated polymers is so low that applications of conjugated polymers in optoelectronic devices are limited. In the 1970s, MacDiarmid and Heeger found that doping improved the conductivity of the conjugated polymer poly(acetylene). This led to a revolution in the field of organic electronics as PEDOT:PSS (poly(3,4-ethylenedioxythiophene):poly(styrenesulfonate)) is an example of a doped conjugated polymer which is widely used as an electrode in many organic electronic devices (Lu *et al.*, 2012).

The tendency of a conjugated polymer material to aggregate is a key factor in controlling both the charge carrier mobility and the ability of excited states to dissociate when combined with an electron-accepting material. In this way, the aggregation process controls the performance of a polymer in solar cell applications as well as in thin-field transistors (Guo *et al.*, 2012). The interdependence of device performance and thin film morphology has been extensively studied for the polymer poly(3-hexylthiophene) (P3HT). The reason why P3HT is so amenable to these processing techniques lies in the semicrystalline nature of P3HT (Bkakri *et al.*, 2015).

Although it adopts a randomly disordered chain conformation in a good solvent, planarization and concomitant crystallization occurs when the solvent quality is deteriorated. Similar effects have been reported for other homopolymers such as poly{[4,4-bis(2-ethylhexyl)-cyclopenta-(2,1-b;3,4-b')dithiophen]-2,6-diyl-alt-(2,1,3benzothiadiazole)2,4,7-diyl} (PCPDTBT), carbazole-based polymers such as PCDTBT, diketopyrrole-based polymers such as PDPP-TPT, thienothiophene-benzodithiophene-based polymers such as PTB7, and so forth (Nelson, 2011). Like P3HT, the performance of bulk heterojunction solar cells made with these polymers depends critically on the processing conditions and the resulting thin film morphology. Consequently, great effort is made to understand and control the bulk heterojunction morphologies, for example, by thermal annealing, solvent vapour annealing, and spin-coating from solutions containing solvent additives (Yang *et al.*, 2015).

3.2 Experimental

3.2.1 Materials

PCDTBT with a molecular weight (M_w) of 20 664 Da, 3-Hexylthiophene (3HT), Iron (III) Chloride ($FeCl_3$), Chlorobenzene (99% HPLC) and anhydrous chloroform $CHCl_3$ (99%), glass/ITO substrates of 2 cm x 2 cm were purchased from Sigma-Aldrich. All materials were used without any further treatment except for the glass slides which were cleaned in deionized water, ethanol, and acetone, respectively for 10 min each under sonication.

3.2.2 Sample preparations

Synthesis of P3HT was achieved by following a route reported by Hussein *et al.* (2015), using Iron (III) Chloride ($FeCl_3$) as catalyst. $FeCl_3$ (2 g, 12.3 mmol) was added to dry Chloroform $CHCl_3$ (~12 mL) and stirred for 15 min at room temperature. The monomer 3-Hexylthiophene(3HT) (0.5 g, 3 mmol) in dry $CHCl_3$ (~12 mL) was then added drop-wise to the $FeCl_3$ solution and the reaction mixture was stirred overnight under argon at room temperature. The polymerization reaction was then terminated by pouring the reaction mixture into excess methanol (MeOH) (~50 mL). The crude polymer precipitate was filtered using a PTFE membrane filter (1 μ m, Millipore) and washed with ethanol (200 mL), distilled water: acetone mixture (1:1, 250 mL:250 mL) and finally with acetone (250 mL). The dark brown solid product obtained was dried under vacuum for 72 h to afford P3HT (0.45 g, 90%). 12.5 mg of P3HT and PCDTBT was added to 0.5 mL OF CB in separate glass vials then sonicated at 50 °C for 24 h for further characterizations.

3.2.3 Instrumentation

FT-IR was used to confirm the synthesis of P3HT in a range from 4000 to 400 cm^{-1} and to confirm the chemical structural properties of both P3HT and PCDTBT. These experiments were performed using Perkin Elmer FTIR model 100 spectrophotometer. Electrochemical experiments were performed at different scan rates at room temperature under nitrogen. The setup is a computer controlled consisting of a potentiostat CH. As an electrolyte a solution of 0.1 M of LiClO_4 in anhydrous acetonitrile (CH_3CN) solution was used. Platinum electrode was used as a working electrode; Ag/AgCl couple and platinum wire as the reference electrode and auxiliary electrode respectively. The UV-vis absorption data and PL emission data was obtained by thermally evaporating a thin layer of the organic compounds approximately 30 μL onto a clean ITO glass substrate. The absorption spectra were acquired at room temperature using UV-Vis spectrometer Nicolet evolution 100 and emission spectra was obtained using IGA-521 X 1 – 50 – 1700 – 1LS, HORIBA JOBIN YVON photoluminescence spectroscopy (PL).

3.3 Results and Discussion

3.3.1 Chemical structures of the polymers

3.3.1.1 Fourier-transform infrared spectroscopy

Figure 11 shows the measured FTIR spectrum of P3HT and PCDTBT. The absorption bands at 3600-3419, 3000 and 2443–2923 cm^{-1} are assigned to the CH_2 out-of-phase stretching, CH_2 in-phase stretching and the CH_3 asymmetric stretching vibrations on the thiophene ring, respectively.

The band at 1652–1291 cm^{-1} and 1485 cm^{-1} represent the C=C asymmetric stretching vibration and the C–C symmetric stretching modes and symmetric ring stretching mode, respectively for P3HT and 1261-1455 cm^{-1} bands are characteristic vibrations of CH_2 and CH_3 for PCDTBT (Romero, 2017). The bands at 1073 cm^{-1} is attributed to the CH_2 stretching vibration. The bands at 668 and 581 cm^{-1} are the characteristic bands for the absorption of sulfate atom (S-atom) on the polythiophene ring in P3HT and PCDTBT respectively.

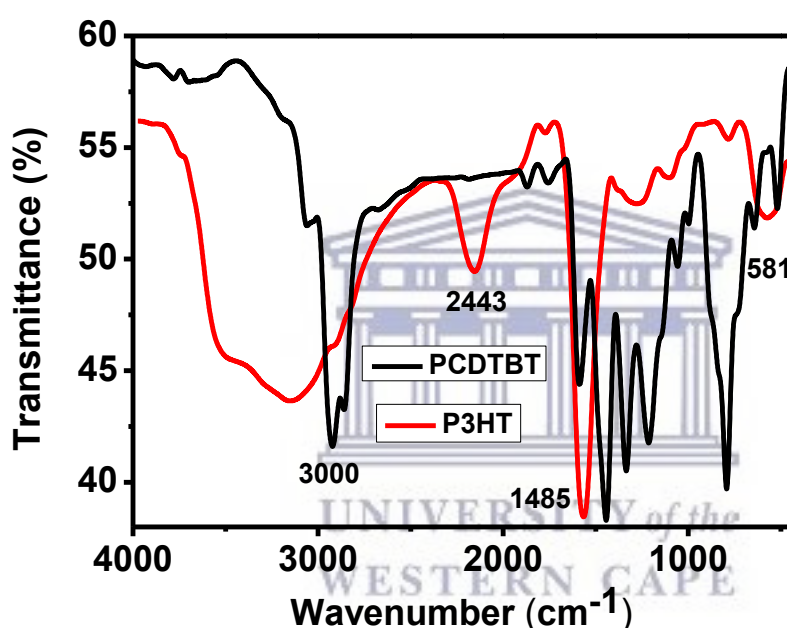


Figure 11: Fourier transform infrared (FTIR) absorption of P3HT and PCDTBT.

3.3.2 Optical analysis

3.3.2.1. Ultra-violet visible spectroscopy

The P3HT and PCDTBT in Chlorobenzene (CB) is initially orange and purple in colour respectively, these solutions were spin coated onto glass substrate to obtain a thin film.

The characteristic spectrum of the P3HT thin film is a broad band at 516 - 520 nm corresponding to the π - π^* transition in conjugated polymer (Anefnaf *et al.*, 2016 and Saini *et al.*, 2009), which indicates the transition between energy levels of the π electronic system. The optical absorption spectra of P3HT and PCDTBT film spin coated onto a glass substrate then annealed at 125 °C for 15 min showed wavelengths between 300 to 850 nm, are shown in **Figure 12**. The UV-Vis spectrum of the P3HT film showed two peaks at $\lambda = 520$ and 550 nm, these bands are known as the vibronic absorption shoulders. The vibronic absorption shoulders can be attributed to the $\pi - \pi^*$ transition in crystalline π - π stacking structure of polymer P3HT chains (conjugated polymer). The increase in the P3HT order, shows more pronounced vibronic shoulders and an increase in the inter-digitation and stacking of the polymer. The absorption coefficient, α was calculated by using Beer-Lambert's law: ($\alpha = 2.303 A/d$) where, A is the absorbance. **Figure 13** shows the absorption coefficient spectra of PCDTBT film, which revealed strong light absorption peaks at wavelength of about 403 nm and 550 nm. The spectra reveal all the films exhibit low absorption in the Visible and Near-infrared region but high absorbance in the UV range. High absorption characteristics in the UV range are due to melanin wide band gap properties.

The determined band gap values are obtained by extrapolating the linear region of the plot $(\alpha h\nu)^2 = 0$. The allowed direct transition optical gap is found at 1.4 and 1.6 eV for PCDTBT and P3HT respectively. This downshift is attributed to the thiophene ring in the polymer P3HT (Xu, 2007). The energy gap values depend in general on the films crystal structure, and the arrangement and distribution of the atoms in the crystal lattice. Also, it is affected by crystal regularity.

E_g can be calculated from the classical relation for near edge optical absorption in semiconductors (Tumuluri *et al.*, 2014) and the relation is drawn between $(\alpha h\nu)^2$ and photon energy ($h\nu$), as shown in **Figures 14** for both P3HT and PCDTBT. The band-gap energy, E_g which is associated with HOMO to LUMO electron transitions between the π and π^* molecular orbitals, were estimated using Tauc's approach $\alpha h\nu = A(h\nu - E_g)^{1/2}$ of direct band-gap energy (where, $h\nu$ is the incident photon energy) by extrapolating the linear curve to the photon energy axis. It was deduced from **Figure 14** that the E_g of PCDTBT and P3HT as a function of film thickness are 1.4 and 1.6 eV, respectively. This obtained values are close to the reported values of synthetic P3HT of 1.9 eV (Liu *et al.*, 2013 and Romero, 2017 and Saini *et al.*, 2009).

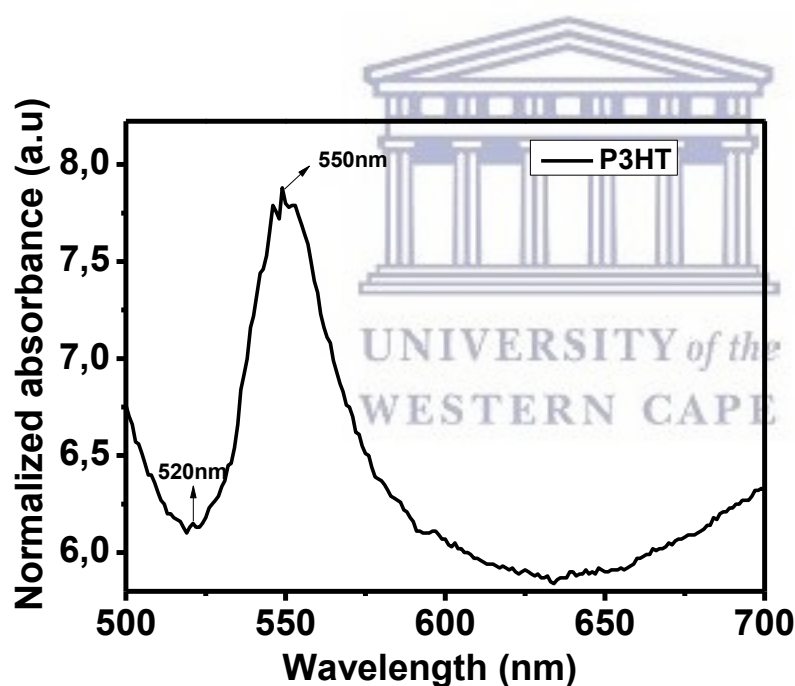


Figure 12: UV-vis absorption spectra of P3HT thin film.

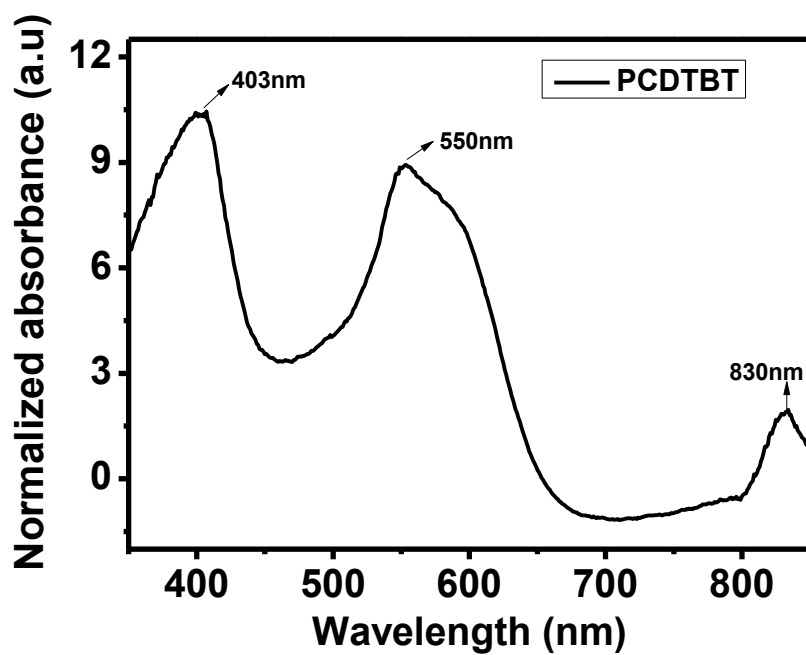


Figure 13: UV-vis absorption spectra of PCDTBT thin film.

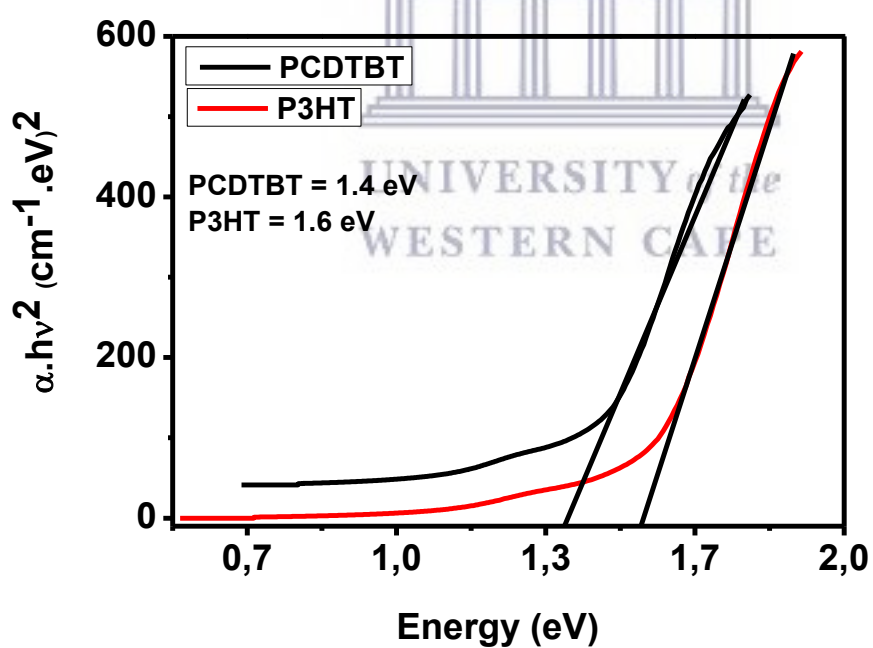


Figure 14: Tauc plot for P3HT and PCDTBT.

3.3.2.2. Photoluminescence spectroscopy

The photoluminescence (PL) of the semiconducting polymers was studied in CB and the results are shown in **Figure 15**. PL or fluorescence is a transition that occurs when a compound in its excited state goes back to its ground state by releasing a photon, singlet excited state of the polymers occurs as an exciton. This exciton hops along the polymer chain until it dissipates by transitions such as fluorescence (Henssler *et al.*, 2009). The PL spectra of polymer films under excitation was observed by using an excitation wavelength of 430 nm in the range from 400 to 800 nm. As shown in **Figure 15** the PL behaviour of the exciton is observed at 422 nm and 691 nm for PCDTBT and P3HT, respectively. The P3HT thin film had the maximum PL peak at 691 nm. The high intensity of PL emission from the polymer P3HT film can be due to the surface oxidation defects of the exposed film. The degree of PL quenching is related to possible structural order of the polymer film on the substrate or on the oxygen adsorbed on surface active sites (John *et al.*, 2016 and Shastry *et al.*, 2016). The fluorescence quantum yields that were calculated were, 0.41 and 0.56 for PCDTBT and P3HT, respectively.

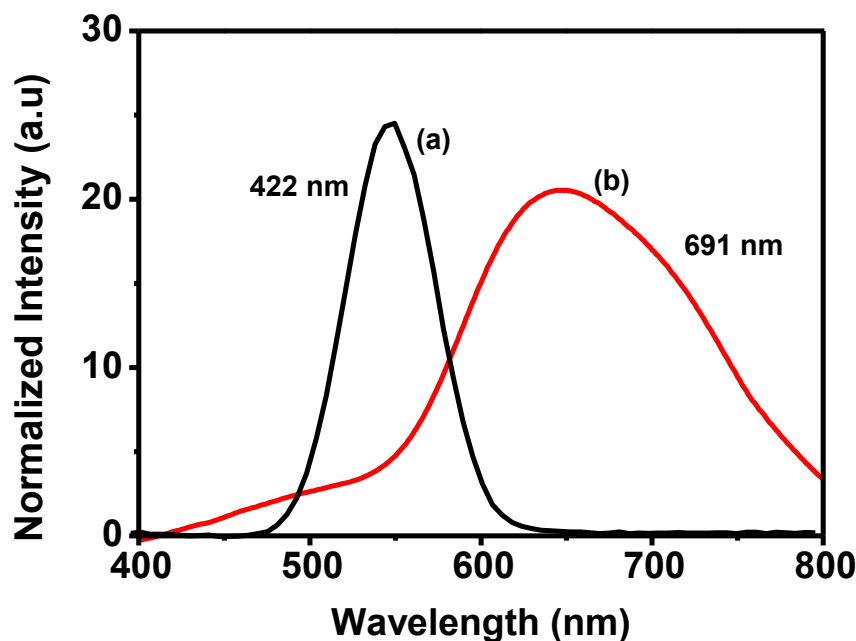


Figure 15: Photoluminescence spectra of (a) PCDTBT and (b) P3HT thin films.

3.3.3 Electrochemical analysis

3.3.3.1. Cyclic voltammetry

Cyclic voltammetry (CV) is a very suitable method for a wide range of applications. This unique technique assists in discovering organic materials with its properties which opens a new approach for fabricating organic photovoltaics devices instead of the conventional inorganic devices. It is very important for device fabrication to select the appropriate materials as the active semiconducting layer, because it is where the charge generation, separation and transfer will take place under the illumination of light. For this to take place the electron transfer from the donor to the acceptor requires the LUMO level of the donor to be higher than that of the acceptor, also the hole transfer from the acceptor to the donor requires the HOMO level of the donor to be above that of the acceptor.

CV is one of the most utilized characterization technique to estimate the energy gap diagram. In organic semiconductors HOMO represents the energy required to extract an electron from a molecule, which is an oxidation process and LUMO is the energy necessary to inject an electron to a molecule, implying a reduction process (Gonçalves *et al.*, 2017). CV was used to measure these processes by measuring the redox potentials E_{red} and E_{ox} . Ferrocene will be used as the known reference to calculate the energy of the HOMO and LUMO levels, including the ferrocene value which is $E_0 = -4.4$ eV. According to *Bredas et al*; the energy levels were calculated using the below empirical equations:

$$E(\text{LUMO}) = (E_0 + E'_{red}) \quad (1)$$

$$E(\text{HOMO}) = (E_0 + E'_{ox}) \quad (2)$$

$$E_g = E(\text{LUMO}) - E(\text{HOMO}) \quad (3)$$

In the organic molecules, the energy levels of the electronic states correspond to the energy carried by the UV-vis radiation. The molecules can absorb quantified energy transported by the electromagnetic radiation and promote electron from the low-energy molecular orbital to higher energy molecular orbital (Yang *et al.*, 2015). These transitions can be measured using a UV-vis spectrometer. E_{opt} corresponds to the energy of the wavelength edge of the exciton absorption band. The longest absorption wavelength λ_{onset} is used to calculate the optical energy gap E_g , according to the equation:

$$E_g = 1242 / \lambda_{onset} \quad (4)$$

Coupling the two methods together, we can estimate which one of the two materials work best as a donor material in the active layer of the photovoltaic device. On the cycle voltammogram regarding P3HT behaviour, a reversible two electron reduction is observed, with the onset of approximately -0.30 mV and -0.68 mV. The band/energy gap was estimated to be 1.68 eV this is in correlation with the band gap estimated from the optical absorption (**Figure 14**). In P3HT, both the oxidation and reduction peak positions were affected by the degradation process, suffering a slight shift towards more positive and negative values, respectively. Such shift in peak position could be considered a change in the energy necessary to ionic intercalation, i.e with polymeric film degradation in this process takes more energy to occur (Wei *et al.*, 2010). An oxidation and reduction peak for PCDTBT is observed at -0.53 mV and 0.46 mV, respectively. An estimate of the HOMO and LUMO energy level is found to be 3.84 eV and 4.46 eV, respectively.

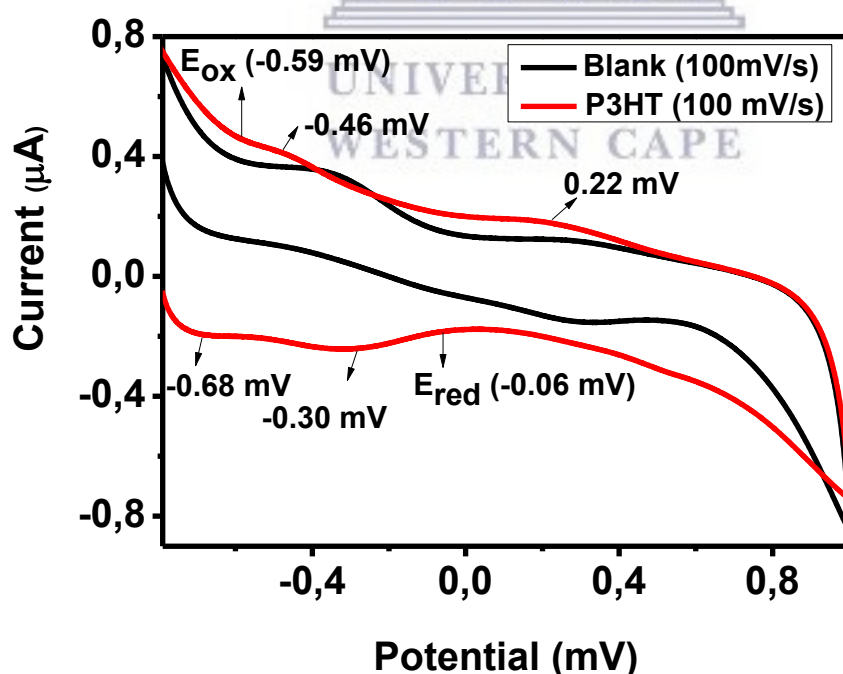


Figure 16: Cyclic voltammogram behaviour of P3HT and bare Pt electrode in 0.1M LiClO₄ at 100 mV/s.

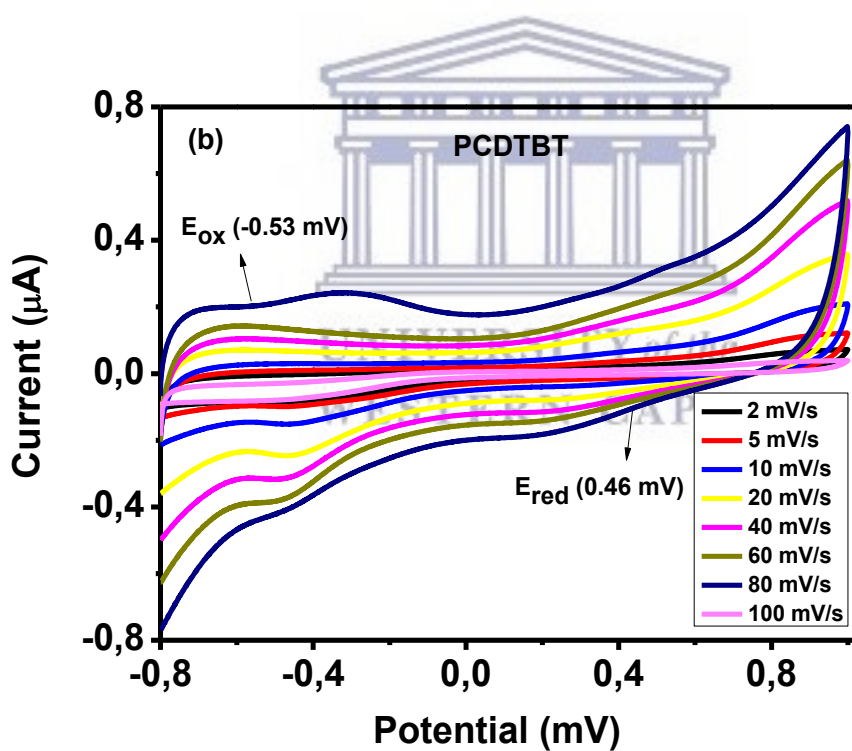
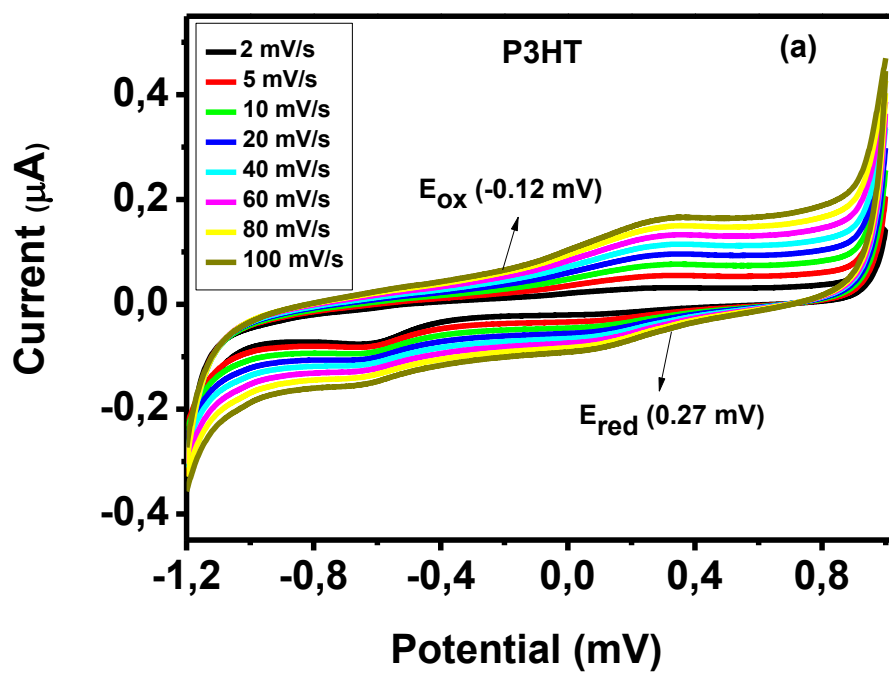


Figure 17: Cyclic voltammogram of (a) P3HT and (b) PCDTBT.

Table 1: Calculated electrochemical and optical bandgaps of the polymers.

Sample	E'ox (V)	E'red (V)	E _{HOMO} (eV)	E _{LUMO} (eV)	E _g (CV) eV	E _g (UV) eV
P3HT	-0.19	1.49	4.21	5.89	1.68	1.6
PCDTBT	-0.56	0.06	3.84	4.46	0.62	1.4

3.3.3.2. Electrochemical Impedance Spectroscopy

The electrochemical impedance analysis of the polymers was done using 0.1 M LiClO₄ as an electrolyte. The analysis of the EIS data can be done using Nyquist plots and Bode plots. This work focused more on the analysis of the EIS data using Bode plots since with Bode plots frequency data is directly supplied. The Bode plots can directly supply the phase angle data and the frequency and the value of the phase angle will determine whether a compound is considered a conductor, semiconductor or an insulator. The increase in the capacitive effect is denoted by the increase in the value of the phase angle (Gonçalves *et al.*, 2017 and Habelhames *et al.*, 2014). The phase angle maximum for bare platinum electrode is occurring at 78.1° and at a frequency of 436 Hz as shown in **Figure 18**. From **Figure 19**, it can be concluded that the phase angle maximum for P3HT occurs at 82.1° and at a frequency of 3290 Hz. The phase angle maximum for the PCDTBT occurring at 81.4° and at a frequency of 2740 Hz. The frequency at which the maxima of the phase angle is reached can be used to conclude the whether there is fast electron transfer or slow electron transfer. The data that was found can lead to the conclusion that there is relatively fast electron transfer occurring in P3HT, since the capacitive effect maximum reached has relatively high frequencies in comparison with PCDTBT (Gonçalves *et al.*, 2017).

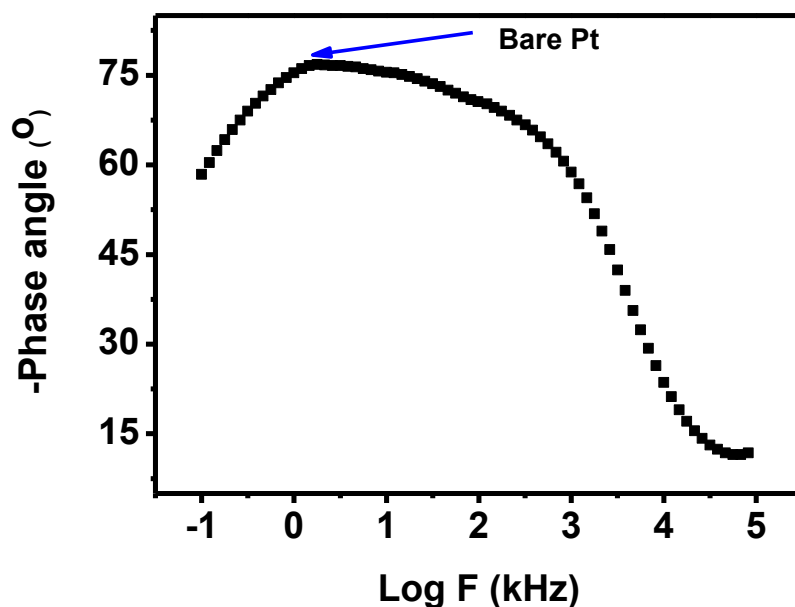


Figure 18: The Bode plots of Bare Pt electrode analysed using 0.1 M LiClO₄.

EIS can be utilized for analytical description of nanomaterials at the electrode/electrolyte interface. The charge dissipation provides information about interactions between electroactive materials or any biological components. The resultant impedance spectra are assessed by fitting the data to an equivalent circuit model with imaginary components that represent the Physico-chemical process. A shortened Randles equivalent circuit is used to fit the impedance data for evaluation of the processes that occur. The circuit consist of solution resistance (R_s) models the solution resistance, charge transfer resistance (R_{ct}), the resistance to the flow of ions and double layer capacitance (Cdl). **Figure 22** shows the Nquist plots for a platinum electrode modified with P3HT and PCDTBT. Lower impedance for PCDTBT is observed with R_{ct} of 4.51×10^5 k Ω in comparison to that of P3HT at 1.09×10^5 k Ω . The parameters for both P3HT and PCDTBT such as i_o (exchange current) and k_{et} (heterogeneous rate constant) are represented in **Table 2**.

These parameters are calculated from:

$$i_o = RT/nFR_{ct} \quad (5)$$

Where R is the gas constant ($8.304 \text{ JK}^{-1} \text{ mol}^{-1}$), F is Faraday constant ($96\,486 \text{ C mol}^{-1}$), n is the number of electrons and,

$$k_{et} = i_o/nFAC_o \quad (6)$$

Where A is the area of the electrode (cm^2) and C_o is the concentration of the solution (mol cm^{-3}).

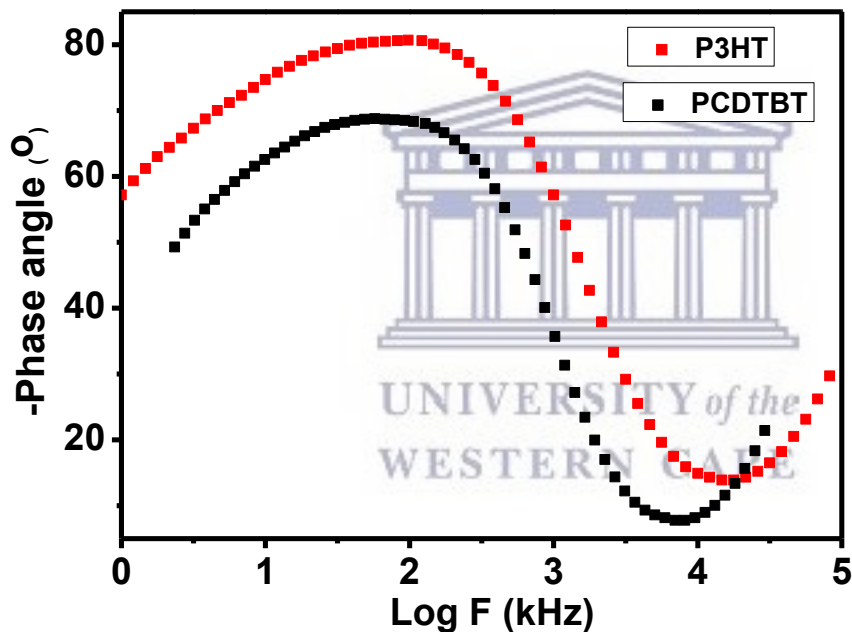


Figure 19: Bode plot that describes impedance behaviour of phase angle for P3HT and PCDTBT analysed using 0.1 M LiClO_4 .

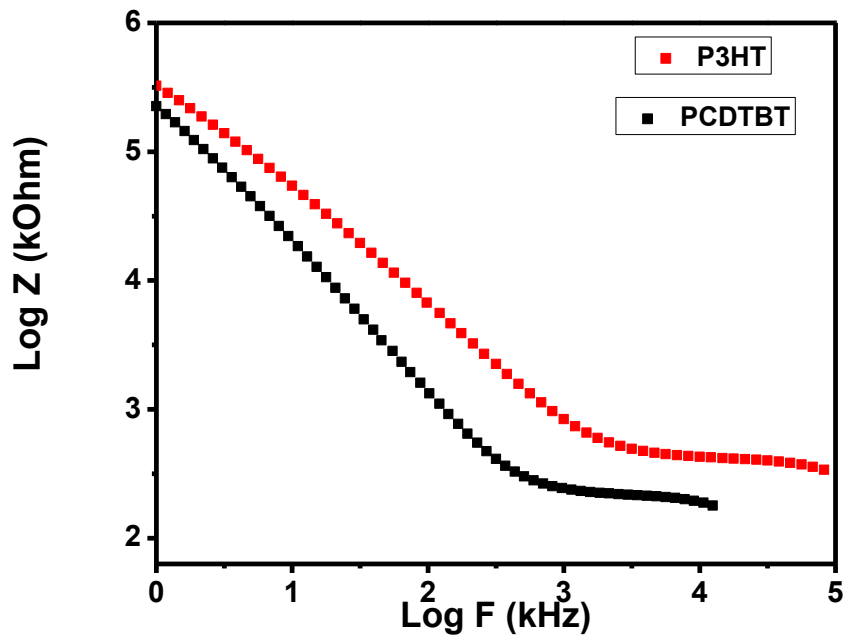


Figure 20: Bode plot that describes impedance behaviour of absolute value for P3HT and PCDTBT analysed using 0.1 M LiClO₄.

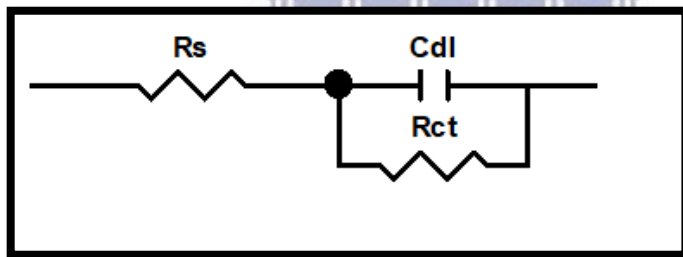


Figure 21: Simplified Randles equivalent circuit for P3HT and PCDTBT.

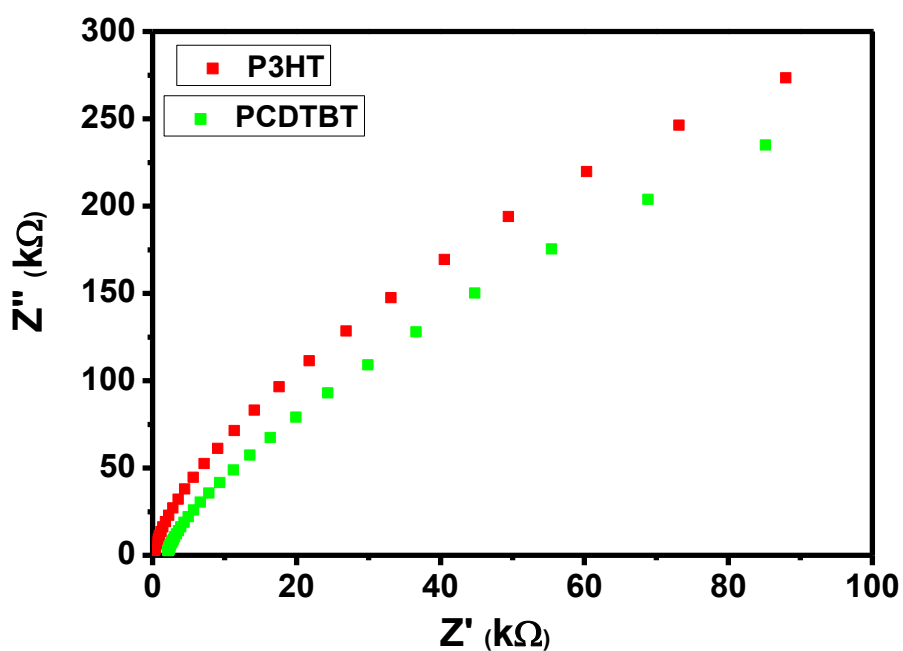


Figure 22: Nyquist plot of P3HT and PCDTBT in 0.1 M LiClO₄ at 80 mV applied potential.

Table 2: Calculated electrochemical impedance parameters from the Nyquist plot.

Sample	R_s (k Ω)	Cdl (μ F)	R_{ct} (k Ω)	I_0	k_{et} (cm ² s ⁻¹)
PCDTBT	248.6	9.57×10^{-7}	4.52×10^5	4.78×10^{-9}	2.47×10^{-12}
P3HT	430.6	2.69×10^{-7}	1.09×10^5	1.97×10^{-9}	1.02×10^{-12}

3.4. Conclusion

From the obtained results the different representations of the EIS showed to be a powerful tool for evaluating the degradation process in the poly (3-hexylthiophene) thin film electrodes. Adjusting the EIS data to an equivalent circuit, it was possible to evaluate an increase in the charge-transfer resistance (R_{ct}) at the P3HT/electrolyte interface than the PCDTBT interface and a decrease in the low-frequency capacitance that is related to the load of intercalated charge within the polymeric film in order to maintain charge neutrality. Such achievement corroborates the cyclic voltammogram, where a shift and a diminishment of the oxidation/reduction peak intensity was assigned to a hindering in the ionic intercalation process within the polymeric film. In order to enhance efficiencies even further research activities for new materials are needed with better aligned energy levels, by narrowing the donor bandgap to enhance light absorption. It can be observed that both polymer exhibit small bandgap within the range of less than 1.7 eV for better light absorption. PCDTBT has the smallest band from both the CV and UV-Vis with 0.62 and 1.4 eV, respectively. Looking specifically at the small bandgap polymers, this class of materials does not show the superior charge dissociation, transport, and morphology control as is the case with P3HT.

Bibliography

- Agarwal, A. (2010). Optical Properties and Application of Metallic Nanoparticles and their Assembled.
- Ahmed, E., Ren, G., Kim, F. S., Hollenbeck, E. C., and Jenekhe, S. A. (2011). Design of new electron acceptor materials for organic photovoltaics: Synthesis, electron transport, photophysics, and photovoltaic properties of oligothiophene-functionalized naphthalene diimides. *Chemistry of Materials*, 23, pp. 4563–4577.
- Ahn, K. S., Yan, Y., Kang, M. S., Kim, J. Y., Shet, S., Wang, H., and Al-Jassim, M. (2009). CoAl₂O₄–Fe₂O₃ p-n nanocomposite electrodes for photoelectrochemical cells. *Applied Physics Letters*, 95, pp. 2.
- An, B. K., Langley, B., Burn, P., and Meredith, P. (2009). Dendrimers for photon harvesting in organic and organic/inorganic hybrid solar cells, pp. 434.
- Anefnaf, I., Benhaddou, N., and Aazou, S. (2016). Optical , Structural and Photoconductivity Properties of Organic Photovoltaic Thin Films Based on Polymer / Fullerene, pp. 3.
- Arendse, C. J. (2012). Temperature-dependence on the optical properties and the phase separation of polymer – fullerene thin films, pp 4282–4289.
- Bakar, N. A., Supangat, A., and Sulaiman, K. (2014). Controlling the morphological, structural, and optical properties of one-dimensional PCDTBT nanotubes by template wetting. *Nanoscale Research Letters*, 9, pp. 1–6.
- Bhosale, S. V., Jani, C. H., and Langford, S. J. (2008). Chemistry of naphthalene diimides. *Chem. Soc. Rev.*, 37, pp. 331–342.

- Bkakri, R., Chehata, N., Kusmartseva, O. E., Kusmartsev, F., and Song, M. (2015). Charge Transfer and Transport Properties in P3HT and P3HT : Graphene Based Organic Solar Cells, 3, pp. 1–5.
- Bond, G. C. (2008). Faraday Discussion 138: Nanoalloys – From Theory to Applications. *Platinum Metals Review*, 52, pp. 107–109.
- Cardon, F., and Gomes, W. P. (1982). Photovoltaic and Photoelectrochemical Solar Energy Conversion. *Solar Energy*, 29, pp. 267.
- Chen, S., Liu, L., and Wang, T. (2005). Investigation of the mechanical properties of thin films by nanoindentation, considering the effects of thickness and different coating-substrate combinations. *Surface and Coatings Technology*, 191, pp. 25–32.
- Chen, Y. T., and Wu, C. W. (2013). Effect of grain size on nanomechanical property Ni80Fe20 thin film. *Intermetallics*, 34, pp. 89–93.
- Choi, W. S., Chisholm, M. F., Singh, D. J., Choi, T., Jellison, G. E., and Lee, H. N. (2012). Wide bandgap tunability in complex transition metal oxides by site-specific substitution. *Nature Communications*, pp. 3.
- Clarke, T. M., Eng, M. P., Barlow, S., and McCulloch, I. (2012). Charge photogeneration in donor / acceptor organic solar cells Charge photogeneration in donor / acceptor organic solar cells, pp. 85.
- Diebold, U. (2003). Structure and properties of TiO₂ surfaces: A brief review. *Applied Physics A: Materials Science and Processing*, 76, pp. 681–687.
- Doeleman, H. (2012). Limiting and realistic efficiencies of multi-junction solar cells, pp. 3.

- Etgar, L. (2013). Semiconductor nanocrystals as light harvesters in solar cells. *Materials*, 6, pp. 445–459.
- Express, O. M. (2017). Efficient photoinduced charge transfer in Efficient photoinduced charge transfer.
- Faculty, T. A., Jung, J., and Fulfillment, I. P. (2015). "Organic-inorganic nanocomposites for renewable energy conversion devices", pp. 6.
- Ge, J., and Yan, Y. (2017). Synthesis and characterization of photoelectrochemical and photovoltaic $\text{Cu}_2\text{BaSnS}_4$ thin films and solar cells. *Journal of Material Chemistry C*, 5, pp. 6406–6419.
- Gliboff, M. (2013). Molecular Level Understanding of Interfaces and Excited State Electronic Structure in Organic Solar Cells Using Soft X-ray Techniques.
- Gonçalves, R., Pereira, E. C., and Marchesi, L. F. (2017). The overoxidation of poly(3-hexylthiophene) (P3HT) thin film: CV and EIS measurements. *International Journal of Electrochemical Science*, 12, pp. 1983–1991.
- Gratzel Michael. (2001). Photoelectrochemical cells. *Nature*, 414, pp. 338–344.
- Guo, X., Kim, F. S., Seger, M. J., Jenekhe, S. A., and Watson, M. D. (2012). Naphthalene diimide-based polymer semiconductors: Synthesis, structure-property correlations, and n-channel and ambipolar field-effect transistors. *Chemistry of Materials*, 24, pp. 1434–1442.
- Gutmann, J. S. (2010). Comparison of Hybrid Blends for Solar Cell Application, pp. 301–312.

- Habelhames, F., Zerguine, W., and Nessark, B. (2014). Improvement of optical and photoelectrochemical properties of conducting polymer by incorporation of ZnO nanoparticles. *Journal of Materials and Environmental Science*, 5, pp. 2139–2144.
- Hankins, M. (1999). of photovoltaic systems in Kenya, pp. 92–99.
- Henssler, J. T., Zhang, X., and Matzger, A. J. (2009). Thiophene/thieno[3,2-b]thiophene co-oligomers: Fused-ring analogues of sexithiophene. *Journal of Organic Chemistry*, 74, pp. 9112–9119.
- Heremans, P., Cheyns, D., and Rand, B. P. (2009). Strategies for increasing the efficiency of heterojunction organic solar cells: Material selection and device architecture. *Accounts of Chemical Research*, 42, pp. 1740–1747.
- Herzog, A. V., Lipman, T. E., and Kammen, D. M. Renewable energy sources, pp. 1–63.
- Higashihara, T., Ohshimizu, K., Ryo, Y., Sakurai, T., Takahashi, A., Nojima, S., and Ueda, M. (2011). Synthesis and characterization of block copolythiophene with hexyl and triethylene glycol side chains. *Polymer*, 52, pp. 3687–3695.
- Hodes, G. (2012). Photoelectrochemical cell measurements: Getting the basics right. *Journal of Physical Chemistry Letters*, 3, pp. 1208–1213.
- Hoppe, H., and Sariciftci, N. S. (2004). Organic solar cells: An overview. *Journal of Materials Research*, 19, pp. 1924–1945.
- Hou, J., and Guo, X. (2013) Active Layer Materials for Organic Solar Cells.
- Hussein, A. A., Sultan, A. A., Obeid, M. T., Abdulnabi, A. T., and Ali, M. T. (2015). Synthesis and Characterization of poly (3-hexylthiophene), 7, pp. 33–38.

- Jardas, D. (2012). Photovoltaic systems. *Chemical Physics Letters*, 682, pp. 301–428.
- Jian, S. R., Chen, G. J., and Hsu, W. M. (2013). Mechanical properties of Cu₂O thin films by nanoindentation. *Materials*, 6, pp. 4505–4513.
- Jiang, H., Moon, K. S., Dong, H., Hua, F., and Wong, C. P. (2006). Size-dependent melting properties of tin nanoparticles. *Chemical Physics Letters*, 429, pp. 492–496.
- Joffe, H. (2012). Challenges for South Africa's Electricity Supply Industry. *Helen Suzman Foundation Focus*, 64, pp. 32–37.
- John, S. V., Mayedwa, N., Ikpo, C., Molefe, L. Y., Ndipingwi, M. M., Dywili, N. R., and Iwuoha, E. (2016). Photoluminescence quenching of poly(octylfluorenylbenzothiadiazole) luminophore by n-type cobalt(II) salicylaldimine metallodendrimer. *Synthetic Metals*, pp. 114–122.
- Kabongo, G. L., Mbule, P. S., Mhlongo, G. H., Mothudi, B. M., Hillie, K. T., and Dhlamini, M. S. (2016). Photoluminescence Quenching and Enhanced Optical Conductivity of P3HT-Derived Ho³⁺-Doped ZnO Nanostructures. *Nanoscale Research Letters*, 11.
- Karzazi, Y., and Arbouch, I. (2014). Inorganic photovoltaic cells : Operating principles, technologies and efficiencies - Review, 5, pp. 1505–1515.
- Kawakami, R., Ito, K., Sato, Y., Mori, Y., Adachi, M., and Yoshikado, S. (2011). Preparation and Evaluation of TiO₂ Nanoparticle Thin Films using Electrophoresis Deposition Method. *Materials Science and Engineering*, 18, pp. 6.

- Kopidakis, N., Mitchell, W. J., Van De Lagemaat, J., Ginley, D. S., Rumbles, G., Shaheen, S. E., and Rance, W. L. (2006). Bulk heterojunction organic photovoltaic devices based on phenyl-cored thiophene dendrimers. *Applied Physics Letters*, 89, pp. 1–4.
- Kümbül, A., Turaç, E., Dursun, T., and Şahmetlioğlu, E. (2009). Synthesis and characterization of conducting copolymer of (N1,N3-bis(thiophene-3-ylmethylene)benzene-1,3-diamine-co-3,4-ethylenedioxythiophene). *Chemical Papers*, 64, pp. 114–117.
- Kwong, C. Y., Choy, W. C. H., Djurišić, A. B., Chui, P. C., Cheng, K. W., and Chan, W. K. (2004). Poly(3-hexylthiophene): TiO₂ nanocomposites for solar cell applications. *Nanotechnology*, 15, pp. 1156–1161.
- Li, Y. (2011). Photovoltaic Systems for Solar Electricity Production, pp 1–4.
- Licht, S. (2002). Photoelectrochemical Solar Energy Storage. *Encyclopedia of Electrochemistry: Semiconductor Electrodes and Photoelectrochemistry*, 6, pp. 317–345.
- Liu, J., Chen, L., Gao, B., Cao, X., Han, Y., Xie, Z., and Wang, L. (2013). Constructing the nanointerpenetrating structure of PCDTBT:PC₇₀BM bulk heterojunction solar cells induced by aggregation of PC₇₀BM via mixed-solvent vapor annealing. *Journal of Materials Chemistry A*, 1, pp. 6216.
- Liu, R. (2014). Hybrid Organic/Inorganic Nanocomposites for Photovoltaic Cells. *Materials*, 7, pp. 2747–2771.

- Lu, X., Hlaing, H., Germack, D. S., Peet, J., Jo, W. H., Andrienko, D., and Ocko, B. M. (2012). Bilayer order in a polycarbazole-conjugated polymer. *Nature Communications*, 3, pp. 795–797.
- Luber, E. J., and Buriak, J. M. (2013). Reporting Performance in Organic Photovoltaic Devices BT. *American Chemistry of Society Nanotechnology*, 7, pp. 4708–4714.
- Luechai, A., Gasiorowski, J., Petsom, A., Neugebauer, H., Sariciftci, N. S., and Thamyongkit, P. (2012). Photosensitizing porphyrin–triazine compound for bulk heterojunction solar cells. *Journal of Materials Chemistry*, 22, pp. 230.
- Malgas, G. F., Arendse, C. J., Mavundla, S., and Fransciious, R. Interfacial analysis and properties of regioregular Poly (3-Hexyl thiophene) spin-coated on an Indium tin oxide coated glass substrate, 12, pp. 1–17.
- Mayedwa, N. (2015). Development of platino-iridium / ruthenium telluride nanoalloy electrode systems for possible application in ammonia fuel cell.
- Minnaert, B., and Veelaert, P. (2012). Guidelines for the Bandgap Combinations and Absorption Windows for Organic Tandem and Triple-Junction Solar Cells, pp. 1933–1953.
- Mohammad Bagher, A. (2014). Comparison of Organic Solar Cells and Inorganic Solar Cells. *International Journal of Renewable and Sustainable Energy*, 3, pp. 53.
- Mora, M. B., Monroy, B. M., and Lugo, J. E. (2017). Solar Energy Materials & Solar Cells Materials for downconversion in solar cells : Perspectives and challenges. *Solar Energy Materials and Solar Cells*, 165, pp. 59–71.
- Nelson, J. (2011). Polymer: Fullerene bulk heterojunction solar cells. *Materials Today*, 14, pp. 462–470.

- Ohshimizu, K., Takahashi, A., Rho, Y., Higashihara, T., Ree, M., and Ueda, M. (2011). Synthesis and characterization of polythiophenes bearing aromatic groups at the 3-position. *Macromolecules*, *44*, pp. 719–727.
- Potratz, S., Mishra, A., and Bäuerle, P. (2012). Thiophene-based donor-acceptor co-oligomers by copper-catalyzed 1,3-dipolar cycloaddition. *Beilstein Journal of Organic Chemistry*, *8*, pp. 683–692.
- Pv, T., and Asso, E. P. I. (2017). Opto-Electronics Review Top PV market solar cells 2016. *Opto-Electronics Review*, *25*, pp. 55–64.
- Rahman, M. Y. A., Umar, A. A., Taslim, R., Roza, L., Saad, S. K. M., and Salleh, M. M. (2014). TiO₂ and ZnO Thin Film Nanostructure for Photoelectrochemical Cell Application: *International Journal of Electroactive Material*, *2*, pp. 4–7.
- Rait, S., Kashyap, S., Bhatnagar, P. K., Mathur, P. C., Sengupta, S. K., and Kumar, J. (2007). Improving power conversion efficiency in polythiophene/fullerene-based bulk heterojunction solar cells. *Solar Energy Materials and Solar Cells*, *9*, pp. 757–763.
- Romero, B. (2017). Optical , morphological and electrical properties of P3HT : SiNWs nanocomposite deposited on flexible substrate. Optical , morphological , and electrical properties of P3HT : SiNWs nanocomposite deposited on flexible substrate : effect of SiNWs concent. *Materials Research Express*, *46*. pp. 1482.
- Saini, V., Li, Z., Bourdo, S., Dervishi, E., Xu, Y., Ma, X., and Carolina, N. (2009). Electrical, Optical, and Morphological Properties of P3HT-MWNT Nanocomposites Prepared by in Situ Polymerization, pp. 8023–8029.

- Scharber, M. C., and Sariciftci, N. S. (2013). Efficiency of bulk-heterojunction organic solar cells. *Progress in Polymer Science*, 38, pp. 1929–1940.
- Schubert, M., Dolfen, D., Frisch, J., Roland, S., Steyrleuthner, R., Stiller, B., and Neher, D. (2012). Influence of aggregation on the performance of all-polymer solar cells containing low-bandgap naphthalenediimide copolymers. *Advanced Energy Materials*, 2, pp. 69–380.
- Seyler, H., Subbiah, J., Jones, D. J., Holmes, A. B., and Wong, W. W. H. (2013). Controlled synthesis of poly(3-hexylthiophene) in continuous flow. *Beilstein Journal of Organic Chemistry*, 9, pp. 1492–1500.
- Shafiee, A., Salleh, M. M., and Yahaya, M. (2011). Determination of HOMO and LUMO of [6,6]-phenyl C61-butyric acid 3-ethylthiophene ester and poly (3-octylthiophene-2, 5-diyl) through voltametry characterization. *Sains Malaysiana*, 40, pp. 173–176.
- Sharma, M. K., Buchner, R. D., Scharmach, W. J., Swihart, M. T., Sharma, M. K., Buchner, R. D., and Swihart, M. T. (2013). Creating Conductive Copper – Silver Bimetallic Nanostructured Coatings Using a High Temperature Reducing Jet Aerosol Reactor Creating Conductive Copper, pp. 32.
- Shastry, T. A., Balla, I., Bergeron, H., Amsterdam, S. H., Marks, T. J., and Hersam, M. C. (2016). Mutual Photoluminescence Quenching and Photovoltaic Effect in Large-Area Single-Layer MoS₂ Polymer Heterojunctions. *American Chemistry of Society Nanotechnology*, 10, pp. 10573–10579.
- Sheng-Rui Jian, G. J. C., and Sheng-Rui Jian, W. M. H. (2006). Mechanical Properties of Cu₂O Thin Films by Nanoindentation. *Chemistry, an Asian Journal*, 1, pp. 148–154.

- Thangavelu, K., Annamalai, R., and Arulnandhi, D. (2013). Preparation and Characterization of Nanosized TiO₂ Powder by Sol-Gel Precipitation Route. *International Journal of Emerging Technology and Advanced Engineering*, 3, pp. 636–639.
- Tumuluri, A., Naidu, K. L., and Raju, K. C. J. (2014). Band gap determination using Tauc 's plot for LiNbO₃ thin films. *International Journal of Chemistry Technology Research*, 6, pp. 3353–3356.
- Usluer, Ö., Kästner, C., Abbas, M., Ulbricht, C., Cimrova, V., Wild, A., and Egbe, D. A. M. (2012). Charge carrier mobility, photovoltaic, and electroluminescent properties of anthracene-based conjugated polymers bearing randomly distributed side chains. *Journal of Polymer Science, Part A: Polymer Chemistry*, 50, pp. 3425–3436.
- Vatansever, D., Siores, E., and Shah, T. (2012). Alternative Resources for Renewable Energy : Piezoelectric and Photovoltaic Smart Structures, pp. 681.
- Vemulamada, P., Hao, G., Kietzke, T., and Sellinger, A. (2008). Efficient bulk heterojunction solar cells from regio-regular-poly(3,3-didodecyl quaterthiophene)/PC₇₀BM blends. *Organic Electronics: Physics, Materials, Applications*, 9, pp. 661–666.
- Watanabe, R., and Miyano, K. (2011). Metal nanoparticles in a photovoltaic cell: Effect of metallic loss. *American Institute of Physics Advances*, 1, pp. 6.
- Wei, D., Andrew, P., and Ryhänen, T. (2010). Electrochemical photovoltaic cells-review of recent developments. *Journal of Chemical Technology and Biotechnology*, 85, pp. 1547–1552.

- Winder, C. (2002). Sensitization of low bandgap polymer bulk heterojunction solar cells. *Thin Solid Films*, 403, pp. 373–379.
- Xu, Q. (2007). Optical Properties of Poly (3-hexylthiophene) / ZnS, pp. 48–63.
- Yang, J., Clark, N., Long, M., Xiong, J., Jones, D. J., Yang, B., and Zhou, C. (2015). Solution stability of active materials for organic photovoltaics. *Solar Energy*, 113, pp. 181–188.
- Yin, H., Lok, K., Hoi, C., Ho, Y., Ka, H., Lee, H., and Kong, S. (2017). Bulk-heterojunction solar cells with enriched polymer contents, 40, pp. 1–7.
- Zeng, X., and Gan, Y. X. (2010). Nanocomposites for Photovoltaic Energy Conversion.
- Zhong, L., Beaudette, C., Guo, J., Bozhilov, K., and Mangolini, L. (2016). Tin nanoparticles as an effective conductive additive in silicon anodes. *Nature Publishing Group*, pp. 1–8.
- Zhou, D., Ji, Z., Jiang, X., Dunphy, D. R., Brinker, J., and Keller, A. A. (2013). Influence of material properties on TiO₂ Nanoparticle agglomeration, 8, pp. 1–7.

CHAPTER FOUR

Summary

One of the challenges in the field of organic photovoltaics is developing alternative to the family of fullerene derivatives that are commonly used as acceptor material. Herein we describe the synthesis and optoelectronic properties of three new electron acceptor materials that are developed from transitional metals. The acceptor materials will be combined with poly(3-hexylthiophene) as electron donor material in bulk heterojunction solar cells. The performance of the photovoltaic devices is limited by incomplete exciton dissociation and a sluggish separation of the photogenerated electrons and holes at low fields. The separation is in competition with charge recombination to the triplet state. In addition, the low electron mobility in the acceptor polymers hampers charge collection. This chapter discusses the results obtained from the study of the novel stannum-based bimetallic nanoparticles synthesised as electron accepting materials in the fabrication of bulk heterojunction photovoltaic cells. The chapter focuses mainly on the characterisation of Sn and SnTi, SnV, SnCr nanoparticles prior to their application in the photovoltaic cells. These polyvinylpyrrolidone (PVP) capped nanoparticles were successfully synthesised by the conventional borohydride reduction of metal precursors at 70 °C. The optical (UV-vis and PL), structural (XRD and SAXS), morphological (HR-TEM) and electrochemical (CV and EIS) properties of these nanoparticles are therefore discussed. The potential application of the nanoparticles as acceptor materials in photovoltaic application was further investigated.

Novel Stannum-based Nanoparticles as Acceptor Material for Organic Photovoltaic Devices

Abstract

The aim of this chapter was to establish design rules for designing and synthesising acceptor bimetallic nanoparticles as potential acceptor materials for photovoltaic cells. The design explored in this chapter was based on the well-known transition metals. Three transition metals using different combinations of stannum transition metal as the core have been synthesised and characterised. The electrochemical properties of the different nanoparticles revealed, however, that stannum-chromium (SnCr) can be used as electron acceptor towards photovoltaic cells. The nanoparticles were formed, then immediately quenched and deposited on a glass substrate. The effect of the stannum content of the mixed bimetallic nanoparticles films on their electrical conductivity was studied systematically, which revealed an abrupt transition from low conductivity to high conductivity. In photovoltaics fabrication, metal nanoparticles offer the prospect of increasing device efficiency by reducing surface reflectance and/or increasing light-trapping within thin-film devices. However, metal nanoparticles can also decrease the efficiency of solar cells. For example, due to absorption of light within the nanoparticle or by increasing reflectance of the front surface due to back-scattering. To enhance light-trapping in bimetallic nanoparticles photovoltaic cells, we require nanoparticles that exhibit low absorption in the visible and near-infrared (NIR), and large scattering cross-sections across the useful solar spectrum. Therefore, metal nanoparticles could remove the need for rough textured surfaces while providing improved light-trapping; however, if utilized incorrectly they could introduce additional loss mechanisms.

These additional loss mechanisms must be minimized by the development of a complete understanding of the optical properties of particles of different size, shape and metal type. Synthetic methods have been discussed in detail to provide the reader with an extensive knowledge of controlling the nanoparticle physical characteristics (size, size distribution, morphology).

4.1 Introduction

The synthesis of metallic nanoparticles is of great current interest and potential future industrial importance. Compared to the corresponding bulk materials, nanoparticles have improved catalytic, optical, and electronic properties due to their high surface to volume ratio, confinement of free electrons within finite domains, and changes in their electronic structure at very small sizes (Okumu *et al.*, 2017). These properties depend upon the size, shape, and composition of the metal nanoparticles. Interesting properties can arise in bimetallic structures through synergistic effects of their components (Toshima and Yonezawa, 1998 and Shah *et al.*, 2012). The design and synthesis of bimetallic nanomaterials (BM) have received considerable interest because of their myriad properties and applications in optics, magnetism, catalysis, and others, due to their high tenability and superior features compared with those of their monometallic counterparts (Okumu *et al.*, 2017). BMs may form core-shell structures, hetero-structures, and alloy nanocrystals, this formation diversity increases the mass specific activity (MSA) of the nanoparticles while also minimizing the cost by using precious metals only on the surface of the particles (Dutta *et al.*, 2012 and Wadams *et al.*, 2014). Nanomaterials properties strongly depend on their size, structure and morphology (Mora *et al.*, 2017).

Size provides an important control over many of the physical and chemical properties of nanoscale materials including luminescence, conductivity, and catalytic activity. Mono-nanoparticles e.g.: Ti, V and Cr have been widely studied, but much room remains for exploring interesting properties of multicomponent nanoparticles (Toshima and Yonezawa, 1998). This project aims at realizing a high efficiency organic device using the multicomponent nanoparticles concept and metal nanoscale features to enhance the overall cell performance. In recent years the unique properties of bimetallic nanoparticles had led to new applications and the possibility of making new products, for example catalyst, sensors, and substrates for surface enhanced Raman scattering (Lee *et al.*, 2018). This area of nanoscience was gaining mounting attention in the field of catalysis also due to the synergistic effects. Bimetallic nanoparticles, either as alloys or as core-shell structures, exhibited unique electronic, optical and catalytic properties compare to pure metallic nanoparticles. It has been reported that the use of bimetallic nanoparticles in solar cells could produce stronger field and greater absorption enhancement. The light absorbed by the absorption layer can contribute to the external electricity, thus it is essential to analyse the absorption enhancement in the absorption layer of the thin film solar cell. There are some concerns regarding these materials, for an example; the particle size. The particles need to be as small possible to achieve the highest line resolution and it is important to minimize the surface contamination on the particle (i.e. oxide or adsorbates) to facilitate further reactions. This may require an active capping of the particles with organic or inorganic protectants.

4.2 Experimental

4.2.1 Materials and Synthesis Procedure

4.2.1.1 Materials

Tin (II) chloride (SnCl_2), sodium borohydride (NaBH_4), polyvinylpyrrolidone (PVP), chromium hexacarbonyl (C_6CrO_6), vanadium (III) chloride (VCl_3), and titanium isopropoxide ($\text{Ti}[\text{OCH}(\text{CH}_3)_2]_4$) were obtained at Sigma-Aldrich and used without any further purification. All solutions were prepared in ultra-pure water (H_2O).

4.2.1.2 Synthesis procedure

➤ Preparation of Sn nanoparticles

Sn nanoparticles were synthesised by following method reported by *Mayedwa* (2015). Briefly, 10 mL of 0.00168 M NaBH_4 solution aged for 3 h was added drop wise into 20 mL of a 0.00018 M SnCl_2 solution with vigorous stirring, using a round bottom flask at a temperature of 90 °C. The surfactant PVP was then added to the solution and the reaction was left for 16 hours to reach completion. The complete reduction of the Sn nanoparticles was centrifuged and washed 3 – 4 times with ultra-pure water. Then dried in a vacuum over night at 60 °C.

➤ Synthesis of SnCr, SnTi and SnMo nanoparticles

SnCr , SnV and SnTi nanoparticles were synthesised by adding drop wise 10 mL of 1.68 mM NaBH_4 solution aged for 3 h to aqueous solution into 20 mL of fixed 0.00018 M SnCl_2 , was varied with 0.00018 M (C_6CrO_6 , VCl_3 and $\text{Ti}[\text{OCH}(\text{CH}_3)_2]_4$). These were added into three different round bottom flasks then stirred vigorously at 90 °C followed by the addition of surfactant PVP.

The reaction was left over night for the reaction to complete. The binary nanoparticles were centrifuged and washed 3 - 4 times with ultrapure water. Then dried over night at 60 °C under vacuum over (Mayedwa, 2015).

4.2.2 Instrumentation

Attenuated total reflection-Fourier transform infrared (ATR-FTIR) spectra were recorded on Perkin Elmer FTIR model 100 spectrophotometer, operating between 400 and 4000 cm^{-1} as pellets in the presence of potassium bromide (KBr). UV-Vis absorption measurements for the prepared stannum-based bimetallic nanoparticles dispersed in CB was obtained using 1 cm quartz cuvette on a Nicolet Evolution 100 UV-Visible spectrophotometer over a wavelength range of 200 to 800 nm. The PL spectra were recorded using a Nanolog Horiba with double grating excitation and emission monochromator wavelength that was used is 200 nm. Small-Angle X-Ray Scattering (SAXS) measurements for were obtained using a 1 mm thin walled capillary (i.e. liquids that contains mainly water or hydrocarbons) at the beamline ID09B. The phase and crystal structure of stannum-based nanoparticles were characterized using X-Ray diffraction (XRD) of using the Williamson-Hall method by referring to the most prominent peak (111). High resolution-transmission electron microscope (HR-TEM) equipped with an energy-dispersed spectroscopy (EDS) detector was used to study the size and morphology of samples. Copper grid (Cu) was used as sample holder for the immobilisation of (2 μL) solution of the nanoparticles, the micrographs were recorded at room temperature. Electrochemical experiments were performed using CH potentiostat at different scan rates. Wherein, platinum electrode, platinum wire and Ag/AgCl (3 M NaCl) acted as the working electrode, the counter electrode and the reference electrode, respectively. As an electrolyte a solution of 0.1 M of LiClO_4 in anhydrous acetonitrile (CH_3CN) solution was used.

4.3 Results and Discussion

4.3.1 Structural properties of nanoparticles

4.3.1.1 Fourier Transform Infrared Spectroscopy

FTIR spectrum in (**Figure 23a**) shows the IR spectra in the 400 – 4500 cm^{-1} range of PVP capped Sn nanoparticles. The broad absorption band centred at 3400 cm^{-1} is attributed to O-H stretching mode of H_2O absorbed on the surface of the product. The most striking evidence from FTIR spectrum of the PVP stabilized Sn is the broad band between 1280 and 1650 cm^{-1} which corresponds to C-N stretching motion and C=O stretching motion of monomer for PVP, respectively (Zhong *et al.*, 2016). The narrow absorption peak centred at 1444 cm^{-1} and 2939 cm^{-1} ascribed to the C–H bonding due to the presence of PVP (Bond, 2008) and this may be due to the formation of coordinate bond between the nitrogen atom of the PVP and the Sn^{2+} (Zhong *et al.*, 2016). **Figure 23b** shows the IR spectra of PVP capped SnCr, SnV and SnTi nanoparticles. The broad absorption band centred at 3219 cm^{-1} (SnCr), 3400 cm^{-1} (SnV), 3409 cm^{-1} (SnTi) is attributed to O-H stretching mode of H_2O absorbed on the surface of the product. The absorption band centred at 1444 cm^{-1} and 2939 cm^{-1} is ascribed to the C–H bonding due to the presence of PVP. This may be due to the formation of coordinate bond between the nitrogen atom of the PVP and the Sn^{2+} , V^{2+} , Ti^{2+} and Cr^{2+} . Observed FTIR band at 1100 cm^{-1} was only observed in SnV NPs which confirmed the formation of SnV bonds between V^{2+} and Sn^{2+} .

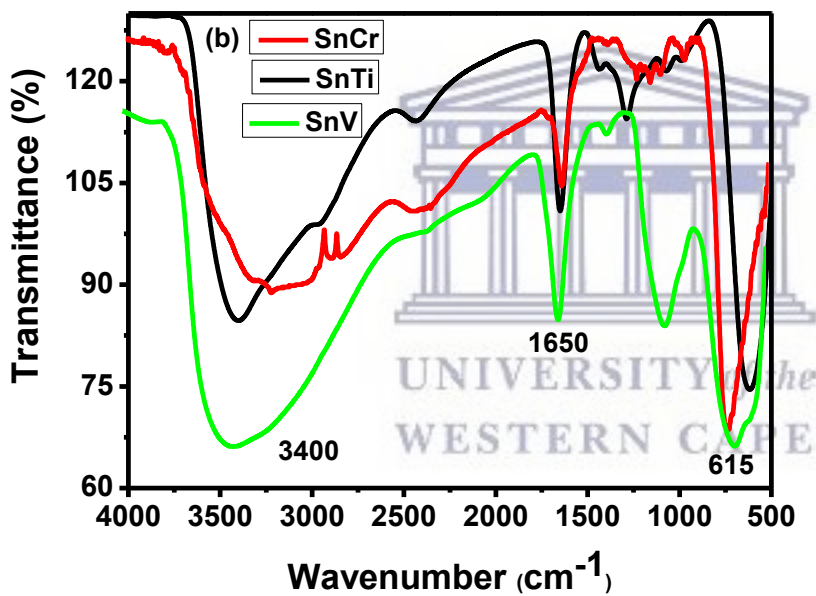
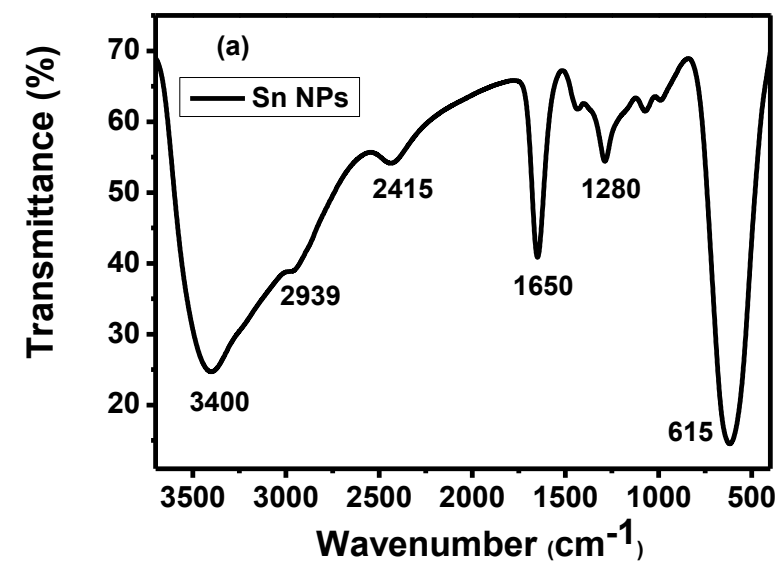


Figure 23: ATR-FTIR interferograms ranging from 500 - 4000 cm⁻¹ for (a) PVP capped Sn nanoparticles and (b) SnCr, SnV and SnTi.

4.3.1.2 X-ray Diffraction analysis

X-ray diffraction (XRD) technique was employed to investigate the crystal structure of the bimetallic nanoparticles. As illustrated in **Figure 24**, the diffractograms of the bimetallic combinations exhibit well defined sharp bands (Jian *et al.*, 2013), this is due to the increase in crystallinity by combination of two metals. The particle sizes of the bimetallic combinations determined from the XRD spectra correlate well with the sizes obtained from HR-TEM measurements. The particle size is calculated on the base of Debye Scherrer equation:

$$D = K\lambda / d \cos\theta \quad (7)$$

Where λ , d and θ attributes to the X-ray wavelength, FWHM peak and the Bragg's diffraction angle, respectively. As illustrated in **Figure 24**, five distinctive diffraction peaks were observed at $2\theta = 26^\circ$, (110), 33.6° , (101), 51.6° , (211), 65° , (301) and 79° , (321), respectively. These reflection peaks are found to be consistent with the spherical structure of the Sn NPs (Jian *et al.*, 2013). The composition of bimetallic nanoparticles in **Figure 25** was identified by the shift in the peaks which were observed at $2\theta = 25^\circ$, 24° and 30° for SnCr, SnTi and SnV, respectively. This could be attributed to combination characteristics of metals onto the tetragonal Sn^{2+} . Characteristics of the stannum based with different metals revealed slightly amorphous characteristic with the spherical structure, this may be due to the H_2O utilized during the synthesis of the nanoparticles. This is because of the temperature at which synthesis was done was lower than 100°C (Jian *et al.*, 2013). These results are in good agreement with HR-TEM and SAXS measurements.

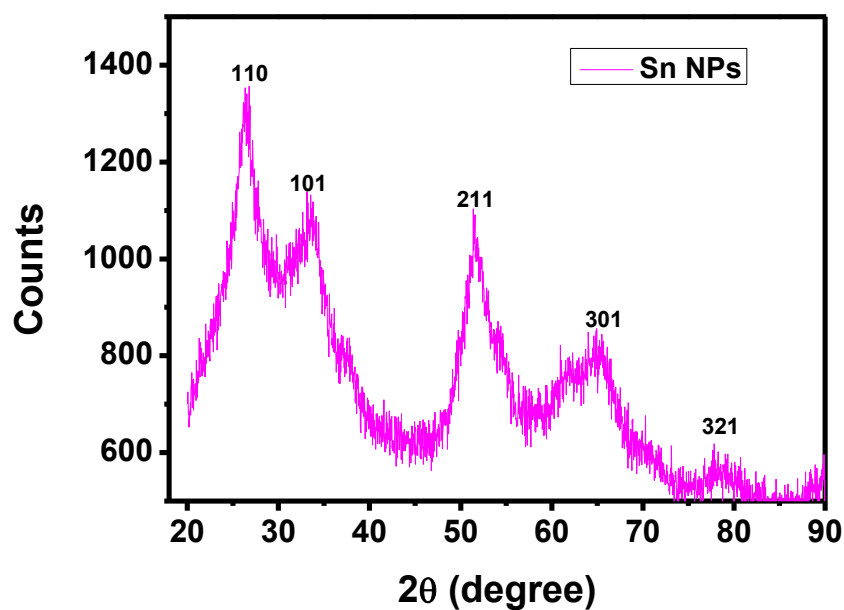


Figure 24: XRD pattern of Sn nanoparticles.

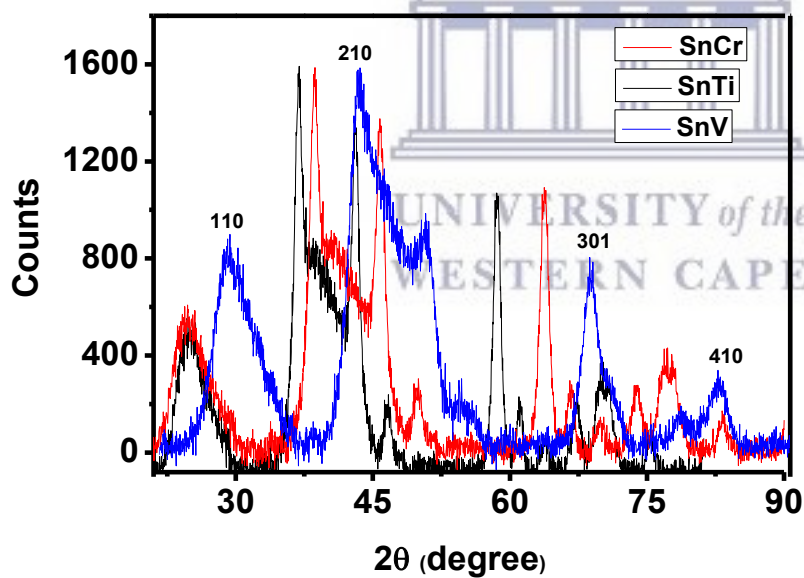


Figure 25: XRD pattern of SnCr, SnTi and SnV nanoparticles.

4.3.2 Morphological properties of nanoparticles

4.3.2.1 High Resolution - Transmission electron microscopy

The size, shape and crystallinity of the nanoparticles were investigated by high resolution transmission electron microscope (HR-TEM). **Figure 26a** shows typical HR-TEM images of the prepared Sn nanoparticles. It is observed that the nanoparticles are spherical, cubic poly-orientated and are uniformly dispersed on the Cu grid with few agglomerates on some parts of the sample. From the micrographs in **(Figure 26 [(b) and (c)])**, it is observed that the spherical nanoparticles were uniformly dispersed on Cu grid without any agglomeration of the sample. Finally; SnTi nanoparticles **Figure 26d** show images of nanoparticles that were agglomerated on the Cu grid with some poly-orientated nanoparticles dispersed on the grid. The particle size and morphology greatly influences the electrochemical activity of the nanoparticles due to the surface area and structure. It can be clearly observed that nanoparticles are poly-orientated which agrees with the results obtained in the XRD that SnCr, SnV and SnTi nanoparticles showed different diffraction patterns (Sharma *et al.*, 2013 and Mayedwa, 2015). Selected area electron diffraction pattern (SAED) shown in **Figure 27** for Sn NPs, SnCr, SnV and SnTi nanoparticles shows characteristic electron diffraction rings for the nanoparticles. The nanoparticles exhibit a high crystallinity as can be deduced from the SAED pattern as seen in **[Figure 27 (a), (b), and (c)]**. **Figure 26d** does not exhibit any crystallinity, this may be due the agglomeration as observed in HR-TEM **(Figure 26d)**. The high crystallinity of the synthesised Sn nanoparticles is observed which reveals well-defined (1 0 1) lattice fringes **(Figure 27a)**.

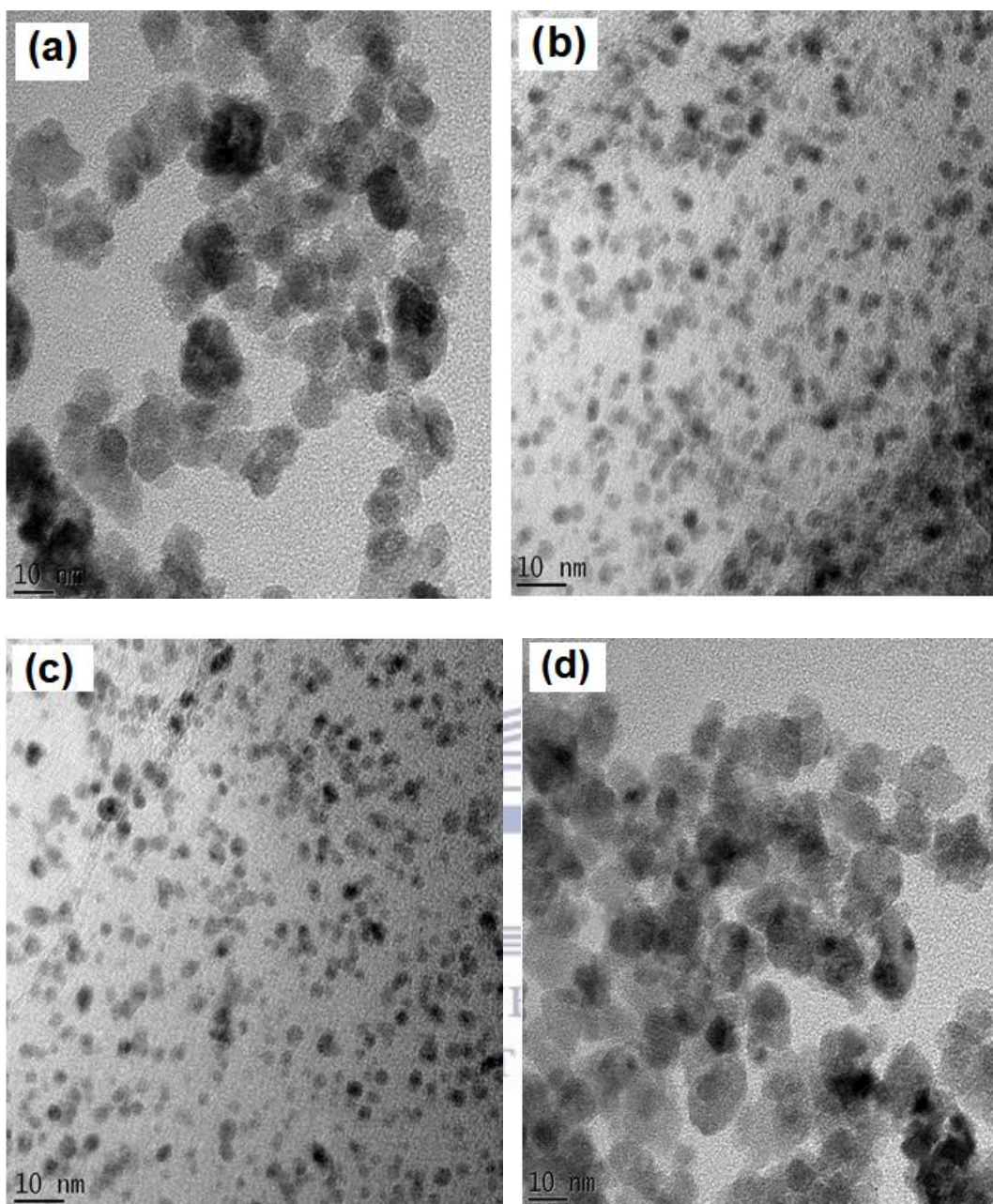


Figure 26: HR-TEM images of (a) Sn nanoparticles, (b) SnCr, (c) SnV and (d) SnTi bimetallic nanoparticles.

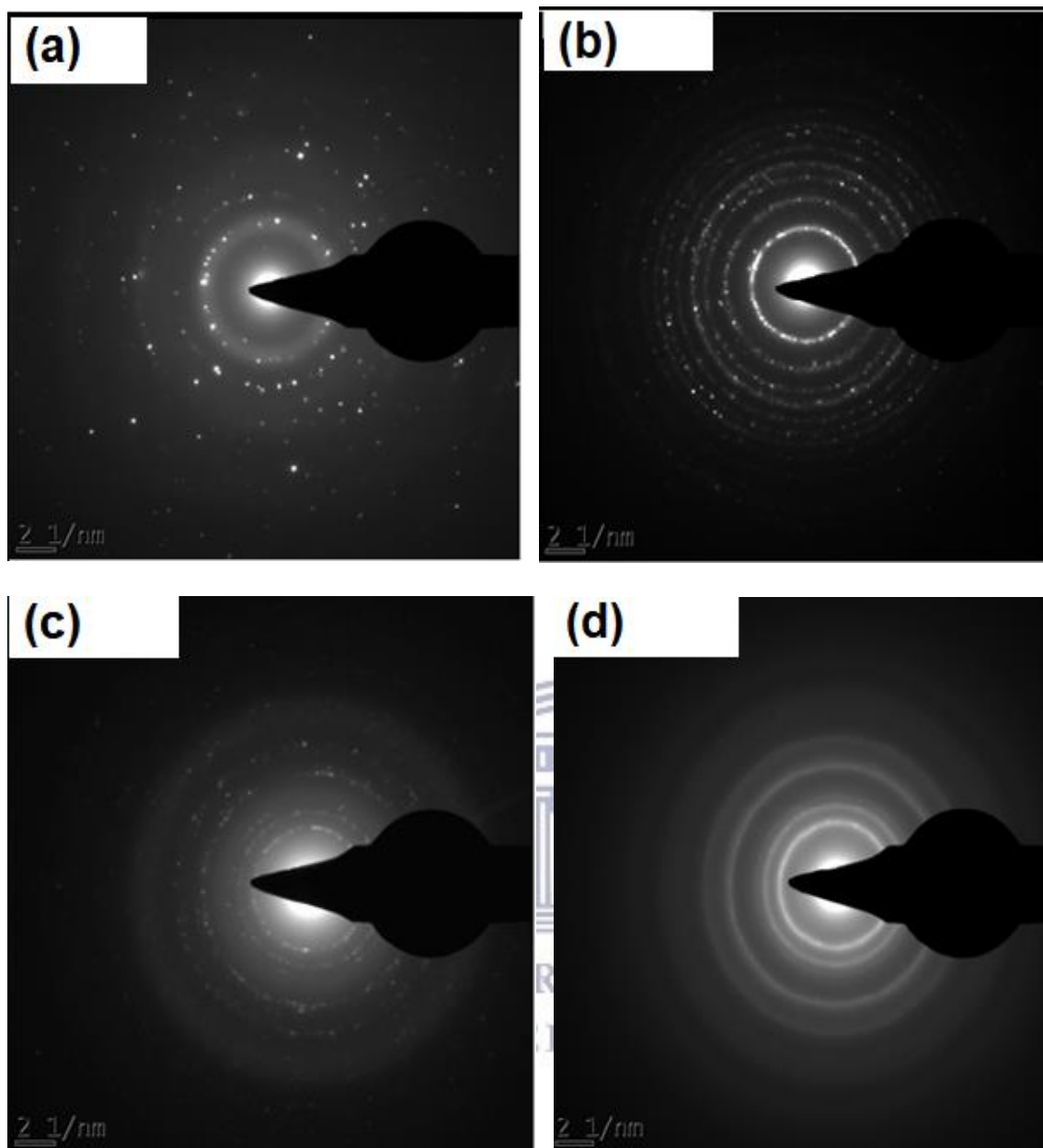
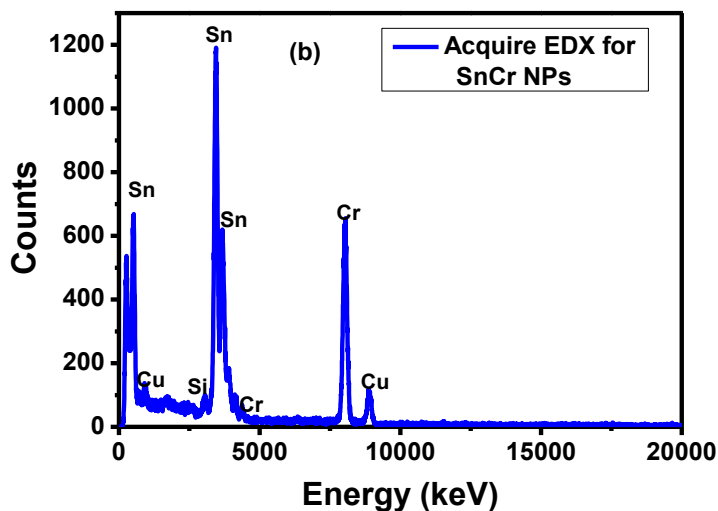
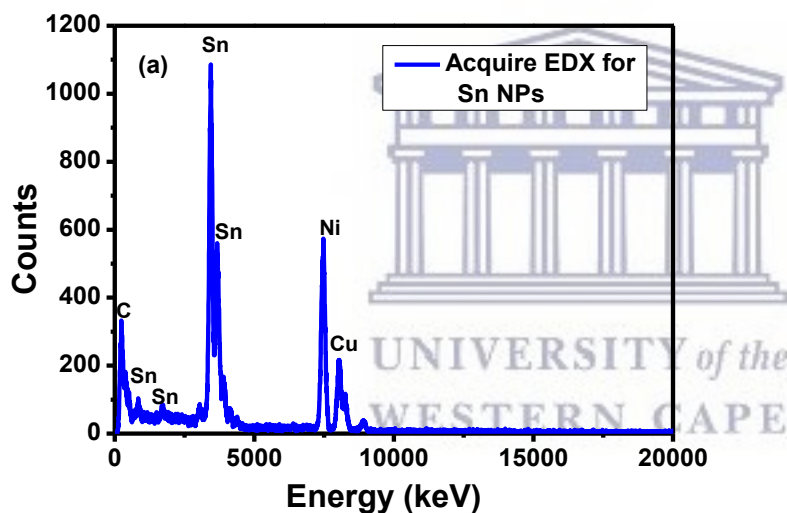


Figure 27: Selected area electron diffraction pattern (SAED) of (a) Sn nanoparticles, (b) SnCr, (c) SnV and (d) SnTi bimetallic nanoparticles.

Investigation of the elemental composition of SnCr, SnV and SnTi, nanoparticles was characterised using energy-dispersed spectroscopy (EDS). The EDS analysis (**Figure 28 (a), (b), and (c)**) of the synthesised SnCr, SnV and SnTi nanoparticles revealed the elemental composition of the nanoparticles and showed that all the three elements; Sn, Cr, V and Ti were present in the bimetallic systems. However, other elemental signals were also recorded namely; carbon, and copper. The presence of carbon may have originated from contamination during sample preparation, while copper is because of the copper grid and nickel grid onto which the nanoparticles were immobilised for the HR-TEM analysis (Trouillet *et al.*, 2000).



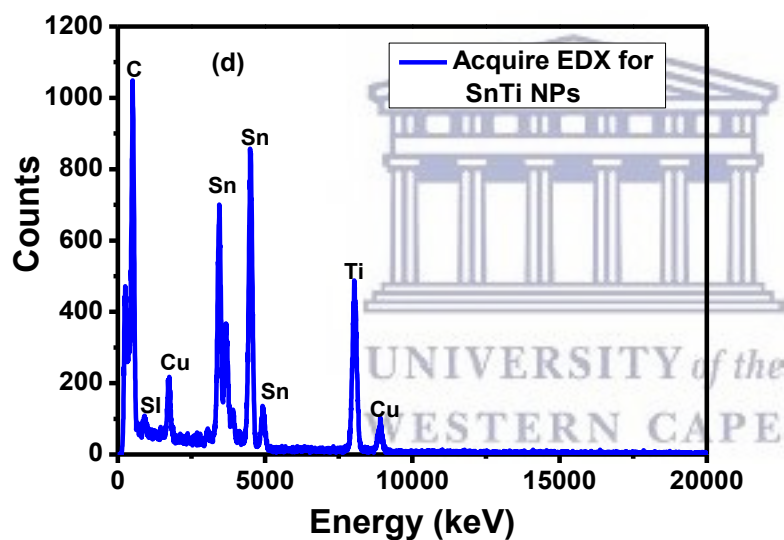
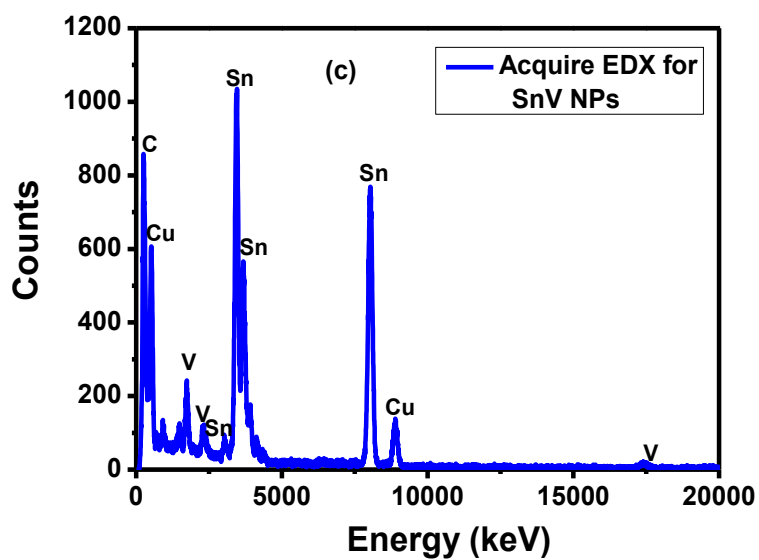


Figure 28: Energy dispersive X-ray spectrum of nanoparticles (a) Sn nanoparticles, (b) SnCr, (c) SnV and (d) SnTi bimetallic nanoparticles.

4.3.3 Optical Properties

4.3.3.1 Ultra-violet Visible spectroscopy for bimetallic nanoparticles

The UV-visible spectra of the bimetallic nanoparticles were done in CB. The generally observed wide absorption spectrum of the nanomaterials is advantageous for photovoltaic cells. This is because with photovoltaic cells, compounds that absorb at a wide spectral range are required to absorb as much energy as it is possible from the sun. The absorption spectrum of the bimetallic nanoparticle showed broad peaks at the high energy area of the UV-visible spectrum, **Figure 29**. The maximum absorption of the band is observed at 240, 218 and 216 nm for SnCr, SnV and SnTi, respectively. The electronic transitions that are observed are because of the excitation of the electron from the valence band to the conduction band, forming the electron hole pair, the exciton (Agarwal, 2010). The band gap of the nanoparticles was extrapolated from the Tauc plot and were found to be 1.8, 1.7 and 2 eV for SnCr, SnV and SnTi, respectively as seen in **Figure 29b**. The low absorption observed for the bimetallic nanoparticles is in the near ultraviolet region (**Table 3**) which is recommended to enhance light-trapping in photovoltaic application. This is indicative of a compound with low conductivity and a very weak semi-conductor material (Saini *et al.*, 2009 and Agarwal, 2010).

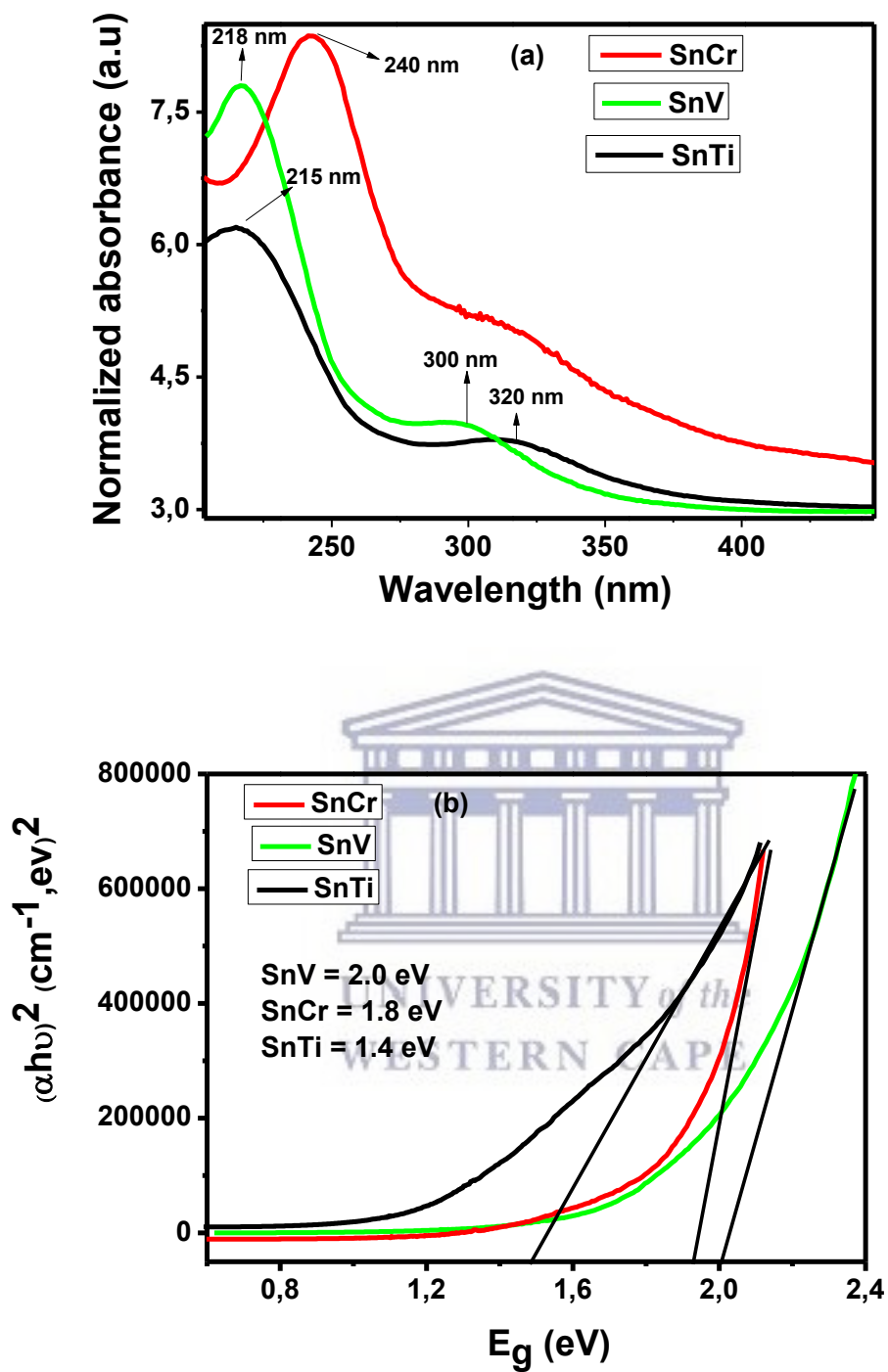


Figure 29: (a) UV-vis spectra and (b) Tauc plots for Sn-based bimetallic nanoparticles.

Table 3: Ultraviolet and Visible light regions for nanomaterials.

Region	λ_m (nm)	Absorbing compounds
Far ultraviolet	Less than 190	Saturated and mono-saturated
Near ultraviolet	190 – 380	Poly-unsaturated and aromatic
Visible light region	380 - 780	Coloured

4.3.3.2 Photoluminescence for bimetallic nanoparticles

Generally; it is agreed upon that when a semiconductor material is exposed to a photon of light, there is excitation of the electron from the valence band to the conduction band thereby leaving a hole in the valence band (Saini *et al.*, 2009). An electron hole pair is formed because of the existence of coulombic forces between the particles. As a result, there can be observation of transitions that are as a result of the charge transfer for transition metal. The emission and excitation spectrum of the nanoparticles is shown in **Figure 30a**, with the excitation and emission peak are enantiomers. This is indicative of that there are no geometric changes within the nanoparticles upon excitation. The emission spectrum of the synthesised bimetallic nanoparticles (**Figure 30b**) showed broad peaks at 330 nm, 330 nm and 347 for SnV, SnTi and SnCr, respectively. The peak at 410 nm for SnV is as a result of the relaxation of the exciton of the nanoparticles from the excited state to the ground state (Saini *et al.*, 2009 and Agarwal, 2010).

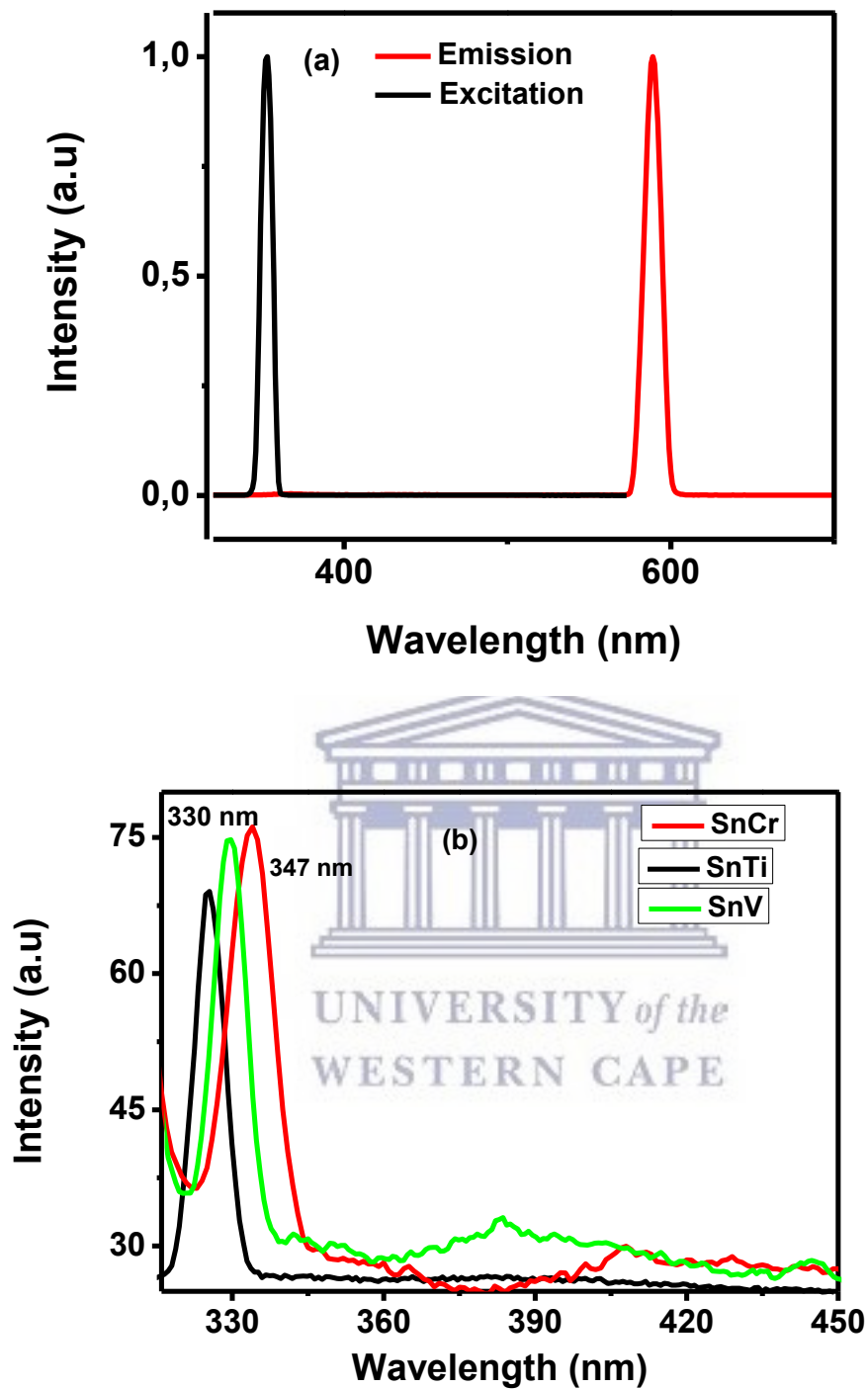
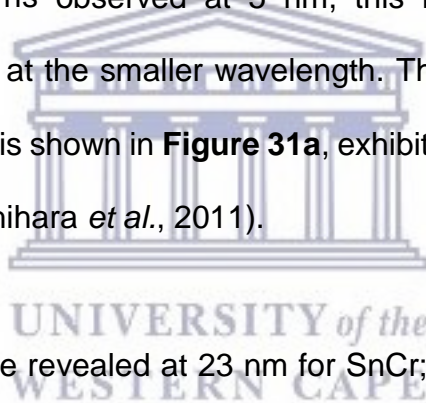


Figure 30: (a) The excitation and emission spectra of SnCr nanoparticles and (b) Photoluminescence spectra of Sn-based nanoparticles.

4.3.4 Structural analysis

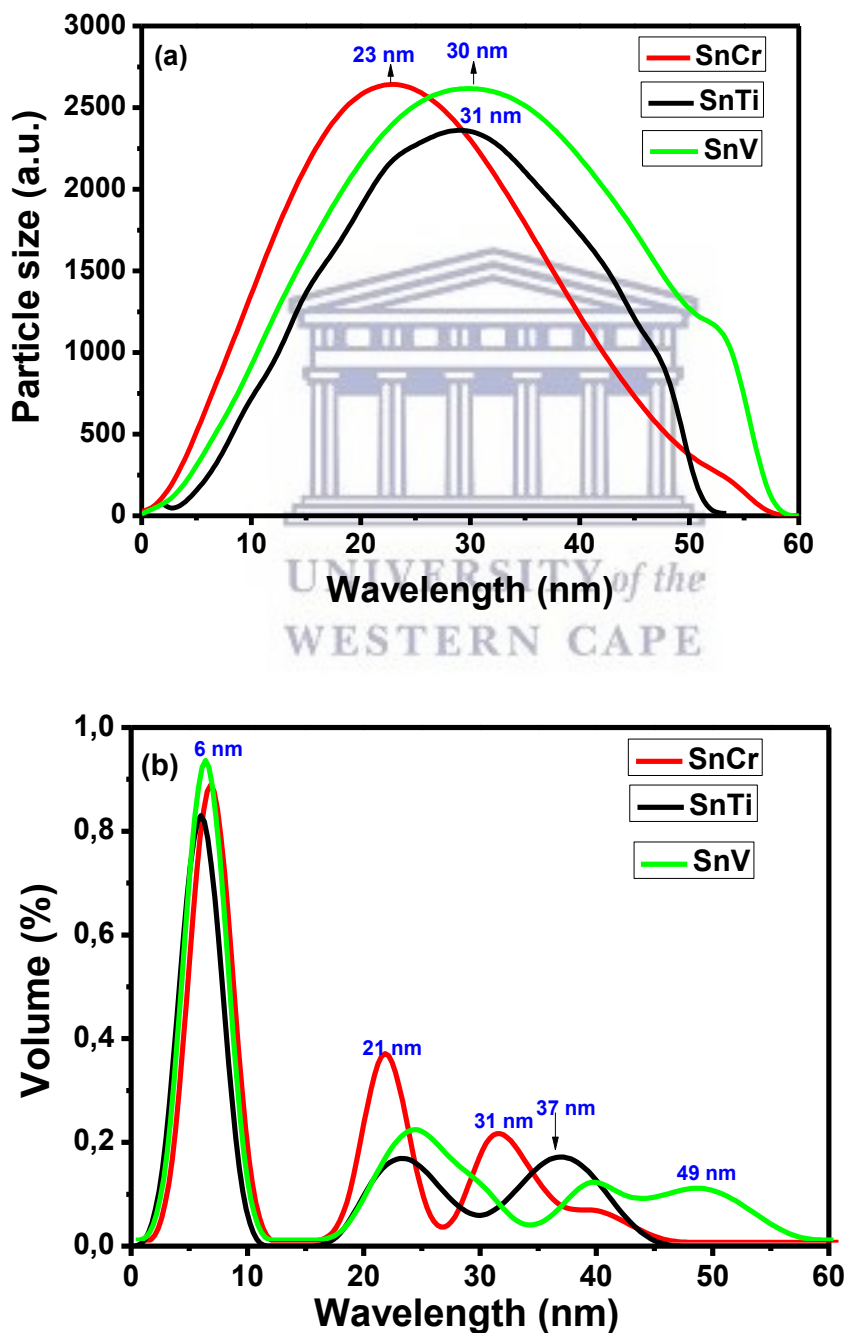
4.3.4.1 SAXSpace for bimetallic nanoparticles

The SAXS has the advantage over other techniques of being able to analyse a wide variety of sample types, including aerosols, colloidal suspensions, powders, solids, and thin films. The SAXS tends to provide more statistically reliable estimates of nanoparticle sizes because the particle size distribution obtained by the SAXS is typically estimated over a large number of nanoparticles. The weighted by volume fraction for SnCr was observed at 5 nm, 21 nm and 31 nm; SnV at 5 nm, 24 nm, 40 nm, 44 nm and SnTi at 5 nm, 24 nm and 37 nm. For all bimetallic nanoparticles there are more prominent patterns observed at 5 nm, this indicates that most of the nanoparticles are occupied at the smaller wavelength. The weighted particle size of the bimetallic nanoparticles is shown in **Figure 31a**, exhibit the particle size and shape of the nanoparticles (Higashihara *et al.*, 2011).



The scattering patterns were revealed at 23 nm for SnCr; 30 nm for SnV and 31 nm for SnTi. The pattern for all bimetallic nanoparticles are well-defined broad peak indicating that the nanoparticles are spherical. These observations are in accordance with the HR-TEM analysis (Thangavelu *et al.*, 2013). **Figure 31b** revealed a series of SnCr weighted by volume fraction at 6 nm, 21 nm and 31 nm, SnTi at 5 nm, 23 nm and 37 nm and SnV at 7 nm, 25 nm, 40 nm and 49 nm, respectively. The volume fraction of the bimetallic nanoparticles at smaller angles (5 nm, 6 nm and 7 nm) for SnTi, SnCr and SnV, respectively were more distinct. This observation indicates that various nanoparticles sizes are mostly occupied at smaller angle scattering pattern.

The intensity of the scattering signal usually collaborates with the particle size distribution, hence; bigger particles obtained at larger angles will obtain much intensity than small particles at small angles. Hence, as indicated in **Figure 31c**, the intensity signals obtained by the bimetallic nanoparticles around (5 nm - 7 nm) were nearly invisible than the intensity at large angles (25 nm - 60 nm). This, therefore, concluded that larger particles overshadowed the intensity signal of the particles at small angles.



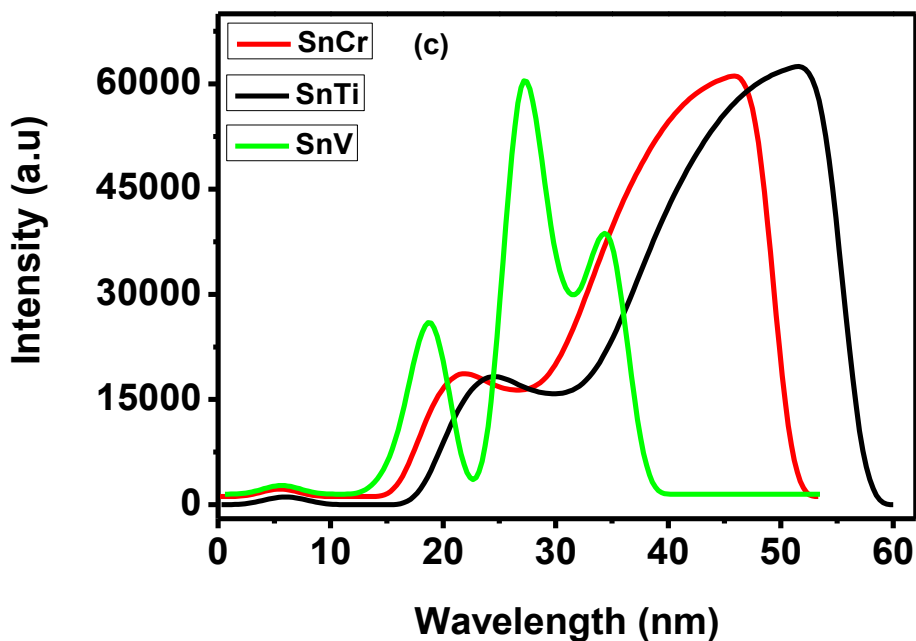
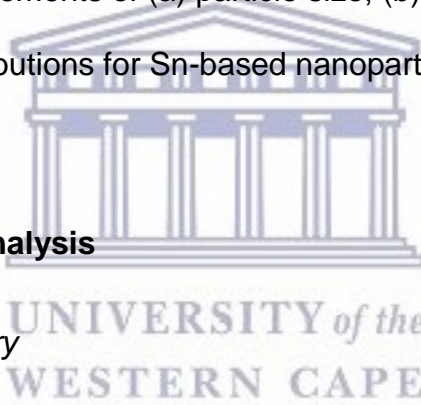


Figure 31: SAXS measurements of (a) particle size, (b) volume size and (c) intensity distributions for Sn-based nanoparticles.

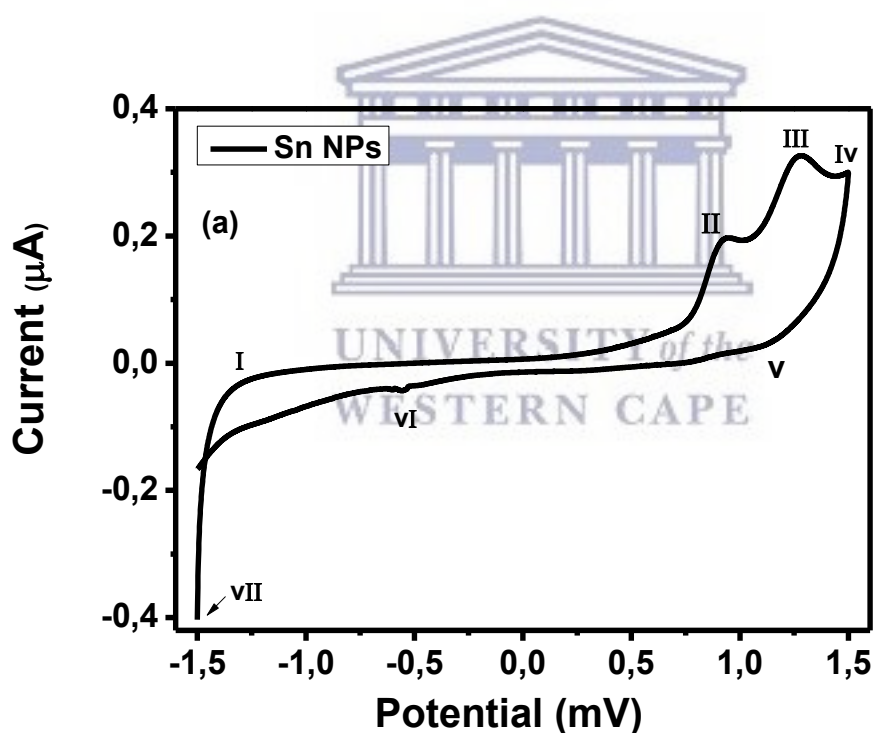


4.3.5 Electrochemistry analysis

4.3.5.1 Cyclic voltammetry

Analysis of the electrochemical kinetics is depicted by the use of two techniques, cyclic voltammetry (CV) and electrochemical impedance spectroscopy (EIS). The use of these techniques determines the ease at which charge transfer occurs for the different bimetallic nanoparticles. This is to ascertain the best bimetallic nanoparticle for photovoltaic application in terms of the electrochemical kinetics that is obtained. From the CV curve of the Sn-based bimetallic nanoparticles composite electrode, a large current and symmetrical type of voltammogram with a rectangular shape is found in both anodic and cathodic directions compared to the Sn nanoparticles voltammogram (Figure 32a).

In **Figure 32a** a pair of oxidation and reduction peaks is clearly found on the positive and negative sweeps at -1.27 V, 0.92 V, 1.28 V, 1.52 V, 1.14 V, -0.56 V and -1.49 V from peak I to VII, respectively. The peak at -1.27 V correspond to the metallic region (Gonçalves *et al.*, 2017). Thus the four oxidation peaks (from I to IV) and three reduction peaks (from V to VII). The current density is higher than that of the bimetallic nanoparticles (Kümbül *et al.*, 2009). Literature reports indicate that the factors affecting the capacitance are particle sizes and electrochemical conditions, namely type of electrolyte, concentration of electrolyte, scan rate, etc. (Zhong *et al.*, 2016). From **Figure 33**, the oxidation and reduction peaks can be used to calculate the HOMO and LUMO in order to obtain the bandgap as seen in **Table 4**.



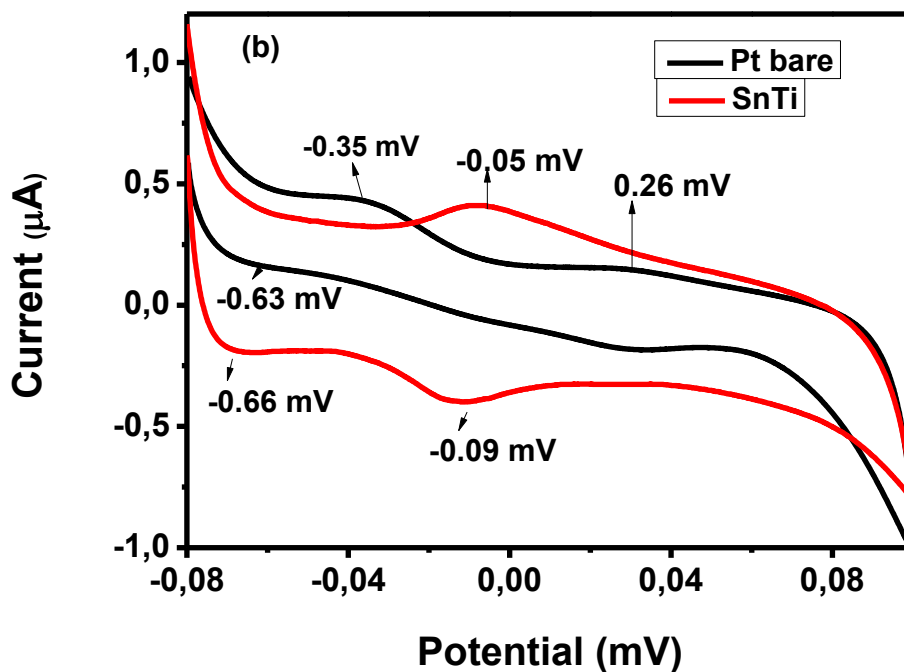
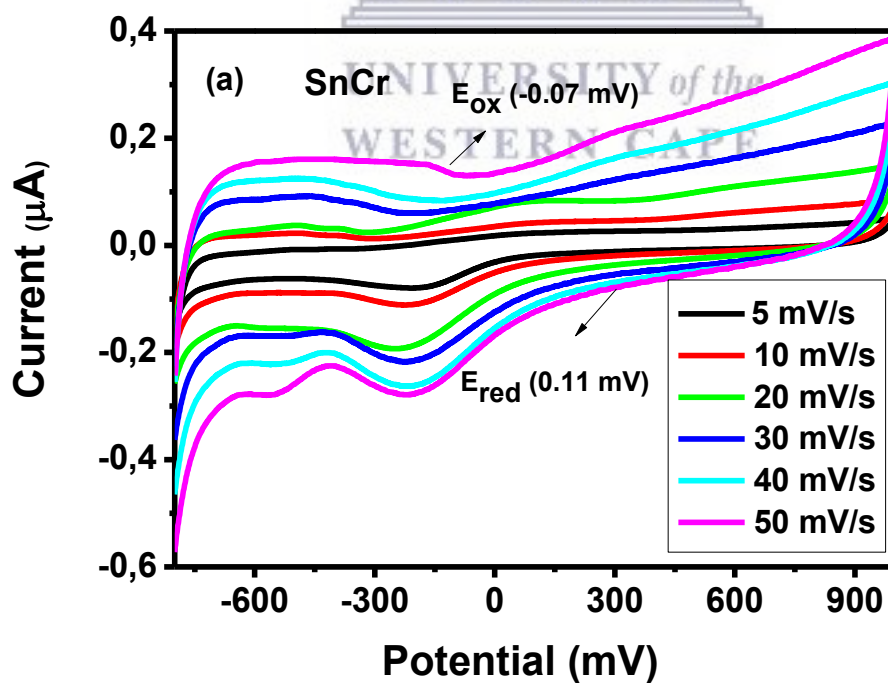


Figure 32: Cyclic voltammograms for (a) Sn nanoparticles and (b) Pt bare electrode with SnTi nanoparticles in 0.1 M LiClO₄.



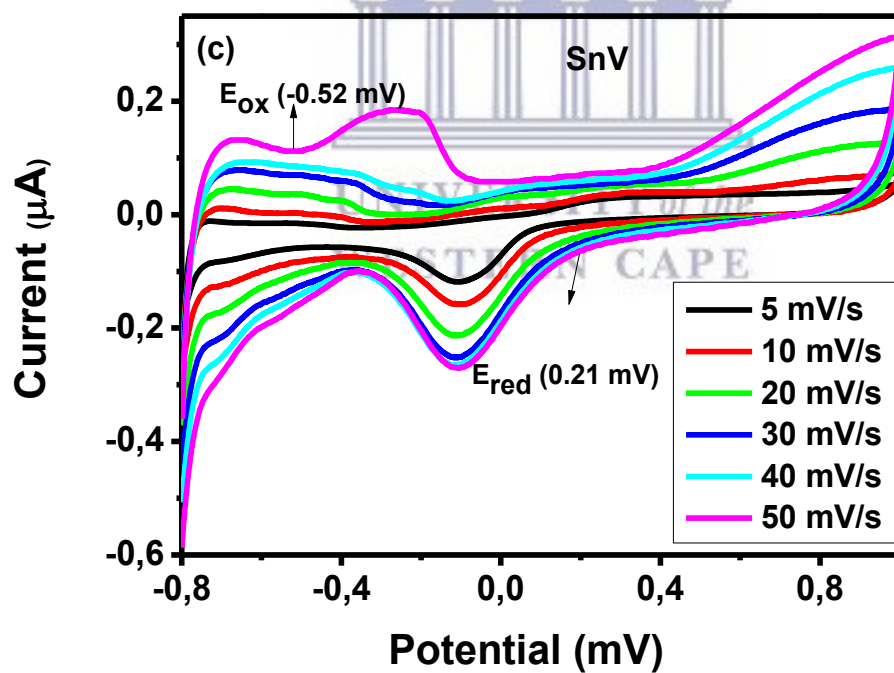
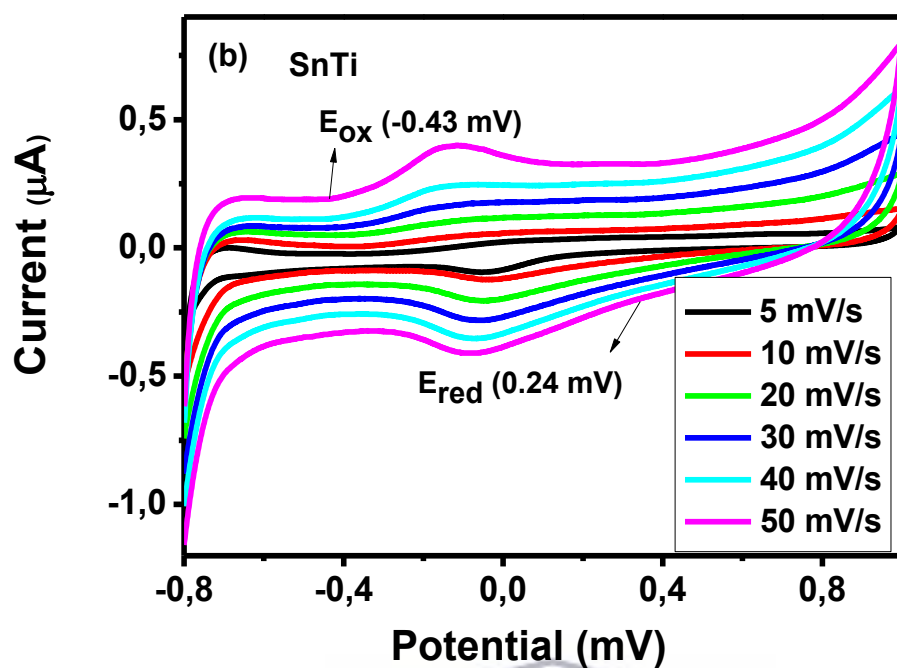


Figure 33: Cyclic voltammograms for (a) SnCr nanoparticles, (b) SnTi nanoparticles and (c) SnV nanoparticles in 0.1 M LiClO₄ at different scan rate.

Table 4. Calculated electrochemical and absorption band gaps for bimetallic nanoparticles.

Compound	E _{ox} (V)	E _{HOMO} (eV)	E _{red} (V)	E _{LUMO} (eV)	E _g (CV) eV	E _g (UV) eV
SnCr	-0.07	4.33	0.11	4.51	0.18	1.8
SnTi	-0.43	3.97	0.24	4.64	0.67	1.7
SnV	-0.52	3.88	0.21	4.61	0.73	2.0

4.3.5.2 Electrochemical impedance spectroscopy

Bode plots (**Figure 34**) give information about the phase angle and frequency for SnCr, SnV and SnTi nanoparticles. The increase in the capacitive effect is denoted by the increase in the value of the phase angle. The phase angle maximum for the bimetallic nanoparticles is occurring at 75°, 58° and 56° for SnCr, SnV and SnTi, respectively. The frequency was observed at 2645 Hz, 2353 Hz and 1105 Hz for SnCr, SnV and SnTi, respectively. The data that was found led to the conclusion that there is relatively fast electron transfer that is occurring at SnCr nanoparticles, since the capacitive effect maximum is observed at relatively high frequencies and phase angle compared to the other compounds (Gonçalves *et al.*, 2017). The Nyquist plot of impedance spectra in (**Figure 36**) for SnCr, SnTi and SnV was immobilized on Pt working electrode. The charge transfer resistance (R_{ct}) at the electrode surface is equal to the semicircle diameter, which can be used to describe the interface properties of the electrode.

In (**Figure 36**) the charge transfer resistance (R_{ct}) of SnV was the lowest ($R_{ct} = 1.804 \times 10^5 \text{ k}\Omega$) compared to that of SnCr and SnTi working electrode ($2.193 \times 10^5 \text{ k}\Omega$ and $2.908 \times 10^5 \text{ k}\Omega$). This indicates that SnCr and SnTi nanoparticles have good conductivity as compared to SnV and played an important role in accelerating the transfer of electrons.

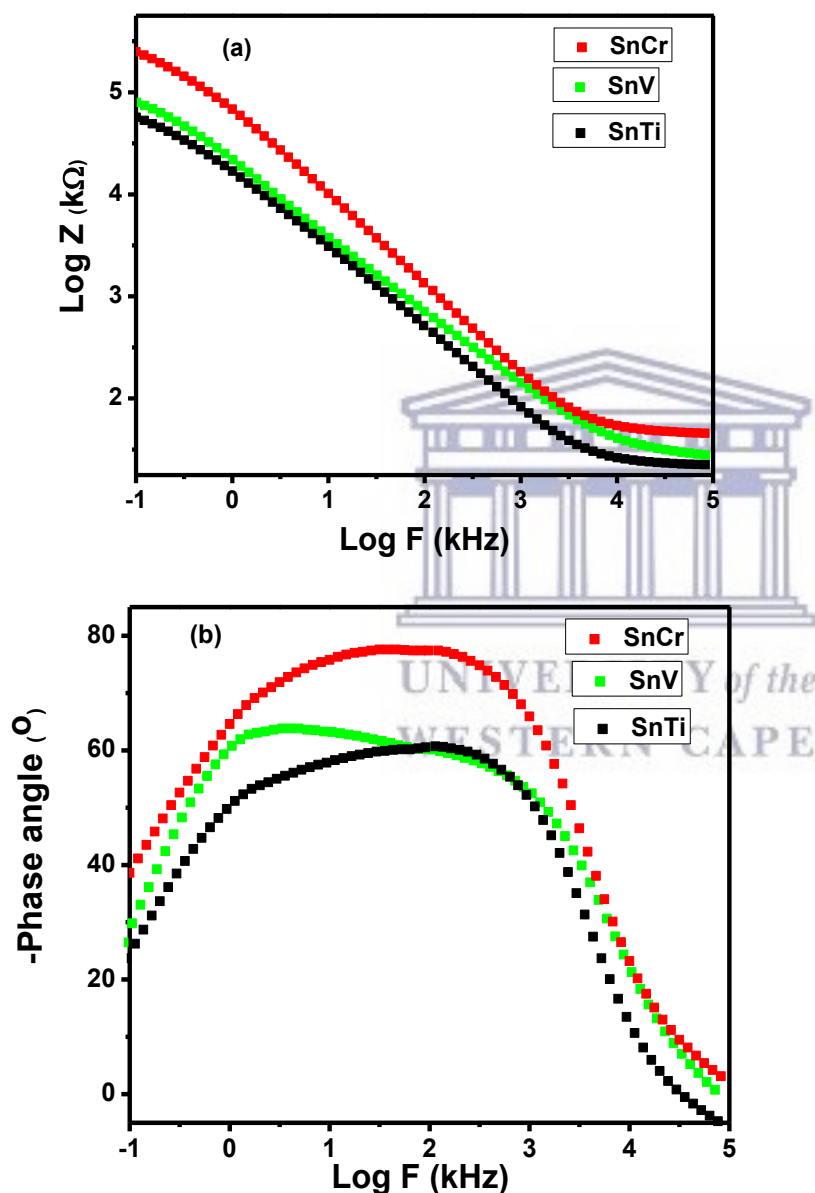


Figure 34: The Bode plot gives direct information on the (a) frequency and (b) phase angle for the bimetallic nanoparticles SnCr, SnV and SnTi.

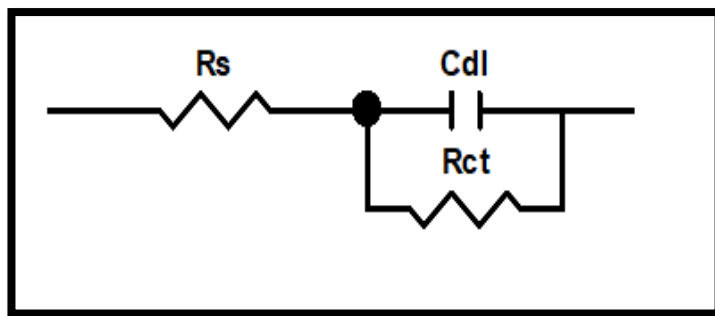


Figure 35: Simplified Randles equivalent circuit for the bimetallic nanoparticles.

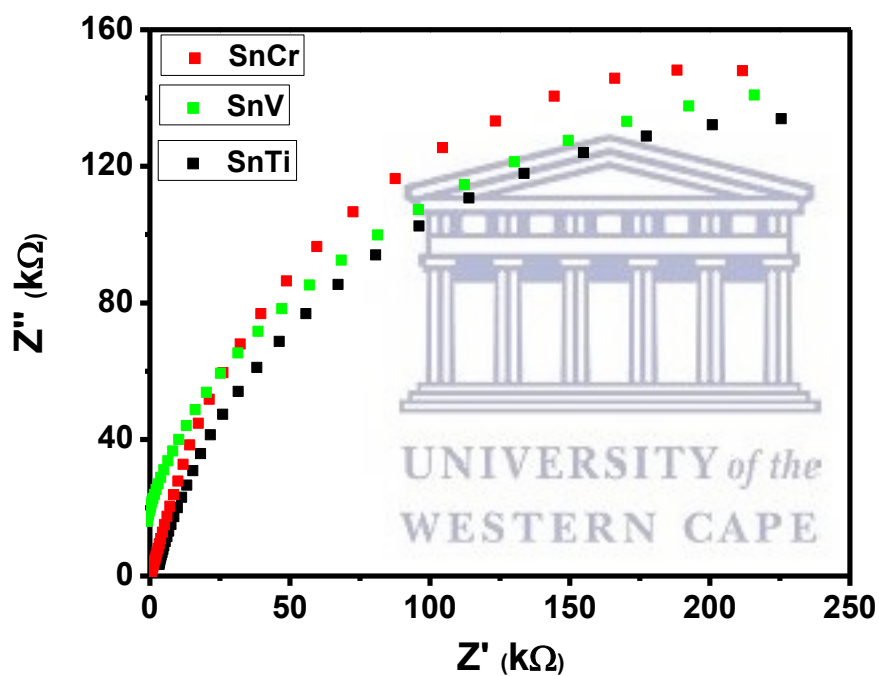


Figure 36: Nyquist plot of the bimetallic nanoparticles SnCr, SnV and SnTi.

Table 5: Summary of the impedance spectroscopy data analysis for bimetallic nanoparticles.

Sample	R_s (k Ω)	C_{dl} (μ F)	R_{ct} (k Ω)
SnCr	49.31	1.341×10^{-6}	2.193×10^5
SnTi	52.06	1.090×10^{-6}	2.908×10^5
SnV	71.31	1.058×10^{-6}	1.084×10^5

4.4 Conclusion

Stannum-based nanoparticles were characterized by XRD. It was found to be highly crystalline except for SnTi due to agglomeration confirmed by HR-TEM. Structural characterization was further confirmed with FTIR and UV-vis, where characteristic bands of PVP capped Sn nanoparticles were between 1280 and 1650 cm^{-1} for C-H bands for presence of nitrogen atom of PVP chemisorbing on Sn^{2+} ion. The UV-vis spectroscopy for Sn-based metallic nanoparticles exhibited the orange shift and the wavelength of 200 - 250 nm which is recommended for acceptor materials in photovoltaic application. HR-TEM was used for morphological analysis and was able to prove that the nanoparticles were poly-orientated as confirmed by XRD. The average particle size was 23 nm, 30 nm and 31 nm for SnCr, SnV, and SnTi, respectively was confirmed by SAXS. The oxidation peak and reduction of the bimetallic nanoparticles revealed the HOMO, LUMO and bandgap and this revealed that the nanoparticles were ~ 2 eV. Electrochemical impedance spectroscopy was done and obtained the charge transfer resistance for Sn-based bimetallic nanoparticles. It was observed that SnV exhibited lower charge transfer resistance concluding has faster charge transfer as compared to SnCr and SnTi.

Bibliography

Agarwal, A. (2010) 'Optical Properties and Application of Metallic Nanoparticles and their Assembled'.

Bond, G. C. (2008) 'Faraday Discussion 138: Nanoalloys Theory to Applications', *Platinum Metals Review*, 52, pp. 107–109.

Dutta, P., Park, H., Lee, W. H., Kang, I. N. and Lee, S. H. (2012) 'A crystalline D- π -A organic small molecule with naphtho[1,2-b:5,6- b']dithiophene-core for solution processed organic solar cells', *Organic Electronics: physics, materials, applications*. 13, pp. 3183–3194.

Gonçalves, R., Pereira, E. C. and Marchesi, L. F. (2017) 'The overoxidation of poly(3-hexylthiophene) (P3HT) thin film: CV and EIS measurements', *International Journal of Electrochemical Science*, 12, pp. 1983–1991.

Higashihara, T., Ohshimizu, K., Ryo, Y., Sakurai, T., Takahashi, A., Nojima, S., Ree, M. and Ueda, M. (2011) 'Synthesis and characterization of block copolythiophene with hexyl and triethylene glycol side chains', *Polymer Elsevier Limited*, 52, pp. 3687–3695.

Jian, S. R., Chen, G. J. and Hsu, W. M. (2013) 'Mechanical properties of Cu₂O thin films by nanoindentation', *Materials*, 6, pp. 4505–4513.

Kümbül, A., Turaç, E., Dursun, T. and Şahmetlioğlu, E. (2009) 'Synthesis and characterization of conducting copolymer of (N1,N3-bis(thiophene-3-ylmethylene)benzene-1,3-diamine-co-3,4-ethylenedioxythiophene)', *Chemical Papers*, 64, pp. 114–117.

Lee, H. K. H., Wu, J., Barbé, J., Jain, S. M., Wood, S., Speller, E. M., Li, Z., Castro, F. A., Durrant, J. R. and Tsoi, W. C. (2018) 'Organic photovoltaic cells – promising indoor light harvesters for self-sustainable electronics', *Journal of Materials Chemistry A*, 6.

Mayedwa, N. (2015) 'Development of platino-iridium / ruthenium telluride nanoalloy electrode systems for possible application in ammonia fuel cell'.

Mora, M. B. De, Monroy, B. M. and Lugo, J. E. (2017) 'Solar Energy Materials & Solar Cells Materials for downconversion in solar cells: Perspectives and challenges', *Solar Energy Materials and Solar Cells*, 165, pp. 59–71.

Okumu, F. O. and Matoetoe, M. C. (2017) 'Electrochemical and optical band gaps of bimetallic silver-platinum varying metal ratios nanoparticles', 11, pp. 1–8.

Saini, V., Li, Z., Bourdo, S., Dervishi, E., Xu, Y., Ma, X., Kunets, V. P., Salamo, G. J., Viswanathan, T., Biris, A. R., Saini, D., Biris, A. S., V, D. U. and Carolina, N. (2009) 'Electrical, Optical, and Morphological Properties of P3HT-MWNT Nanocomposites Prepared by in Situ Polymerization', pp. 8023–8029.

Shah, A. and Qureshi, R. (2012) 'Synthesis, characterization and applications of bimetallic (Au-Ag, Au-Pt, Au-Ru) alloy nanoparticles', 30, pp. 133–149.

Sharma, M. K., Buchner, R. D., Scharmach, W. J., Swihart, M. T., Sharma, M. K., Buchner, R. D., Scharmach, W. J., Papavassiliou, V., Swihart, M. T., Conductive, C., Silver, C., Sharma, M. K., Buchner, R. D., Scharmach, W. J., Papavassiliou, V. and Swihart, M. T. (2013) 'Creating conductive copper – silver bimetallic nanostructured coatings using a high temperature reducing jet aerosol reactor temperature reducing jet aerosol reactor', pp. 6826.

Thangavelu, K., Annamalai, R. and Arulnandhi, D. (2013) 'Preparation and Characterization of Nanosized TiO₂ Powder by Sol-Gel Precipitation Route', *International Journal of Emerging Technology and Advanced Engineering*, 3, pp. 636–639.

Toshima, N. and Yonezawa, T. (1998) 'Bimetallic nanoparticles and novel materials for chemical and physical applications', pp. 1179–1201.

Trouillet, L., de Nicola, A. and Guillerez, S. (2000) 'Synthesis and characterization of a new soluble, structurally well-defined conjugated polymer alternating regioregularly alkylated thiophene oligomer and 2,2'-bipyridine units: Metal-free form and Ru(II) complex', *Chemistry of Materials*, 12, pp. 1611–1621.

Wadams, R. C., Yen, C., Butcher, D. P., Koerner, H., Durstock, M. F., Fabris, L. and Tabor, C. E. (2014) 'Gold nanorod enhanced organic photovoltaics: The importance of morphology effects', *Organic Electronics*, 15, pp. 1448–1457.

Zhong, L., Beaudette, C., Guo, J., Bozhilov, K. and Mangolini, L. (2016) 'Tin nanoparticles as an effective conductive additive in silicon anodes', *Nature Publishing Group*, pp. 1–8.

CHAPTER FIVE

Summary

Titanium dioxide also known as titania (TiO₂) nanoparticles is a promising material, widely used in many applications due to its high photocatalytic activity, excellent gas-sensitive properties, dielectric properties, high stability, low cost and non-toxicity. The unique optical property and chemical stability of titania makes it well suited in the many fields including photovoltaic cells. As a nanosized particle, this material exhibit excellent mechanical properties, a benefit that currently has been exploited in photovoltaics. Also, the addition of an organic material like a polymer would likely enhance the stiffness, toughness and service life of polymeric materials. The sol-gel method is an attractive method for the synthesis of titania. Since this method is carried out in solution, tailoring of certain desired structural characteristics such as compositional homogeneity, grain size, particle morphology and porosity is possible. A uniform distribution of the particles is important for optimal control of grain size and micro structure to maintain high reliability. This chapter will focus on the synthesise of high efficient nanosized titania particles and to characterize the prepared sample using techniques like XRD, AFM, TEM and nanoindentation.

Investigation of Mechanical Properties by Nanoindentation for P3HT Thin Films Prepared by Sol-Gel Process

Abstract

In physical deposition technique, mechanical or electromechanical methods are used to deposit the thin films on the substrate. Materials to be deposited on the substrate depend upon the temperature, pressure and other physical conditions. In these physical methods, the thin films formed are directional in nature because particles will follow a straight path from the target to the substrate. Thin films are formed by depositing material on a clean suitable substrate to grow up film thickness instead of thinning down the bulk material. The mechanical strength of thin films is analysed in this study, the structural properties of poly(3-hexylthiophene) P3HT thin films were investigated by X-ray diffraction (XRD), the morphological properties probed by the transmission electron microscope (TEM), thickness was confirmed by the optical profilometry and mechanical properties were investigated utilizing the nanoindentation technique. The P3HT thin films are deposited on a glass substrate by spin coating technique. The XRD show that the films are predominated (101)-oriented the peak assigned from TiO₂ nanoparticles. The hardness and modulus of the thin films are measured using the Berkovich nanoindenter operated with a continuous stiffness measurement (CSM). The results showed that the increase in the nanoparticles content lead to an increase in the particle size. The relation between the particle size and hardness tend to obey the Hall-Petch equation.

5.1 Introduction

Due to the demand of inexpensive clean energy, renewable energy have considerable attention in the past several decades. Semiconducting polymers have immense potential for cost effectiveness and a wide field of applications due to their mechanical flexibility and low weight of polymer materials (Saini *et al.*, 2009). Polythiophenes specifically poly(3-hexylthiophene) (P3HT) are the most leading and probed representatives of semiconducting polymers. These p-type semiconducting material stand out due to their affordable and easy processing at a large scale (Chen *et al.*, 2013). They are an important class of semiconducting systems which have been widely studied due to their fundamental mechanical properties and have also been applied in various devices such as solar cells (Chen *et al.*, 2013 and Kwong *et al.*, 2004 and Sheng-Rui *et al.*, 2006). The high-quality properties and benefits of titanium dioxide (TiO₂) nanoparticles have generated an active area of research where many investigations have shown potential applications in various technological fields. In this case, the particle size of the nanoparticles is a key factor for the performance and physical properties of the materials (Sheng-Rui *et al.*, 2006). Considering the hasty evolution in the field of nanotechnology over the last decade, there has been an increasing demand for handling materials at nanoscale for making nanostructures or nano-devices. For this reason, understanding the behavior of the materials at the nanometer scale has become essentially important. Previous literature have reported that when the materials are at a lower scale, the mechanical properties (hardness and Young's modulus) tend to behave very differently than those of the bulk form (Saini *et al.*, 2009). Thus, in this study measurements of the mechanical properties of materials will be studied (Sheng-Rui *et al.*, 2006).

Nanoindentation is a rare though very dynamic technique used for investigating the mechanical characteristics of thin films as well as other various materials within the micro or nanoscale (Jian *et al.*, 2013). In the preparation technology of new materials, the sol-gel method has attracted special interest. This is due to Sol-gel process is preferred due to its economical feasibility and the low-temperature process which gives us control over the composition of the product achieved. Small amounts of dopants like rare earth elements and organic polymers can be used in the sol which homogeneously disseminates in the product formed finally (Jian *et al.*, 2013). Preparation of pure and titanium dioxide doped P3HT thin films (1, 5 and 10 wt%) derived by the sol-gel process are described. The structure and morphology of P3HT thin films are characterized by using X-ray diffraction (XRD) and transmission electron microscopy (TEM) techniques. The thickness of the thin films was determined using the optical profilometry. Hardness and Young's modulus of P3HT thin films were measured by means of the Berkovich nanoindentation operating at a continuous stiffness measurement (CSM) mode (Chen *et al.*, 2005). The difference in mechanical properties for P3HT thin films are discussed concurrently with the increase in the nanoparticle content and the particle size is also reported. These thin films from sol-gel were deposited using the spin coating technique. Spin coating process is known to be the simplest thin fabrication technology because it leads to reduction of production costs and provides high optical and quality films (Kwong *et al.*, 2004 and Chen *et al.*, 2005).

5.2 Experimental

5.2.1 Materials and sample preparation

5.2.1.1 Materials

Regio-regular poly (3-hexylthiophene) rr-P3HT, titanium (IV) isopropoxide, propanol, formic acid and glass substrates were purchased from Sigma-Aldrich and were utilized without any further purification. For the proper adhesion of the films, cleaning procedure of the glass substrates is very important. The 2.5 cm x 2.5 cm glass substrates were first cleaned with detergent water for 30 min, then distilled water 30 min, acetone for 10 min, isopropanol for 10 min and dried with nitrogen.

5.2.1.2 Synthesis procedure

Titanium dioxide (TiO₂) nanoparticles were prepared by sol-gel method at room temperature following *Zhou et al.* (2015) method. Titanium (IV) isopropoxide (TTIP) was hydrolysed through the esterification reaction between formic acid and propanol. TTIP (20 mL) was dissolved in propanol (42 mL) and then mixed with formic acid (10 mL) while stirring. A white precipitate was formed, and this was stirred for 4 hours and further aged for another 2 h. The resulting sol was dried at 80 °C overnight and calcined in air in a furnace at a ramp rate of 10 °C/min, from 25 °C to 500 °C for 3 h (*Zhou et al.*, 2013). Nanocomposites of poly(3-hexylthiophene) (P3HT) containing TiO₂ at different weight percentages (1, 5 and 10 wt%) have been prepared through the chemical process from toluene medium at room temperature (25 °C) then spin coated onto a glass substrate to obtain the thin films. The thin films of P3HT_xTi_yO₂ were deposited on a glass substrate using spin coating at 2000 rpm for 30 s and then annealed at 50 °C for 2 h (*Kwong et al.*, 2004 and *Yang et al.*, 2015).

5.2.2 Instrumentation

The structural properties of the thin films were characterized by X-ray Diffractometer: Bruker AXS D8 Advance, mechanical properties were examined by Nano Indenter XP (Spain) and the thickness of the thin films was obtained from Zeta profilometer 0.50x Coupler (Spain). Surface morphology was analysed by Nanosurf easyScan 2 controller Atomic Force Microscopy (AFM) on the spin coated thin films and high resolution-transmission electron microscope (HR-TEM) was used to study the size and morphology of samples. Copper grid (Cu) was used as sample holder for the immobilisation of (2 μ L) solution of the nanocomposites and the micrographs were recorded at room temperature.

5.3 Results and discussion

5.3.1 Structural properties

5.3.1.1 X-ray diffraction spectroscopy

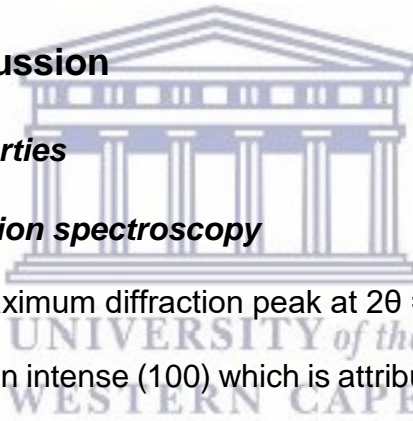
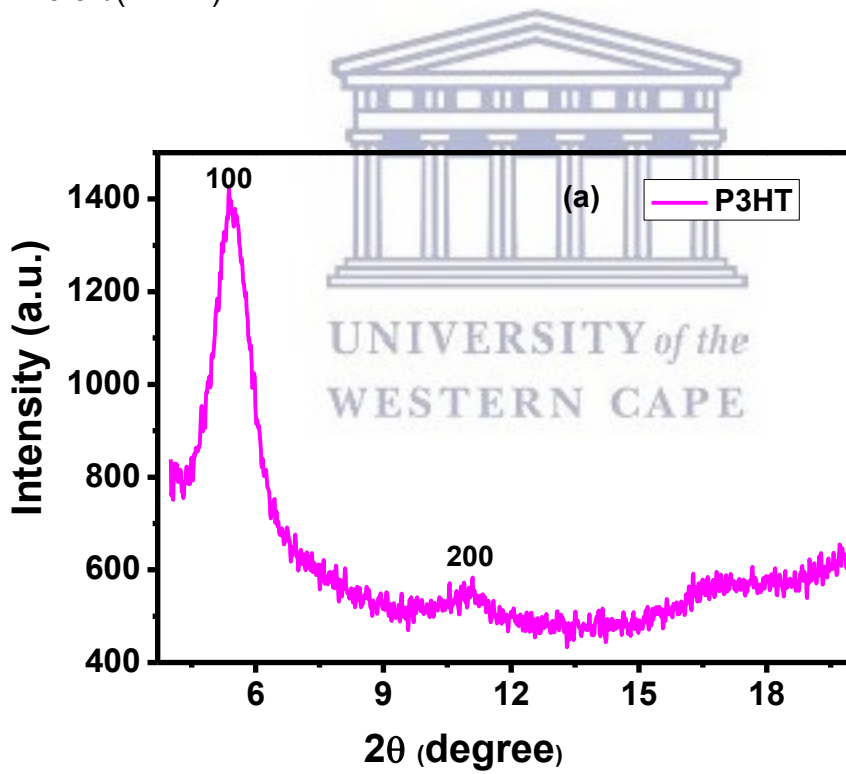


Figure 37a show the maximum diffraction peak at $2\theta = 5.24^\circ$ corresponding to the P3HT thin film showing an intense (100) which is attributed to the lamellar structure with an interlayer spacing formed by parallel stacks included in the P3HT chains (Jian *et al.*, 2013). The XRD patterns of the TiO₂ nanoparticle sample synthesized by sol-gel method are depicted in **Figure 37b**, and the structure reveals a crystalline structure corresponding to the anatase phase with diffraction peaks at $2\theta = 25.41^\circ, 37.79^\circ, 48.71^\circ, 54.55^\circ, 62.70^\circ$ and 69.11° corresponding to (101), (004), (200), (105), (203) and (116) planes (Zhou *et al.*, 2013). The XRD patterns of the P3HT thin films obtained with various content of 1, 5 and 10 wt% are shown in **Figure 38**.

It is evident that the intensity and the full width at half maximum (FWHM) of TiO₂ (101) is more dominant in the nanocomposites and the diffraction peak has shown an improvement with the increasing content of the nanoparticles, indicating a slight increase in particle size and better film crystallinity (Arendse C.J. 2012 and Chen *et al.*, 2013). The particle size (D) can be determined by Scherrer's equation below (**equation 8**), where λ , d and θ attributes to the X-ray wavelength, FWHM (101) peak and the Bragg's diffraction angle, respectively. The estimated particle sizes for the thin films are 5.18, 5.90 and 6.48 nm for the various increase content of nanoparticles of 1, 5 and 10 wt%, respectively (Kwong *et al.*, 2004).

$$(D = 0.9\lambda/(d\cos\theta)) \tag{8}$$



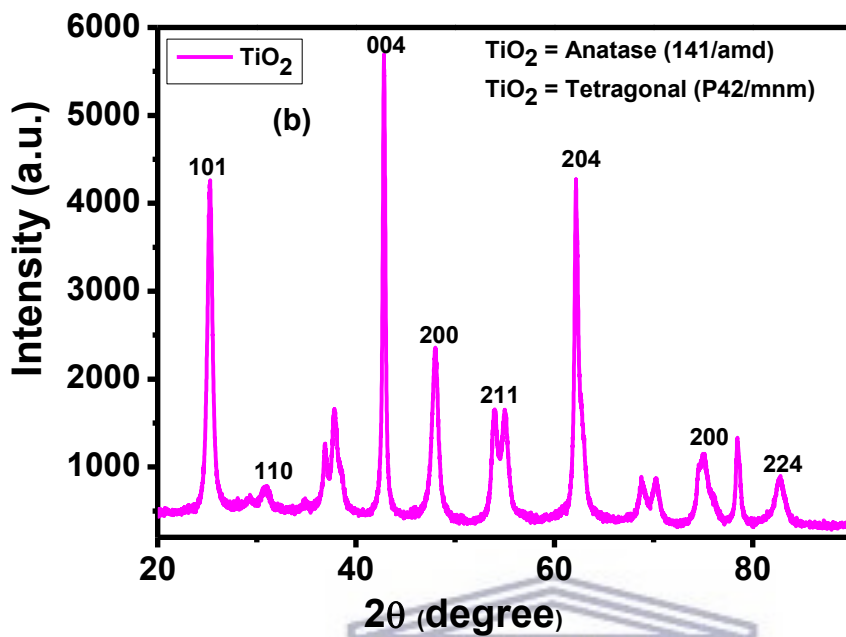


Figure 37: XRD patterns of (a) P3HT thin film and (b) TiO₂ nanoparticles.

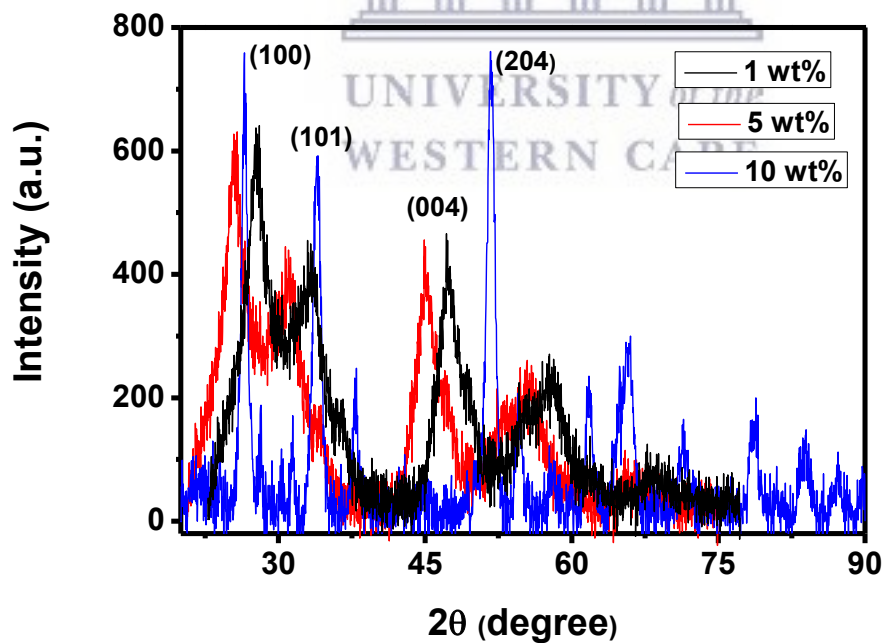


Figure 38: XRD patterns for P3HT thin films with 1 wt%, 5 wt% and 10 wt% TiO₂ nanoparticles content.

5.3.2 Morphological properties

5.3.2.1 High-Resolution Transform Electron Microscopy

TEM image in **Figure 39a** of the 10 wt% thin film indicates spherical but non-homogeneous structure, the SAED in **Figure 39b** confirmed the strong and crystalline ring indicating the formation of the anatase structure. It is evident that the nanoparticles tend to agglomerate thus resulting in the increase of the particle size as observed by the XRD (Kwong *et al.*, 2004 and Zhou *et al.*, 2013).

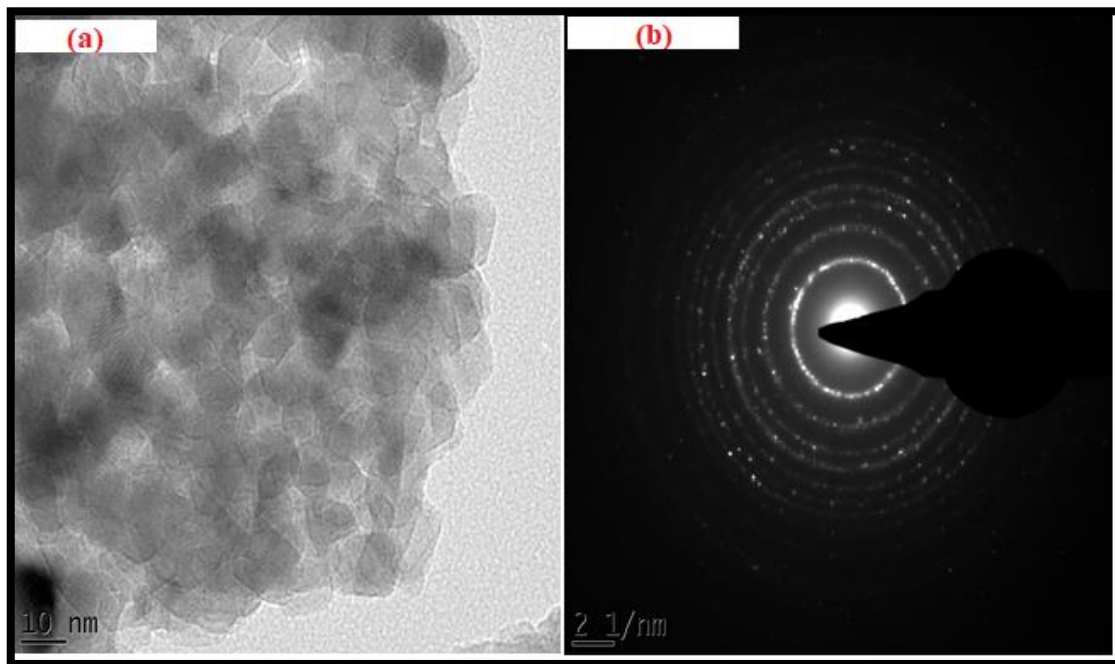


Figure 39: (a) TEM image of P3HT thin film with 10 wt% content of the TiO₂ nanoparticles and (b) SAED image of P3HT thin film with 10 wt% content of TiO₂ nanoparticles.

5.3.2.2 Atomic Force Microscopy

AFM image gives information about the height differences and constituency of the composite thin film at the surface, because the hard nanoparticles can easily be distinguished from the soft polymer. The surface topography of TiO_2 exhibit very rough surface and this may be due to the fact that TiO_2 tend to agglomerate. For the nanocomposites film, it is observed that the surface is smoother. And it's shown in **Figure 40** the addition of TiO_2 nanoparticles decreases the root mean square (RMS) roughness of the polymers and the values are tabulated in **Table 6**.

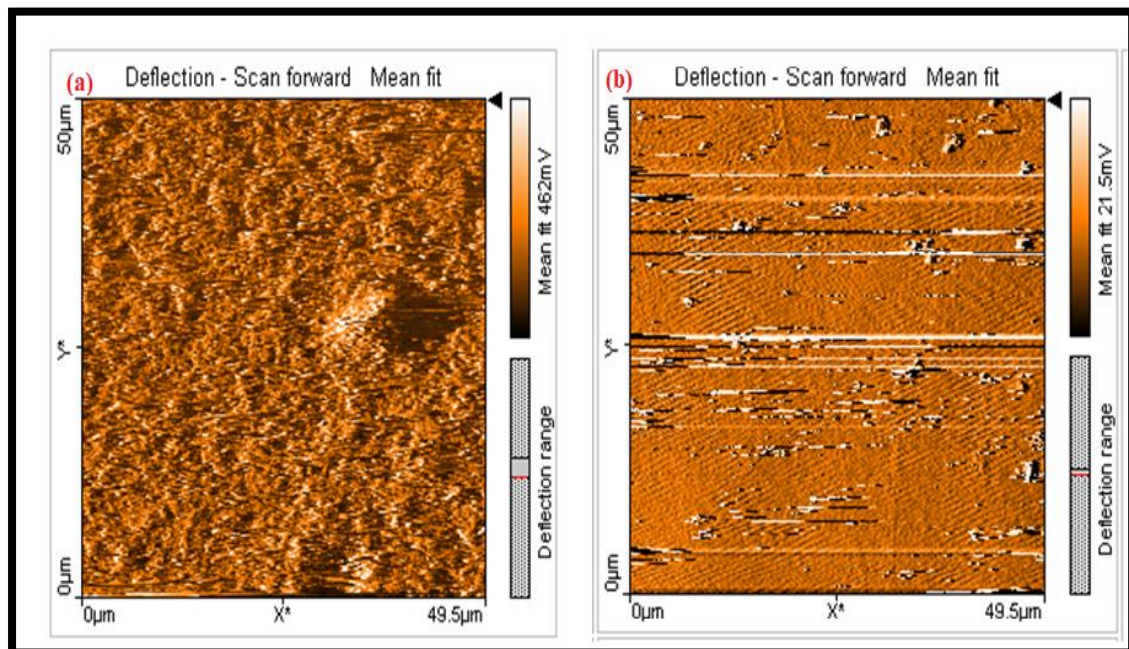


Figure 40: AFM topography of (a) TiO_2 and (b) P3HT: TiO_2 (10 wt%) of films spin-coated from toluene solvent.

Table 1: Root mean square roughness values for the compounds.

Compound	RMS
TiO ₂	18.62
P3HT-TiO ₂	14.01

5.3.3 Optical Profilometry

Profilometry is a good method to study the surface roughness and thickness of the nanocomposite or thin films. The thin film were achieved by deposition of a nanocomposite onto a glass surface by spin coating technique. The thickness achieved for the thin film is 200 nm as shown in **Figure 41**. In photovoltaic application the recommended thickness of the thin film is 100 - 200 nm (Diebold *et al.*, 2003 and Zhou *et al.*, 2013). The film show non-homogeneous yet smooth surface. It has been previously reported by *Diebold* (2003) that the mixing between P3HT and TiO₂ is strongly dependent on the solvent used. It is known that the solvent evaporation rates influences the surface morphology of polymer thin films. Toluene have a magnitude of higher vapour pressure, hence evaporate significantly faster, leading to less polymer chain in the solid state and thus showing a non-homogeneous surface.

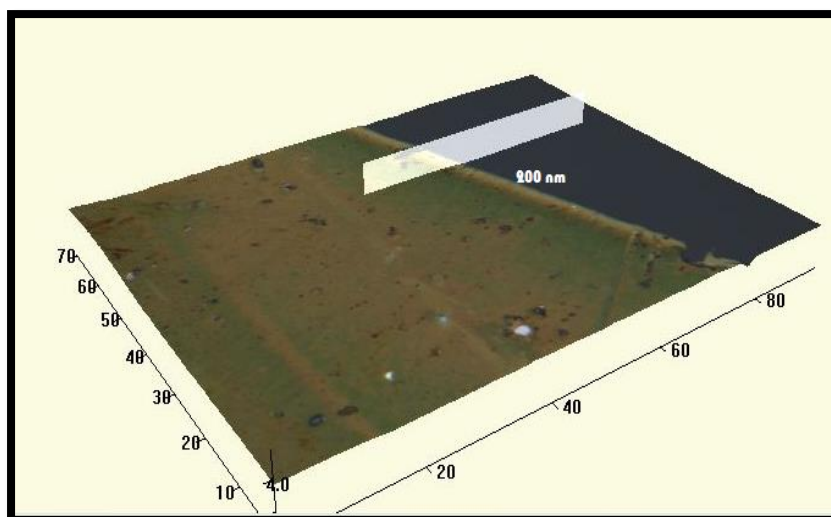


Figure 41: Thickness image of the 10 wt% content P3HT film obtained from the optical profilometry.

5.3.4 Mechanical properties

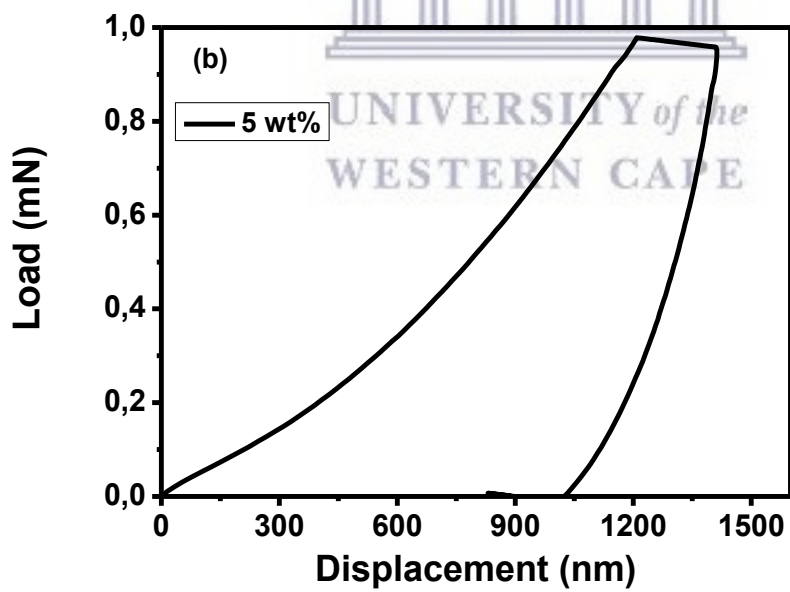
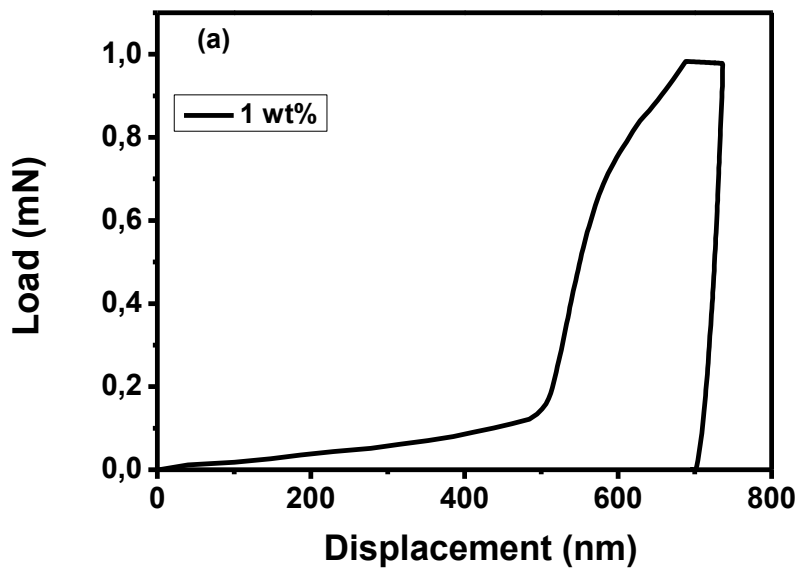
5.3.4.1 Nanoindentation technique

The load-displacement curves for the thin films deposited at 1 wt% shows deformation behaviour during the penetration of the indenter loaded CSM mode, due to the displacement/penetration depth (**Figure 42**). It is accepted that the depth should always be less than 30% of the film's thickness to prevent the substrate effect. At lower content of the nanoparticles (1 wt%), the thickness of the film is very low thus making it easy during the indentation depth to exceed the 30% measurement (Chen *et al.*, 2005 and Sheng-Rui *et al.*, 2006). At 5 and 10 wt%, the curves appear to be regular and smoother. This shows there's absence of discontinuities during the loading and unloading segment. It is observed that the patterns are continuous indicating no cracks on the films during the measurements (Jian *et al.*, 2013). **Figure 43** presents the hardness and Young's modulus graph for 1, 5 and 10 wt% thin films.

The graph shows comparable results from the loading curve for 1 wt% indicating the deformation behaviour. It is evident that with the increase content of nanoparticles the hardness increases attributing to the transition of elastic and plastic contact (Chen *et al.*, 2005). The hardness is represented by the mean contact pressure developed by the plastic zone. The hardness usually decreases with the increase of the displacement or penetration depth, involving dislocation and fine particle structure of the thin films. It will then reach a constant value with a moderate indentation depth suggesting that a single material is measured. The hardness values obtained are regarded as the most essential properties for the thin films (Wang *et al.*, 2005). The Young's modulus in this case behaves like that of the hardness, both mechanical parameters were determined from the CSM loading scheme (Bhosale *et al.*, 2008 and Chen *et al.*, 2013). **Table 7** summarizes the hardness and Young's modulus for the thin films obtained from the nanoindentation. It is known that the dependence of the hardness on the particle size can be described by **equation 9** (Hall-Petch equation). Where H_0 is the lattice friction stress and k_{HP} is the Hall-Petch constant (Chen *et al.*, 2005 and Sheng-Rui *et al.*, 2006).

$$H(D) = H_0 + k_{HP} D^{-1/2} \quad (9)$$

Increase in nanoparticles content leads to larger particle size and better crystallinity as discussed in the TEM. This will result in an increase of the hardness and Young's modulus. **Figure 43** is a fit experimental data from the Hall-Petch equation with the form $H(D) = 0.68 \text{ GPa} + 17.6 \text{ GPa } D^{-1/2}$ (Chen *et al.*, 2005). The obtained parameter $H_0 = 0.68 \text{ GPa}$ indicates that the lattice friction stress is low. This may be due to the lack of disorder in the thin films during loading measurements (Zeng *et al.*, 2010).



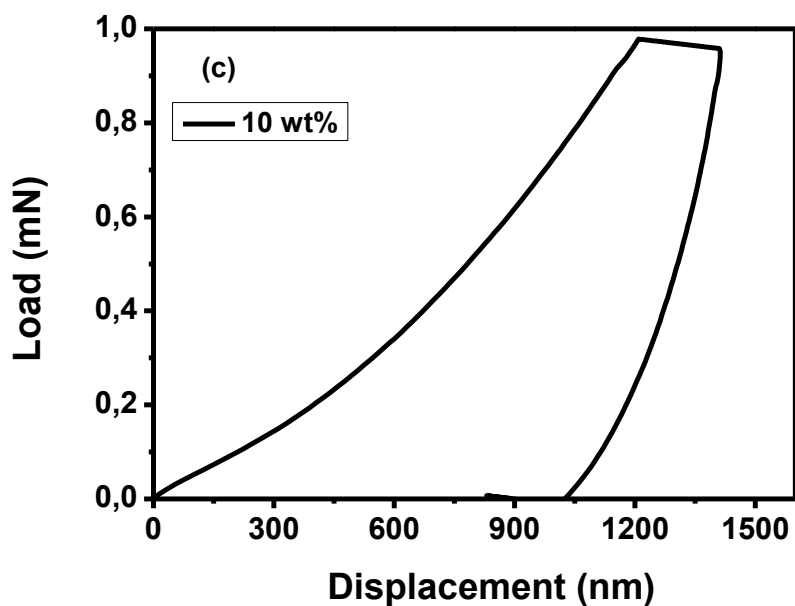


Figure 42: A load-displacement curve for the P3HT thin films at (a) 1 wt%, (b) 5 wt% and (c) 10 wt% content of TiO₂ nanoparticles.

Table 2: Hardness, Young's modulus and particle size of the P3HT thin films.

Sample	Hardness		Young's modulus		Particle size (nm)
	Std. dev	Mean value	Std. dev	Mean value	
P3HT/TiO ₂ (1 wt%)	0.001	0.025	0.016	0.689	5.18
P3HT/TiO ₂ (5 wt%)	0.112	0.048	4.712	5.111	5.90
P3HT/TiO ₂ (10 wt%)	0.497	0.185	17.511	10.779	6.98

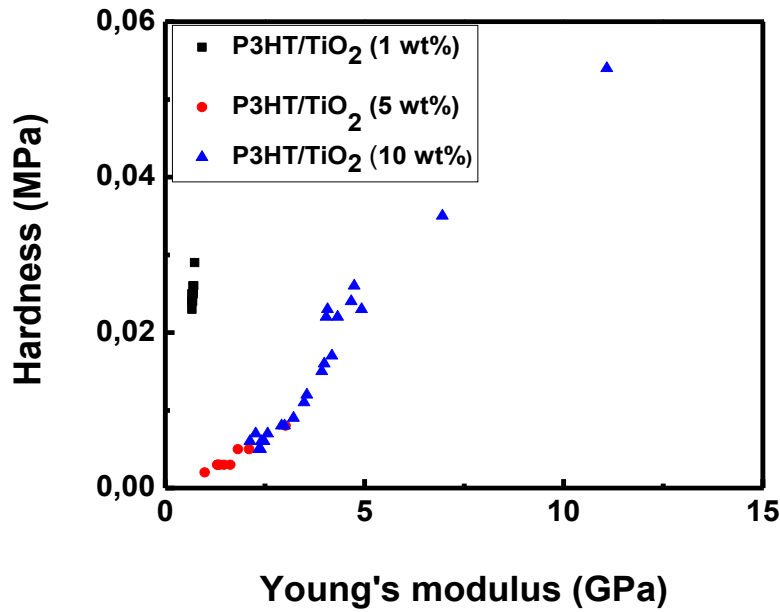


Figure 43: The Hardness-Young's modulus curves for the P3HT thin films at 1, 5 and 10 wt% content of the TiO₂ nanoparticle.

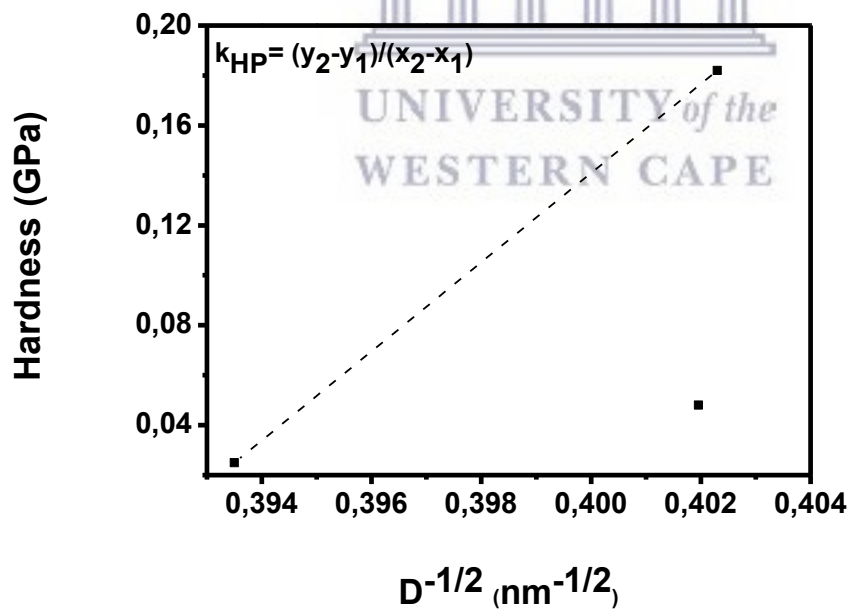


Figure 44: Plot of experimental data of hardness versus the particle size. The dashed line is a fit to the data obtained from the Hall-Petch equation.

5.4 Conclusion

The combination of XRD, TEM, optical profilometry and nanoindentation techniques has been utilized to investigate the structural and mechanical properties of the P3HT thin films at different content of TiO₂ nanoparticles. XRD showed that the particle size and crystallinity improved with an increase in the nanoparticles content. This was also confirmed by the TEM which showed highly crystalline structure and significant rings on the SAED image. The nanoindentation results showed that the particle size is proportional to the hardness and Young's modulus. The increase in hardness with the increase in nanoparticle content is mainly due to the particle size. The fitting experimental hardness data using the Hall-Petch equation showed a lower constant of 17.6 GPa.nm^{1/2}. Due to the improvement, crystalline quality of the thin films the Young's modulus also increased.

Bibliography

- Arendse, C. J. (2012) 'Temperature-dependence on the optical properties and the phase separation of polymer – fullerene thin films', pp. 4282–4289.
- Bhosale, S. V., Jani, C. H. and Langford, S. J. (2008) 'Chemistry of naphthalene diimides', *Chemical. Society. Reviews*, 37, pp. 331–342.
- Chen, S., Liu, L. and Wang, T. (2005) 'Investigation of the mechanical properties of thin films by nanoindentation, considering the effects of thickness and different coating-substrate combinations', *Surface and Coatings Technology*, 191, pp. 25–32.
- Chen, Y. T. and Wu, C. W. (2013) 'Effect of grain size on nanomechanical property Ni₈₀Fe₂₀ thin film', *Intermetallics*, 34, pp. 89–93.

Diebold, U. (2003) 'Structure and properties of TiO₂ surfaces: A brief review', *Applied Physics A: Materials Science and Processing*, 76, pp. 681–687.

Jian, S. R., Chen, G. J. and Hsu, W. M. (2013) 'Mechanical properties of Cu₂O thin films by nanoindentation', *Materials*, 6, pp. 4505–4513.

Kwong, C. Y., Choy, W. C. H., Djuri I. A. B., Chui, P. C., Cheng, K. W. and Chan, W. K. (2004) 'Poly(3-hexylthiophene):TiO₂ nanocomposites for solar cell applications', *Nanotechnology*, 15, pp. 1156–1161.

Saini, V., Li, Z., Bourdo, S., Dervishi, E., Xu, Y., Ma, X., Kunets, V. P., Salamo, G. J., Viswanathan, T., Biris, A. R., Saini, D., Biris, A. S., V, D. U. and Carolina, N. (2009) 'Electrical , Optical , and Morphological Properties of P3HT-MWNT Nanocomposites Prepared by in Situ Polymerization', pp. 8023–8029.

Sheng-Rui, G. J. C. and W. M. H. (2006) 'Mechanical Properties of Cu₂O Thin Films by Nanoindentation', *Chemistry, an Asian journal*, 1, pp. 148–154.

Yang, J., Clark, N., Long, M., Xiong, J., Jones, D. J., Yang, B. and Zhou, C. (2015) 'Solution stability of active materials for organic photovoltaics', *Solar Energy*, 113, pp. 181–188.

Zeng, X. and Gan, Y. X. (2010) 'Nanocomposites for Photovoltaic Energy Conversion'.

Zhou, D., Ji, Z., Jiang, X., Dunphy, D. R., Brinker, J. and Keller, A. A. (2013) 'Influence of material properties on TiO₂ Nanoparticle agglomeration', *Public Library of Science One*, 8, pp. 1–7.

CHAPTER SIX

Summary

Organic solar cells have the potential to be portable power sources that are lightweight flexible, and inexpensive. However, the highest power conversion efficiency for organic solar cells to date is ~8%, and most high-efficiency solar cells have an area of less than 1 cm². This chapter will advance the field of organic solar cells by studying the physics and electrochemistry of the devices to understand the charge current, which is related to efficiency. The novel acceptor material in the presence of well-known semiconductor towards organic photovoltaic application are applied and studied. The equivalent circuit Bio Logic VMP300 model developed for organic photovoltaic cells has shown to work well to describe the behaviour of organic devices and parameterise their current-voltage characteristics with five parameters. The origin of the open-circuit voltage is studied using cells with different electrodes and an electrolyte. Study of the thermal behaviour will also be studied because thermal stability in the nanomaterials improve conversion efficiency of the device.

Effect of Bimetallic Nanoparticle Properties on the Performance of Photoelectrochemical Cell

Abstract

Electrochemistry is largely applied in synthesis, chemical analysis and energy storage. Photoelectrochemistry as a branch of electrochemistry attracts extensive attention from scientists worldwide for its use to convert light energy into electricity with efficiencies competing with silicon-based photovoltaics. This chapter will focus on the area of photoelectrochemical cell (PEC) and its applications in photovoltaic cells. Stannum–chromium bimetallic nanoparticles blended with p-type P3HT was used as the active layer in the preparation of photovoltaic cells. The current investigation focuses on the effect of bimetallic nanoparticles on the performance of photovoltaics. Different concentration of SnCr were prepared (1:1, 1:3 and 1:6). We found significant improvement on the power conversion efficiency of the photovoltaic cells from the 1:6 concentration. Results show that the introduction of SnCr into the nanocomposite layer could be beneficial to improve the charge transport processes in the preparation of photovoltaic cell. The P3HT-SnCr nanocomposite and the device properties were presented and discussed in terms of optical, electrical and film morphologies of the devices. The properties were correlated to the performance of PEC such as short-circuit (I_{sc}), fill factor (FF) and open voltage (E_{oc}).

6.1 Introduction

A typical type of the photocurrent-generated device has a semiconductor in contact with an electrolyte, and this is often referred as photoelectrochemical cells. A photoelectrochemical cell consists of a photoactive semiconductor working electrode (either n- or p-type) and counter electrode made of either metal (e.g. Pt) or semiconductors. Both electrodes are immersed in the electrolyte containing suitable redox couples (Cardo *et al.*, 1982). In a metal-electrolyte junction, the potential drop occurs entirely on the solution site, whereas in a semiconductor-electrolyte junction, the potential drop occurs on the semiconductor site as well as the solution site. The charge on the semiconductor side is distributed deep in the interior of the semiconductor, creating a space charge region (Ahn *et al.*, 2009 and Kopidakis *et al.*, 2006). If the junction of the semiconductor-electrolyte is illuminated with a light having energy greater than the bandgap of the semiconductor, photogenerated electrons/holes are separated in the space charge region. The photogenerated minority carriers arrive at the interface of the semiconductor-electrolyte (Kümbül *et al.*, 2009). Photogenerated majority carriers accumulate at the backside of the semiconductor. With the help of a connecting wire, photogenerated majority carriers are transported via a load to the counter electrode where these carriers electrochemically react with the redox electrolyte. A pioneering photoelectrochemical experiment was realised by obtaining photocurrent between two platinum electrodes immersed in the electrolyte containing metal halide salts by Michael Gratzel in 1991 (Gratzel, 2001). It was later found that the photosensitivity can be extended to longer wavelengths by adding a dye to silver halide emulsions (Potratz *et al.*, 2012). The interest in photoelectrochemistry of semiconductors led to the discovery of wet-type photoelectrochemical photovoltaic cells (Hodes, 2012 and Licht, 2002).

These studies showed electron transfer to be the prevalent mechanism for photoelectrochemical sensitization processes. **Figure 45** shows various types of the photoelectrochemical cells. When shining the light, oxidation reaction will happen on the surface of n-type semiconductors, whilst reduction reaction will happen on the surface of p-type semiconductors. In the electrochemical photovoltaic cell, which is based on a narrow bandgap semiconductor and a redox couple as shown in **Figure 45a**, optical energy is converted into electrical energy without change of the free energy of the redox electrolyte ($\Delta G=0$). Electrochemical photovoltaic cells have the following advantages comparing with the solid photovoltaics: 1) it is not sensitive to the defects in semiconductors, 2) the solid/liquid junction is easy to form, and the production price will be much reduced, 3) it is possible to realize the direct energy transfer from photons to chemical energy. Unlike conventional solid state photovoltaic cells, the potential of the working electrode can be varied with respect to the reference electrode by means of an external voltage source connected between working and counter electrode.

6.1.1 Working principle of photoelectrochemical cell

The photoelectrochemical cell consists of four components, namely, transparent conducting oxide (TCO), metal oxide semiconductor (MOS) film as photovoltaic material, electrolyte as redox mediator and platinum counter electrode as shown in **Figure 46**. Under illumination, PEC undergoes six processes, namely, (1) absorption of light by semiconductor, (2) generation of electron–hole pairs in the semiconductor according to the equation $h\nu - e^- + h^+$, (3) motion of electrons from TCO photoanode to counter electrode to produce electric current, (4) reduction at the interface of counter electrode/electrolyte, (5) oxidation at the interface semiconductor/electrolyte and (6) recombination between electrons and holes in the semiconducting material.

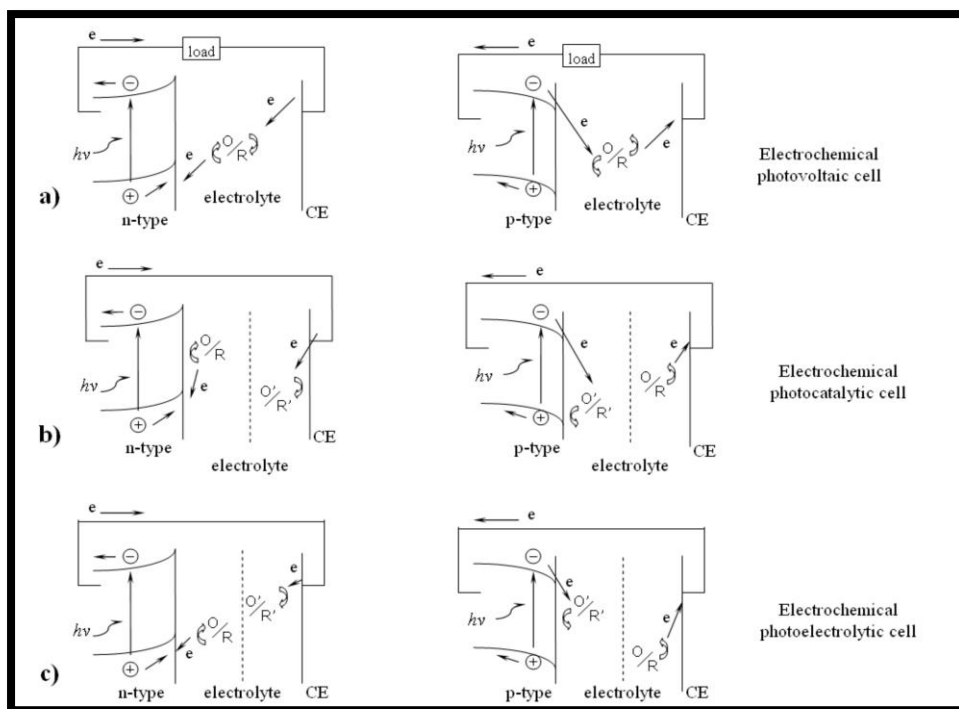


Figure 45: Different types of photoelectrochemical cells with the working electrode (WE) made of semiconductor (n- or p-type) and the counter electrode (CE) (Licht, 2002).

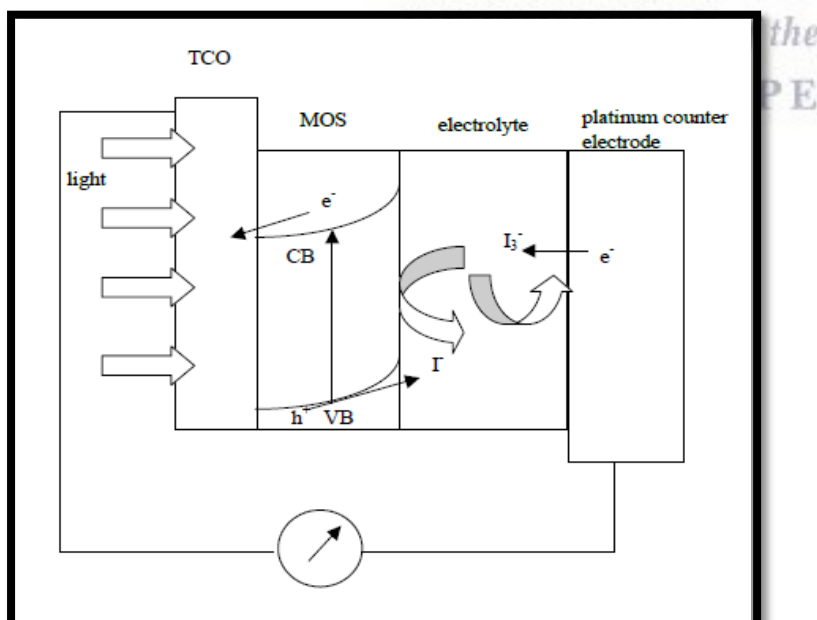


Figure 46: Working principle of photoelectrochemical cells (Gratzel, 2001 and Rahman *et al.*, 2014).

6.2 Experimental

6.2.1 Sample preparations

The Polymers (P3HT) and different concentrations of stannum-chromium nanoparticles (SnCr) were dissolved in a suitable chlorobenzene solvent for 24 h. The indium tin-oxide (ITO, from Sigma Aldrich with a sheet resistance $\sim 10 \text{ Ohm/sq}$) substrates are successively cleaned for 20 min in water and acetone in an ultrasonic bath and finally dried at $120 \text{ }^\circ\text{C}$. Once dissolved, polymers and SnCr are deposited by spin-coating on the ITO substrate at 900 rpm (round per minute) for 90 s. Following deposition, films are dried at $140 \text{ }^\circ\text{C}$ during 15 min to evaporate the solvent.

6.2.2 Instrumentation

The thermal gravimetric analysis was done using a Perkin-Elmer thermal gravimetric analyser. The samples were all analysed using a heat rate of $20 \text{ }^\circ\text{C}/\text{min}$ starting from $50 \text{ }^\circ\text{C}$. The range that was analysed was from $50 \text{ }^\circ\text{C}$ to $900 \text{ }^\circ\text{C}$. The fluorescence and atomic force microscopy measurements were obtained by the using of the Horiba Jobin Yvon NanoLog and Nanosurf STM easyscan 2, respectively. The measurements were done as a film on a glass and ITO substrate. **Device Testing:** Photoelectrochemical (PEC) measurements were carried out using potentiostat (Bio Logic VMP300) in the standard 3-electrode cell configuration using an Ag/AgCl (1 M KCl) reference electrode with a platinum wire as the counter electrode and the semiconducting film as the photovoltaic material. A neutral electrolyte solution of 0.1 M LiClO_4 in acetonitrile was used as the redox mediator.

6.2.3 Characterizations

6.2.3.1 Photoluminescence behaviour of P3HT with different concentrations of SnCr nanoparticles thin films

Sariciftci *et al.* (Sariciftci, 2004) showed that the comparison of photoluminescence (PL) of a donor with that of the donor/acceptor composite provides an important, which is indicated by the quenching effect of the composite with the presence of nanoparticles. **Figure 47 and 48** shows the photoluminescence spectra of blends of P3HT with different SnCr ratios glass and ITO coated substrates respectively. The effect of the presence of the nanoparticles in the photoluminescence spectra of the polymers is a very important parameter that needs to be explored to determine the applicability of a compound as an acceptor in the photovoltaic system. The importance of looking at the interaction of the donor and acceptor is to determine whether there is any interaction of the donor and acceptor at the excited level. The interaction is observed by the quenching of the fluorescence of the donor. The interaction was done using (1:1, 1:3 and 1:6) ratios. The importance of spin coating onto substrate before measurements, is that a trade-off between transparency and conductivity must be made. There is an observation of complete quenching of the fluorescence of the acceptor with the donor in both glass and ITO coated substrates. This implies that there is charge dissociation that is occurring on the donor in the presence of SnCr as an acceptor (Kabongo *et al.*, 2016). This gives a potential system that can be used in photovoltaic cells from this observation it can be concluded that the quenching is more on the glass substrate than the ITO coated substrate.

The photoluminescence was measured for the polymers in the presence of nanoparticles. This exhibit an orange shift for 1:1 compared to the spectra of lower concentrations (1:3 and 1:6) which exhibit the blue shift, suggesting that the polymer chains are twisted and not π -stacked on each other for films with lower concentrations. It has been reported that materials with high absorption coefficient are necessary for application in photovoltaic cells (Express, 2017 and Kopidakis *et al.*, 2006).

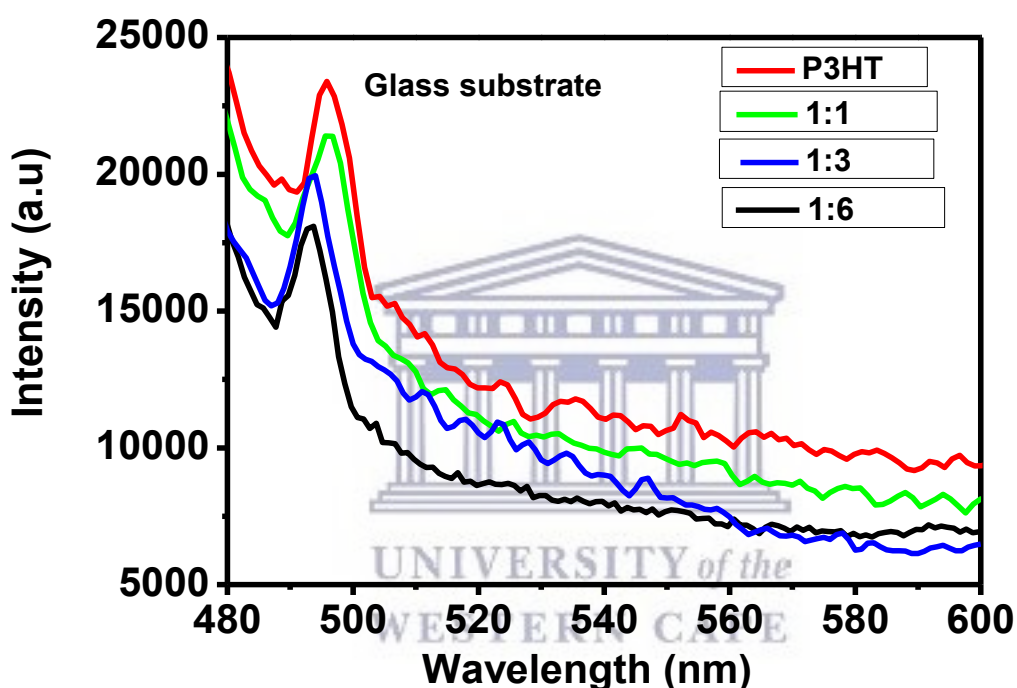


Figure 47: PL spectra of P3HT: SnCr for different concentrations at room temperature on glass substrate.

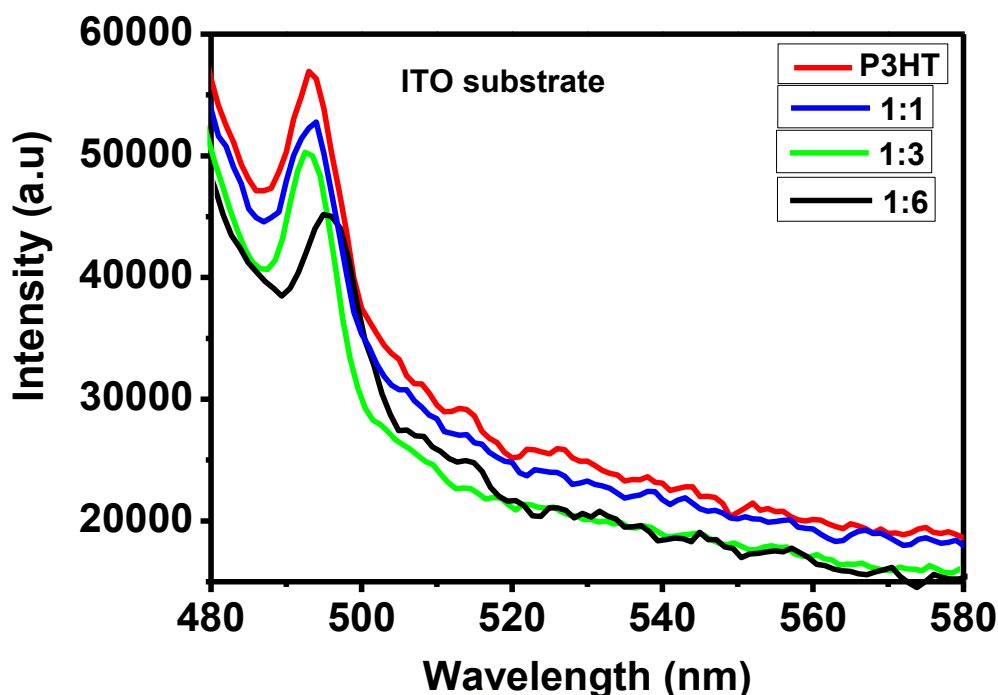
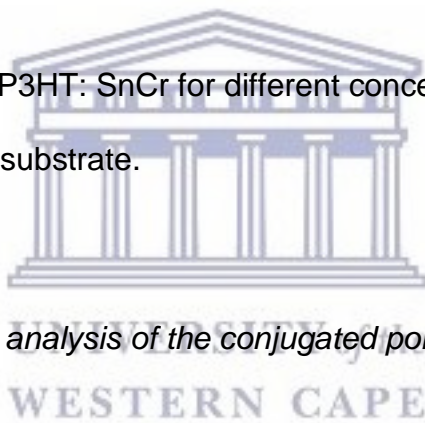


Figure 48: PL spectra of P3HT: SnCr for different concentrations at room temperature on ITO coated substrate.



6.2.3.2 Thermal gravimetric analysis of the conjugated polymer and bimetallic nanoparticles

The thermal gravimetric analysis (TGA) of the P3HT exhibit the mass loss in a two-step mechanism, **Figure 49**. The polymer is very stable against thermal decomposition. The differential thermal analysis consists of two maxima at temperatures around 465 °C and 635 °C indicating two different components of similar oxidation behaviour (Ohshimizu *et al.*, 2011 and Saini *et al.*, 2009). The first step of the mass loss began at about 460 °C and the second step began at about 600 °C. Such an oxidation at high temperature obviously cannot be due to physisorbed species.

The beginning of the mass loss is due to the loss of an alkyl side group attached to the aromatic thiophene backbone (hexyl group) (Malgas *et al.*, 2015). As the temperature increases above 500 °C, the oxidation is accelerated and the pyrolysis of the aromatic backbone of polymer chains is ignited. These products further underwent degradation to form ammonia at temperatures above 450 °C (Kümbül *et al.*, 2009 and Ohshimizu *et al.*, 2011). The thermal analysis graphs of the nanocomposite of P3HT-SnCr shows that the initial degradation temperature (IDT) has been found to take place at 650 °C while the mass loss has been found to occur at 800 °C. From this observation it can be concluded that the addition of the bimetallic nanoparticles improved the stability of the polymer under high temperatures (Sariciftci, 2004 and Jiang *et al.*, 2006 and An *et al.*, 2009).

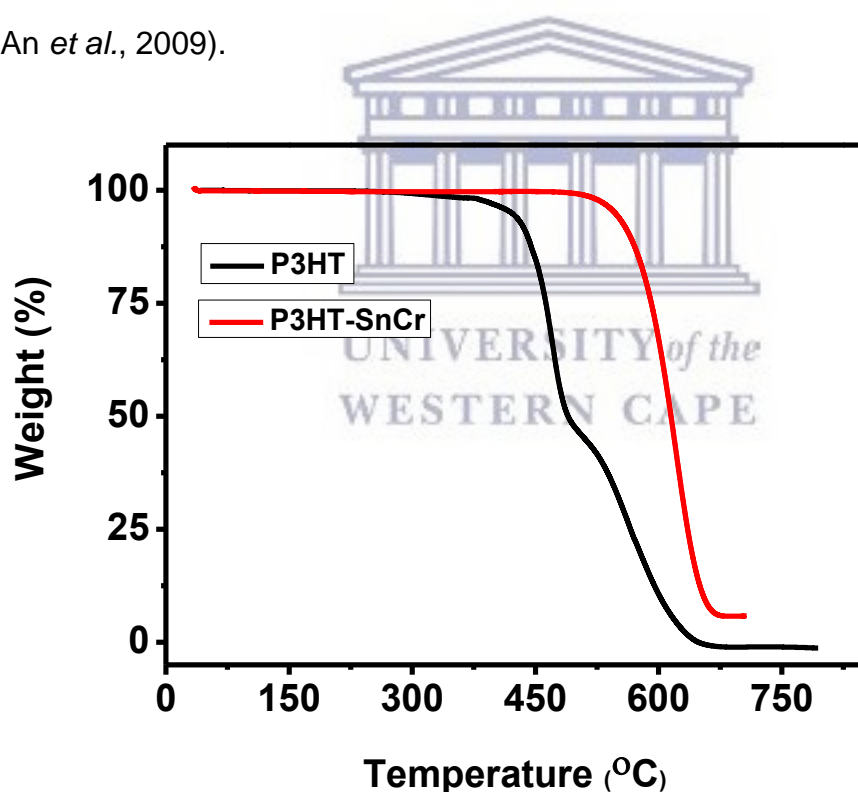


Figure 49: Thermal gravimetric curves of P3HT and P3HT-SnCr.

6.2.3.3 Atomic force microscopic analysis of the conjugated polymer and bimetallic nanoparticles

AFM is a powerful tool to study the nano-morphology of organic blends in thin films. The surface topography usually gives a good insight into the film formation ability and the tendency of the components to phase separate. **Table 8** displays AFM images of thin films prepared from chlorobenzene, from the P3HT thin film we observe phase separation of about 0.2 μm . From the 3D (3 dimension) image, it is seen that the SnCr nanoparticles are found to agglomerate on the surface of the film indicating the granular nature of the nanoparticles. This observation indicates that the film surface is somewhat rough. The blended film prepared from P3HT-SnCr shows a smooth surface with less area roughness and even distribution as compared to that of P3HT and SnCr. We observe a very small-scale phase separation of less than 0.1 μm which is favourable for charge separation, charge transport, or charge collection in photovoltaic application (Luechai *et al.*, 2012).

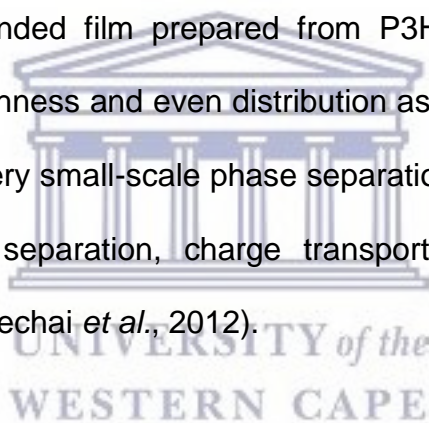
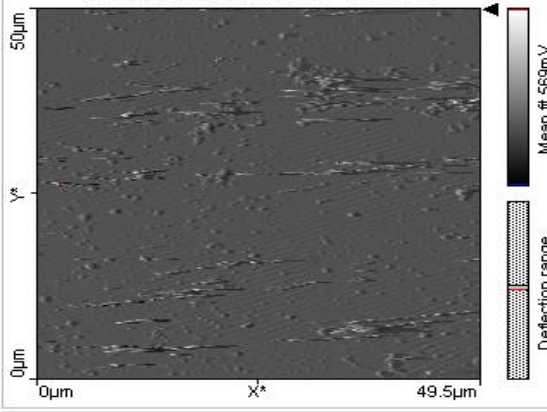
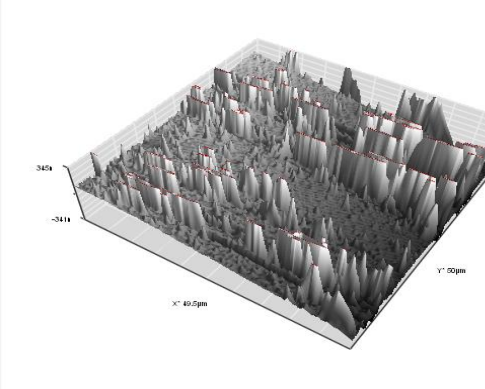
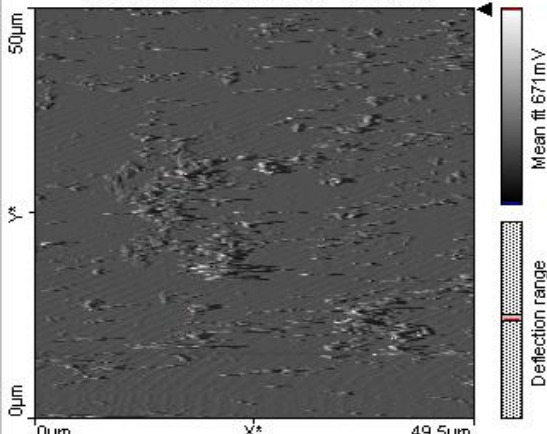
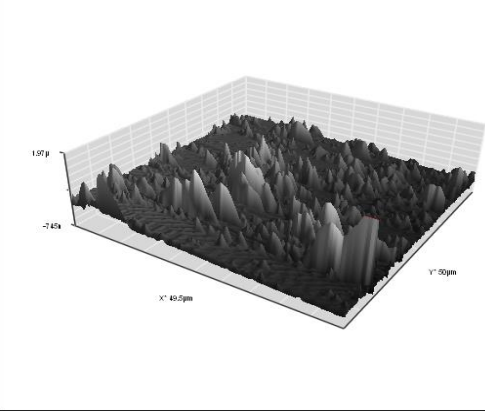
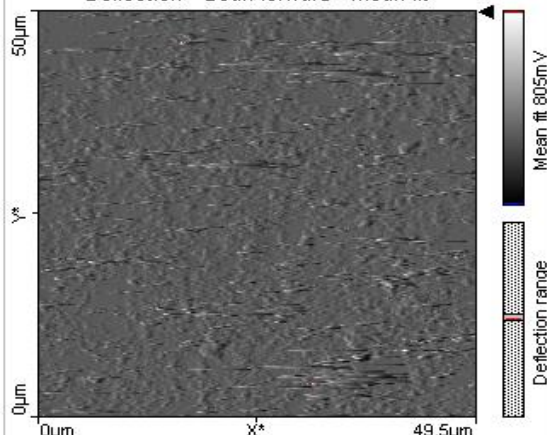
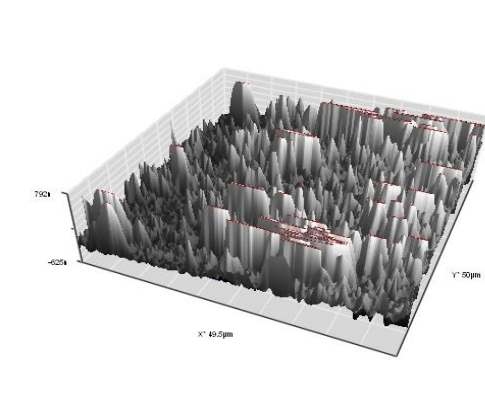


Table 8: AFM topographical images of (50 x 50 μm^2) of P3HT, SnCr and P3HT-SnCr spin coated from chlorobenzene.

Compound	Morphology	Topography
P3HT	<p>Deflection - Scan forward Mean fit</p>  <p>Mean fit 569mV Deflection range</p>	
SnCr	<p>Deflection - Scan forward Mean fit</p>  <p>Mean fit 671mV Deflection range</p>	
P3HT-SnCr	<p>Deflection - Scan forward Mean fit</p>  <p>Mean fit 805mV Deflection range</p>	

6.2.3.4 Photoelectrochemical measurements for photovoltaic application

It has been previously stated in previous studies that charge generation in organic photovoltaic cells involves the absorption of light by the donor, upon absorption an exciton is formed that is able to dissociate into separate charge or recombination. The way in which to limit the degree of recombination is the use of an acceptor that has a lower HOMO level to the LUMO of the donor (**Table 9**). This is the reason that SnCr is introduced as an acceptor conduction band is a good match with the polymer (Vemulamada *et al.*, 2008). The current-voltage (I-V) characteristics of the constructed photovoltaic cells were done and are denoted under 0.1 M LiClO₄ in acetonitrile electrolyte at a potential window of 0.01 to 0.1 V. The parameters that characterise a photovoltaic cell was calculated and are denoted in **Table 10, 11 and 12**. The photovoltaic parameters of the polymer (P3HT) and SnCr nanoparticles were investigated individually. The current-voltage curves are illustrated in **Figure 50 and 51**. The overall response is very weak as can be seen by the fact that the intersection of the curve is very close to zero. This was confirmed by the values that were found for the photovoltaic parameters, the efficiency in power conversion of P3HT is much lower in comparison with that of SnCr nanoparticles. In addition of the nanoparticles to the semiconducting material it is observed that the efficiency increased. The open circuit voltage E_{oc} decreases in both cases, resulting in an increase in the fill factor FF.

Table 9: Comparison of HOMO and LUMO between P3HT and SnCr nanoparticles.

Compound	HOMO (eV)	LUMO (eV)
SnCr	4.33	4.51
P3HT	4.21	5.89

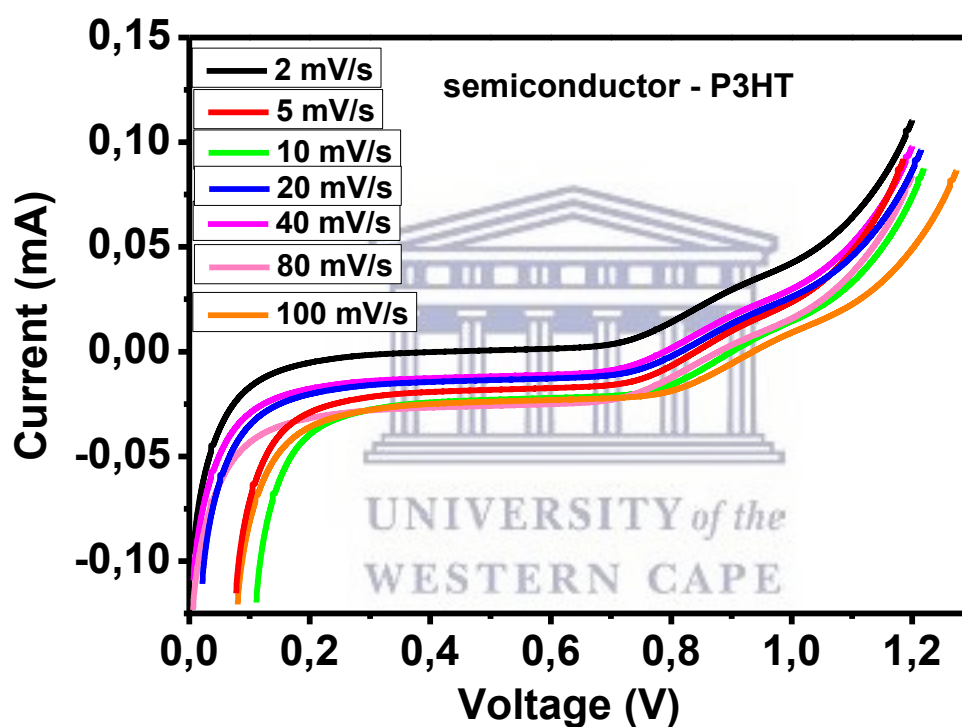


Figure 50: The I-V curves of the P3HT photoelectrochemical cell.

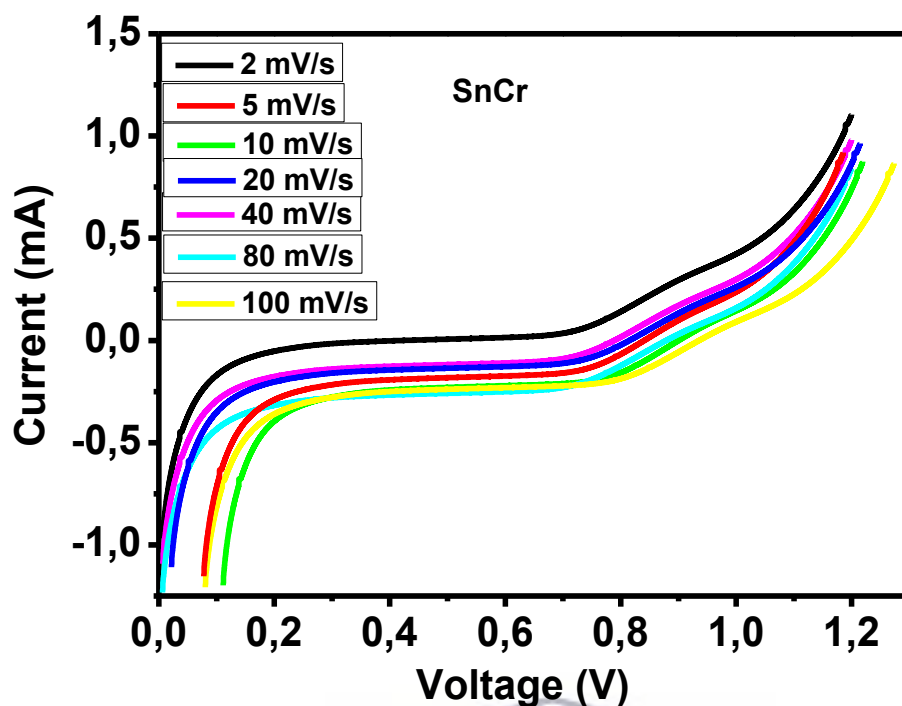


Figure 51: The I-V curves of the SnCr photoelectrochemical cell.

Table 10: The photovoltaic response of the conjugated polymer (P3HT) in different scan rates for photoelectrochemical cell.

Scan rates (mV/s)	E_{oc} [V]	I_{sc} [μ A]	η [%]	FF
2	0.716	0.159	6.79×10^{-6}	7.1
5	0.699	0.062	5.79×10^{-6}	7.4
10	0.690	0.054	5.42×10^{-6}	7.6
20	0.640	0.050	5.33×10^{-6}	8.7
40	0.622	0.049	5.19×10^{-6}	8.8
80	0.586	0.046	5.17×10^{-6}	9.0
100	0.578	0.044	5.14×10^{-6}	9.2

Table 11: The photovoltaic response of the acceptor (SnCr) in different scan rates for photoelectrochemical cell.

Scan rates (mV/s)	E_{oc} [V]	I_{sc} [μA]	η [%]	FF
2	0.091	0.751	0.698×10^{-3}	3.6
5	0.089	0.745	0.601×10^{-3}	3.7
10	0.088	0.728	0.515×10^{-3}	3.98
20	0.053	0.712	0.510×10^{-3}	5.1
40	0.050	0.652	0.507×10^{-3}	6.2
80	0.047	0.543	0.498×10^{-3}	7.9
100	0.042	0.464	0.472×10^{-3}	9.1

The photovoltaic parameters of the polymer with the SnCr nanoparticles were investigated, the current-voltage curves are illustrated in **Figure 52** for different concentration content of the bimetallic nanoparticles. The addition of SnCr nanoparticles in the polymer film increases the intensity of the photocurrent generated with a surface area of 28.5 cm^2 and incident solar power P_{in} of 175 W/m^2 . This suggests that the inorganic semiconductor increasing the number of charge carriers occurs in the composite material. This results agree with p-type polymer conducting behaviour reported by *Winder (2002)* and *Usluer et al., (2012)*. **Figure 52** shows the output characteristics and the cell parameters are given in **Table 11**. It is clearly observed that SnCr gives a significant improvement in the performance because of its low band gap of 1.8 eV , this is an indication that a large portion of the light spectrum is utilized to generate electron and holes.

Lower concentration of the bimetallic nanoparticles (1:1) shows better results with $\eta = 1.40\%$ due to less agglomeration of the nanoparticles on the substrate. Lower bandgap layer on a semiconducting material convert larger portion of optical energy into electricity (Rait *et al.*, 2007 and Heremans *et al.*, 2009), because larger band gap material absorb the shorter wavelength portion of the incident light and cannot be absorbed by it. The morphology of the nanoparticles displayed to be spherical, and this is not favourable in photovoltaic cells (Watanabe *et al.*, 2011), tubular morphology for nanomaterials is more conducive in photovoltaic applications and result in better efficiency of $\sim 8\%$.

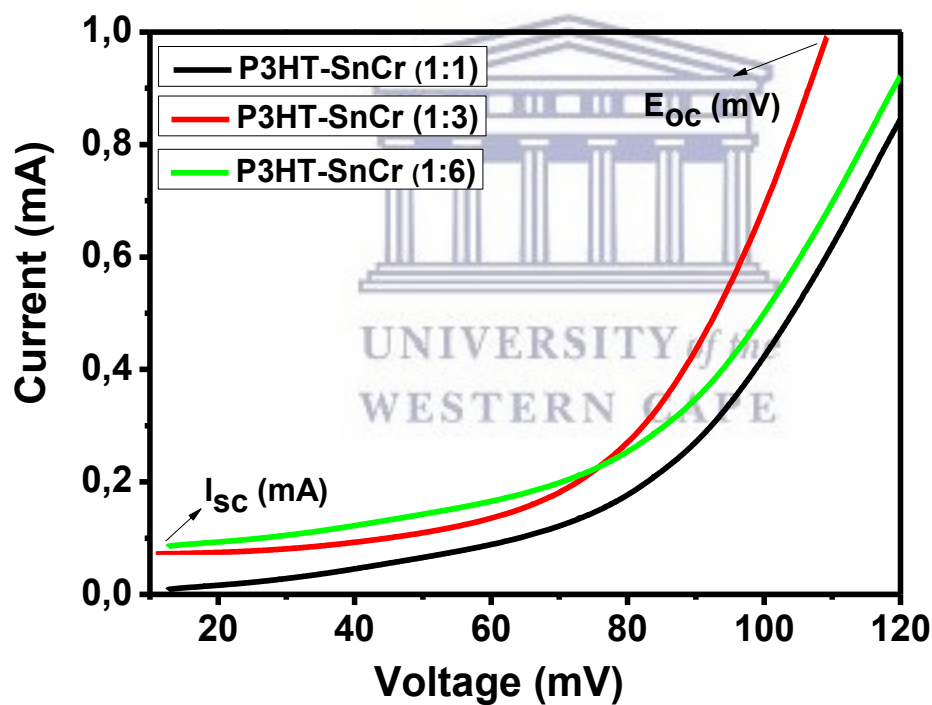


Figure 52: The I-V Curves of the P3HT-SnCr photoelectrochemical cell.

Table 12: The photovoltaic response of the active layer (P3HT-SnCr) in different concentrations for photoelectrochemical cell.

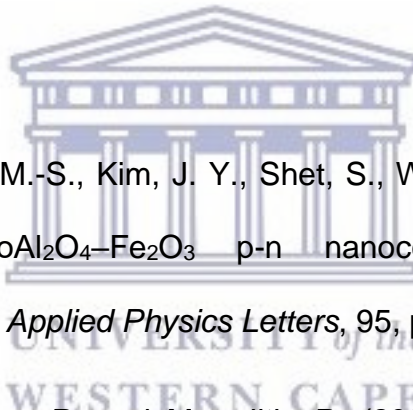
Compound [P3HT-SnCr]	E_{oc} [mV]	I_{sc} [mA]	η [%]	FF
1:1	119.286	0.999	1.40	10.67
1:3	118.675	0.980	1.03	28.10
1:6	109.452	0.977	0.56	45.74

6.3 Conclusion

Organic/inorganic composite films have been obtained by dissolving of P3HT with SnCr nanoparticles and were deposited by spin coating on indium thin oxide (ITO) substrates. It's shown that the additions of SnCr nanoparticles improve the absorption of the polymers film this is concluded by observing the increase in photocurrent of the nanocomposites (Winder, 2002 and Schubert *et al.*, 2012). The study showed that the presence of SnCr nanoparticles in the polymeric film improves the optical and the photoelectrochemical properties of P3HT. Effective photovoltaics, light emitting and photoelectrochemical cells can be realized by means of electrochemical methods. Polymer/nanoparticles and electrochemical light emitting cells will have a promising future for the development of efficient and flexible optoelectronics. Thermal stability of the polymer (P3HT) and nanoparticles showed that the polymer is very stable with presence of the nanoparticles against thermal decomposition until around 465 °C of pristine P3HT.

The complete reduction of photoluminescence of P3HT after mixing with SnCr indicates an effective charge transfer from P3HT to SnCr (Arendse, 2012). In general the value of the efficiencies of the photoelectrochemical cell showed a significant improvement at the efficiency of ~1%. This can be attributed to the morphology of the polymers that were synthesised that did not allow to produce higher efficiencies. Incorporation of the nanoparticles within the polymer improved the efficiency though it still show lower level of efficiency of the photovoltaic application. The use of the bimetallic nanoparticles increases the band gap, it is more advisable to make use of metal nanoparticles that are composed of only one metal in order to lower the band gap, consequently increasing the conductivity of the compounds.

Bibliography



Ahn, K. S., Yan, Y., Kang, M.-S., Kim, J. Y., Shet, S., Wang, H., Turner, J. and Al-Jassim, M. (2009) 'CoAl₂O₄-Fe₂O₃ p-n nanocomposite electrodes for photoelectrochemical cells', *Applied Physics Letters*, 95, pp. 116.

An, B. K., Langley, B., Burn, P. and Meredith, P. (2009) 'Dendrimers for photon harvesting in organic and organic/inorganic hybrid solar cells', *Proceedings of SPIE*, 7416, pp. 9.

Arendse, C. J. (2012) 'Temperature-dependence on the optical properties and the phase separation of polymer – fullerene thin films', pp. 4282–4289.

Cardon, F. and Gomes, W. P. (1982) 'Photovoltaic and Photoelectrochemical Solar Energy Conversion', *Solar Energy*, 29, pp. 267.

Gratzel, M. (2001) 'Photoelectrochemical cells', *Nature*, 414, pp. 338–344.

Heremans, P., Cheyns, D. and Rand, B. P. (2009) 'Strategies for increasing the efficiency of heterojunction organic solar cells: Material selection and device architecture', *Accounts of chemical research*, 42, pp. 1740–1747.

Hodes, G. (2012) 'Photoelectrochemical cell measurements: Getting the basics right', *Journal of Physical Chemistry Letters*, 3, pp. 1208–1213.

Hoppe, H. and Sariciftci, N. S. (2004) 'Organic solar cells: An overview', *Journal of Materials Research*, 19, pp. 1924–1945.

Jiang, H., Moon, K. S., Dong, H., Hua, F. and Wong, C. P. (2006) 'Size-dependent melting properties of tin nanoparticles', *Chemical Physics Letters*, 429, pp. 492–496.

Kabongo, G. L., Mbule, P. S., Mhlongo, G. H., Mothudi, B. M., Hillie, K. T. and Dhlamini, M. S. (2016) 'Photoluminescence Quenching and Enhanced Optical Conductivity of P3HT-Derived Ho³⁺-Doped ZnO Nanostructures', *Nanoscale Research Letters*. *Nanoscale Research Letters*, 11.

Kopidakis, N., Mitchell, W. J., Van De Lagemaat, J., Ginley, D. S., Rumbles, G., Shaheen, S. E. and Rance, W. L. (2006) 'Bulk heterojunction organic photovoltaic devices based on phenyl-cored thiophene dendrimers', *Applied Physics Letters*, 89, pp. 1–4.

Kümbül, A., Turaç, E., Dursun, T. and Şahmetlioğlu, E. (2009) 'Synthesis and characterization of conducting copolymer of (N1,N3-bis(thiophene-3-ylmethylene)benzene-1,3-diamine-co-3,4-ethylenedioxythiophene)', 64, pp. 114–117.

Licht, S. (2002) 'Photoelectrochemical Solar Energy Storage', *Encyclopedia of Electrochemistry: Volume 6, Semiconductor Electrodes and Photoelectrochemistry*, pp. 317–345.

Luechai, A., Gasiorowski, J., Petsom, A., Neugebauer, H., Sariciftci, N. S. and Thamyongkit, P. (2012) 'Photosensitizing porphyrin–triazine compound for bulk heterojunction solar cells', *Journal of Materials Chemistry*, 22, pp. 23030.

Malgas, G. F., Arendse, C. J., Mavundla, S. and Franscious, R. (2015) 'Interfacial analysis and properties of regioregular Poly (3-hexylthiophene) spin-coated on an Indium tin oxide coated glass substrate', 6, pp. 1–17.

Ohshimizu, K., Takahashi, A., Rho, Y., Higashihara, T., Ree, M. and Ueda, M. (2011) 'Synthesis and characterization of polythiophenes bearing aromatic groups at the 3-position', *Macromolecules*, 44, pp. 719–727.

Potratz, S., Mishra, A. and Bäuerle, P. (2012) 'Thiophene-based donor-acceptor co-oligomers by copper-catalyzed 1,3-dipolar cycloaddition', *Beilstein Journal of Organic Chemistry*, 8, pp. 683–692.

Rahman, M. Y. A., Umar, A. A., Taslim, R., Roza, L., Saad, S. K. M. and Salleh, M. M. (2014) 'TiO₂ and ZnO Thin Film Nanostructure for Photoelectrochemical Cell Application. *International Journal of Electroactive Materials*, 2, pp. 4–7.

Rait, S., Kashyap, S., Bhatnagar, P. K., Mathur, P. C., Sengupta, S. K. and Kumar, J. (2007) 'Improving power conversion efficiency in polythiophene/fullerene-based bulk heterojunction solar cells', *Solar Energy Materials and Solar Cells*, 91, pp. 757–763.

Saini, V., Li, Z., Bourdo, S., Dervishi, E., Xu, Y., Ma, X., Kunets, V. P., Salamo, G. J., Viswanathan, T., Biris, A. R., Saini, D., Biris, A. S., V, D. U. and Carolina, N. (2009) 'Electrical , Optical , and Morphological Properties of P3HT-MWNT Nanocomposites Prepared by in Situ Polymerization', 12, pp. 8023–8029.

Schubert, M., Dolfen, D., Frisch, J., Roland, S., Steyrlleuthner, R., Stiller, B., Chen, Z., Scherf, U., Koch, N., Facchetti, A. and Neher, D. (2012) 'Influence of aggregation on the performance of all-polymer solar cells containing low-bandgap naphthalenediimide copolymers', *Advanced Energy Materials*, 2, pp. 369–380.

Usluer, Ö., Kästner, C., Abbas, M., Ulbricht, C., Cimrova, V., Wild, A., Birckner, E., Tekin, N., Sariciftci, N. S., Hoppe, H., Rathgeber, S. and Egbe, D. A. M. (2012) 'Charge carrier mobility, photovoltaic, and electroluminescent properties of anthracene-based conjugated polymers bearing randomly distributed side chains', *Journal of Polymer Science, Part A: Polymer Chemistry*, 50, pp. 3425–3436.

Vemulamada, P., Hao, G., Kietzke, T. and Sellinger, A. (2008) 'Efficient bulk heterojunction solar cells from regio-regular-poly(3,3-didodecyl quaterthiophene)/PC₇₀BM blends', *Organic Electronics: physics, materials, applications*, 9, pp. 661–666.

Watanabe, R. and Miyano, K. (2011) 'Metal nanoparticles in a photovoltaic cell: Effect of metallic loss', *American Institute of Physics Advances*, 1, pp. 6.

Winder, C. (2002) 'Sensitization of low bandgap polymer bulk heterojunction solar cells', *Thin Solid Films*, 6, pp. 373–379.

CHAPTER SEVEN

Conclusive Summary

The Polymers that absorbed in the visible region, these polymeric materials were highly crystalline and the bimetallic nanoparticles were successfully synthesized and revealed the structural properties from SAXS where; the average particle size was 23 nm, 30 nm and 31 nm for SnCr, SnV, and SnTi, respectively and exhibited spherical compounds that were confirmed by HR-TEM. Relationship between crystallinity and conductivity was displayed by the compounds. The high level of crystallinity and band gap is as a result of the higher level of conjugation of the P3HT in comparison with PCDTBT. The emission of the polymers was not quenched by the presence of the stannum-based nanoparticles. Generally; the value of the efficiencies of the photovoltaic devices is low. The bandgap of P3HT was higher in both electronic and optical properties than PCDTBT. As anticipated that the photovoltaic will give good response, it revealed a high-power conversion efficiency, and this might be due the properties of the nanoparticles absorbing the near ultraviolet region and lowered the bandgap of the polymer. The nanoindentation results showed that the particle size is proportional to the hardness and Young's modulus. Increased in TiO₂ content showed better mechanical property as the hardness also increased. The polymers display a highly fluorescent characteristic, this is an indication that they can be useful in the manufacturing of light emitting devices. Since for light emitting devices the requirement is that the compound must be a good fluorophore.

The luminescent properties of the polymers were not affected by the incorporation of the SnCr nanoparticles into the polymers when placed as a thin film on ITO glass. Instead there was a small shift, thus, it can be concluded that the P3HT-SnCr nanocomposites can be used for electroluminescent devices. A synergistic effect may be demonstrated in the electroluminescence of the composite in comparison with the polymer alone. There is also the thermal and environmental stability of the polymers that make them very attractive in this area. Thermal stability of the polymer (P3HT) and nanoparticles showed that the polymer is very stable with presence of the nanoparticles against thermal decomposition. In previous studies the emphasis is been on increase the surface area of the photovoltaic device in order to increase the power conversion efficiency, the addition of SnCr nanoparticles in the polymer film increases the intensity of the photocurrent generated with a surface area of 28.5 cm². Thus; the attained efficiency was 1.40% at 1:1 concentration and a fill factor of 10.67. Interaction of the polymers with the SnCr (acceptor) was investigated using photoluminescence spectroscopy, it was able to quench the photoluminescence of the polymers. Hence it was used as an acceptor in the construction of the photovoltaic cells. Incorporation of the nanoparticles within the polymers lowered the efficiency of the photovoltaic cell, the use of the bimetallic increases the band gap, it seems to be advisable to make use of metal nanoparticles consisting of only one metal in order to lower the band gap, therefore increasing the conductivity of the compounds.



UNIVERSITY *of the*
WESTERN CAPE